UNIVERSITY OF CALIFORNIA, SAN DIEGO

DEVELOPMENT OF A DNA MULTIPLEXING SYSTEM UTILIZING ENCODED POROUS SILICA PHOTONIC CRYSTAL PARTICLES

A dissertation submitted in partial satisfaction of the requirements for the degree Doctor of Philosophy

in

Chemistry

by

Shawn O. Meade

Committee in charge:

Professor Michael J. Sailor, Chair
Professor Seth M. Cohen
Professor Sadik C. Esener
Professor Clifford P. Kubiak
Professor Jerry Yang

2008

The dissertation of Shawn O. Meade is approved, and it is acceptable in quality and form for publication on microfilm:

_____

_____

_____

_____

_____

chair

University of California, San Diego

2008

DEDICATION

This work is dedicated to the memory of my oldest sister, Amanda, who passed away due to cancer.

This work is also dedicated to the rest of family and friends, especially my Mom, who always encouraged me to be creative and ask questions.

For a successful technology, reality must take precedence over public relations, for nature cannot be fooled.

-Professor Richard P. Feynman

TABLE OF CONTENTS

LIST OF FIGURES

Chapter 1

Chapter 2

Chapter 3

Chapter 4

Chapter 5

Appendix A

Appendix B

Appendix C

Appendix D

LIST OF EQUATIONS

Chapter 2

LIST OF TABLES

Chapter 2

Chapter 5

Appendix B

ACKNOWLEDGMENTS

Professor Mike Sailor has been the most influential person in my career. He took me in as an undergrad, helped get me my first job (Illumina) and let me come back to the lab to work on a PhD (he must have had jet lag that day). Mike's taught me how to be a scientist as well as a promoter. He also taught me that science doesn't always have to be a serious business – it can be enjoyable too.

Sailor Group II (2003-2007): Michelle Chen contributed a great amount to this project by helping me write a proper decoding program. She ran ROC analysis on assay results presented in chapter 5. I'm very happy that she will be taking this project over. **Luo Gu** volunteered his time and photography skills to help document much of the procedures outlined in this dissertation. Additionally, I'm grateful for all his sound advice on scientific and technical issues. **To everyone in the group:** thanks for sharing resources and ideas. Also, thanks for making the Sailor lab a fun and slightly crazy place to work.

Sailor Group I (1998-1999): Dr. Keiki-Pua Dancil and Dr. Doug Greiner changed the direction of the Sailor lab toward bio-applications. It's a very exciting place to be now, due in large part to their contributions. I gained a strong understanding of what it takes to develop a biotech application while working with them as an undergraduate researcher.

Dr. Todd Dickinson, Dr. Steve Barnard, Dr. Chanfeng Zhao and so many others that I don't have room to mention them all. I'd like to thank Todd, Steve and

Chanfeng for teaching me the scientific, technical, and organizational skills needed to successfully run an R&D project.

Ryan Anderson and Larry Grissom from the **Nano3** facility offered guidance that made the work presented in chapter 4 possible.

Dr. Austin Derfus and Prof. Sangeeta Bhatia let me use their fluorescence microscope (before I put together the system described in chapter 3) for the bandpass decoding study of appendix B.

Chapters 3, 4, and 5, in part are a reprint of the material as it will appear upon submission of the manuscript in progress: Meade, S.O., Chen, M., Sailor, M.J. "A bioassay multiplexing system utilizing porous silica photonic crystal particles containing spectral barcodes" (2008)

VITA

June 1992	High School Diploma, Dana Hills High School
Sept 1992 - June 1995	Saddleback Community College
June 1999	B.S. Chemistry, University of California, San Diego
Fall 1998 – Sept 1999	Undergraduate Researcher, Dept. of Chemistry and Biochemistry, University of California, San Diego
Sept. 1999 – Dec. 2002	Research Associate, Illumina, Inc.
Spring 2003 – Spring 2004	Teaching Asst., Dept. of Chemistry and Biochemistry, University of California, San Diego
Jan 2003 – Nov 2007	Research Asst., Dept. of Chemistry and Biochemistry, University of California, San Diego
June 2008	Ph.D., Chemistry, University of California, San Diego

PUBLICATIONS

"A bioassay multiplexing system utilizing porous silica photonic crystal particles containing spectral barcodes" **Shawn O. Meade**, Michelle Chen, Michael J. Sailor

Manuscript in progress

"Porous silicon-based polymer replicas formed by bead patterning." Jennifer S. Park, **Shawn O. Meade**, Ester Segal, Michael J. Sailor *Physica Status Solidi A: Applications and Materials Science* (2007) 204(5), 1383-1387

"Microfabrication of freestanding porous silicon particles containing spectral barcodes." **Shawn O. Meade**, Michael J. Sailor *Physica Status Solidi RRL: Rapid Research Letters* (2007), 1(2), R71-R73.

"Porous silicon photonic crystals as encoded microcarriers." **Shawn O. Meade**, Myeong Sik Yoon, Kyo Han Ahn, Michael J.Sailor *Advanced Materials* (2004), 16(20), 1811-1814.

"Optically encoded particles, system and high-throughput screening" Michael J. Sailor, **Shawn O. Meade** United States Patent Application 20070051815, March 8, 2007

"Optically encoded particles with grey scale spectra" Michael J. Sailor, **Shawn O. Meade** United States Patent Application 20070148695, June 28, 2007

"Polymer composite photonic crystal particle preparation." Yang Yang Li, Vijay S.Kollengode, Michael J.Sailor, **Shawn Meade**, PCT Int. Appl. (2006), WO 2006065806

"Array compositions for improved signal detection" Todd A. Dickinson, **Shawn Meade,** Steven M. Barnard, Anthony W. Czarnik, James Bierle**,** Bahram G. Kermani**,** Mark S.Chee United States Patent 6,942,968, September 13, 2005

ABSTRACT OF THE DISSERTATION

Development of a DNA Multiplexing System Utilizing Encoded Porous Silica Photonic Crystal Particles

by

Shawn O. Meade

Doctor of Philosophy in Chemistry

University of California, San Diego, 2008

Professor Michael J. Sailor, Chair

A DNA multiplexing system utilizing encoded porous silica photonic crystal particles has been developed. The critical components necessary to achieve this were the development of (1) a high capacity encoding methodology, (2) instrumentation and methods for decoding and assay readout, (3) a microfabrication technique and a means to stabilize the microparticles in assay conditions as well as allow for the use of existing surface chemistries for probe immobilization, and (4) a model system multiplexed DNA assay. Once, these components were in place an experiment was carried out that demonstrated multiplexed detection.

The encoding method produces a one dimensional photonic structure that exhibits optical reflectivity spectra with multiple peaks. The height of a given peak can be modulated, or the peak can be deleted all together. The resultant spectral peaks can be

used as a spectral barcode, where the number of codes possible is the number of resolvable peak intensity levels (states) raised to the maximum number of wavelength resolved peaks (bits) present in the spectral code. The capacity to encode over 1 million codes has been demonstrated using the method.

Instrumentation and methods for high-throughput decoding and assay readout of the encoded microparticles were developed. The readout system is comprised of a fluorescence microscope modified for high resolution spectral imaging. A decoding method, which identifies codes based on the number of peaks present, the relative distances between neighbor peaks, and thresholds of the peak intensity, was also developed.

A method for the microfabrication of freestanding porous silica particles containing spectral barcodes was developed and shown to produce uniform populations of particles, approximately 25 μm in diameter. Additionally, thermal oxidation of the porous silicon to porous silica was demonstrated not to have a detrimental effect on the optical codes, thus creating an encoded particle with increased chemical resistance and compatibility with common glass-based immobilization chemistries.

A model system multianalyte assay based on 50-mer oligonucleotide probes and perfect match fluorescently labeled targets was used as a means to demonstrate multiplexed detection and act as a benchmark for the accuracy of the photonic encoding method. Essentially, a set three particle types, each with a unique photonic code, were each immobilized with a specific oligonucleotide probe and reacted with a pool of fluorescently labeled targets. Each target was dyed a different color. The results agreed

with the experimental design, thus demonstrating both multiplexed detection and validation of the photonic encoding method. Finally, the successful decoding and assay readout demonstrated chemical stability of both the photonic codes and the immobilized probes through the biological assay conditions.

CHAPTER 1

Introduction to multiplexing technologies

1.1 Genetic analysis and the study of complex disease

The association of genes and genomic regions with cellular growth processes, namely tumor development, is a major goal in the study of complex diseases. Knowing which genes to turn on or off is critical for the successful development of powerful diagnostics and therapeutics.[1] The study of genetic variation and function falls into four main fields: sequencing, genotyping, gene expression and epigenetics.[2] The latter three methods share the need to screen for a large number of biological target molecules in a single patient sample. This need has led to the development of highly parallel assays and readout technologies, allowing researchers to begin extracting medically valuable information from the genome in a high throughput manner.

1.1.1 Gene expression assays

Gene expression assays are designed to look for genes associated with a particular phenotype such as cancer. The measurement of variable levels of mRNA between sick and healthy organisms is the basis for gene expression assays. Lockhart et al. were one of the original groups to use DNA microarrys as a readout platform for highly parallel genomic assays.[3] This work demonstrated that the expression levels of thousands of genes could be quantified in parallel by measurement of the corresponding mRNA sequences present in a single multiplexed sample. Microarray based gene expression assays have been used to classify certain types of cancer on a molecular level. Golub et al. demonstrated both class discovery and class prediction of Leukemia through the use of an array based gene expression assay.[4] Golub et al. were fully warranted to point out the leap they made over previous methods to classify cancers, such as histological or

antibody testing. However, other researchers have found that gene expression profiling carries with it a lot of noise. Fan et al. attribute the noisy data to the nonspecific hybridization and signal to noise ratio issues commonly found with assays that rely only on sequence-specific probe hybridization.[2]

1.1.2 Genotyping

Another way to find genes, or genomic regions associated with cancer or other complex diseases, is by genotyping. The aim of these studies is to draw correlations between genetic mutation patterns and a disease state (phenotype). Single nucleotide polymorphisms (SNPs) have proven to be reliable markers for measuring genetic variation in highly parallel assays.[5, 6] Engle et al. identify four main types of SNP genotyping studies: allelic imbalance, direct association, linkage, and indirect association studies.[1]

1.1.3 Epigenomics

Assays based on epigenetics screen for genetic variation that does not involve a change in the sequence of nucleotides composing a gene or genomic region, yet still affect gene function. These assays are designed to screen for patterns in cytosine methylation and histone modification markers. The Human Epigenome Project is tasked with profiling methylation patterns in all major genes in all major tissues.[7] It is hoped that the project will be able to tie together disease, genetics and the environment because methylation, capable of altering genome function, can be caused by external or environmental factors.

1.2 Multiplexing technologies

1.2.1 Introduction to multiplexing technologies

A multiplexing system describes a system that allows researchers to detect multiple analytes in a single sample. There are two major classes of multiplexing systems: microarrays and encoded particles. The platforms are similar in that specific chemical probes are utilized to detect a desired analyte, or target in solution. Almost all systems use fluorescence or chemiluminescence for signal transduction, by labeling the targets with fluorophores. However, there are differences - discussed below.

1.2.2 Microarrays and spatial encoding

In microarrays, the chemically specific probe is immobilized to a surface at a known location on a grid, providing the identity of the chemical probe. This concept is known as spatial encoding.

1.2.2.1 GeneChip™

Foder et al. took the concepts of conventional photolithography used for making computer chips and developed a method for producing high density oligonucleotide arrays.[8] In this method, gene specific oligonucleotide probes are synthesized directly to the surface of the substrate in a series of steps. In the first step, the surface of a quartz wafer is coated with a photoactive material, selective regions are masked off and a solution of a single type of nucleotide, A, G, T, or C is exposed to the surface. This

process is repeated until the surface is functionalized with unique 25-mer oligonucleotide probes with precise spatial coordinates.[9] Once in the hands of the user, the fluorescently labeled genomic sample is exposed to the surface of the chip, allowed to incubate and is then washed away. High resolution, fluorescence laser scanners are used to readout the assay results. Any location that fluoresces designates a hit for the particular probe, synthesized at that location.

1.2.2.2 cDNA spotted microarray

The cDNA spotted array, made popular, mainly by Brown et al. [10] is similar in concept to the photolithographically synthesized array discussed above. However, there are differences. First, the probes are generated by PCR from biological samples, are usually longer (around 50 nucleotides in length) and are spotted to the surface. The benefit of spotting down the probes is that longer lengths can be used than are able to be synthesized using the Affymetrix technology. Longer oligonucleotide probes have been shown to provide for more sensitivity and selectivity.[11] Unfortunately, the technique of spotting is quite variable because it's difficult to control the amount of probes per spot and the probe distribution within each spot, leading to noisy assay results.

1.2.2.3 Microelectronic arrays

Another type of spatially encoded multiplexing technology is the microelectronic array developed by Heller et al.[12] As the name suggests this platform utilizes microelectronic manufacturing techniques to create micron scale (~ 80 μm in diameter) probe features which act as electrodes to assist in the hybridization of the probe/target

interaction. The electrophoretic field increases the rate of hybridization and the reversal of the field allows for more stringent conditions that increase the selectivity of the array. [13]

1.2.2.4 BeadArray™

Invented by Walt et al.[14], and commercialized by Illumina, Inc.[15], the BeadArray™ utilizes spherical silica beads, functionalized with oligonucleotides probes that act in the capacity of both a code and a gene specific probe. The probe functionalized beads are pooled together into sets where the types of probes are selected depending on the intended application. After pooling, the beads are randomly assembled into one of two substrate formats. The first format is based on dense fiber optic bundles, composed of up to 50,000 individual fibers. The bundle surface covers an area of approximately 1 mm^2. The core of each fiber is selectively etched to provide a well for a bead to assemble into. The second format consists of arrays of wells microfabricated into silica, similar in size to the fiber optic array. In both formats, each bead type (containing a unique probe) is usually, represented by around 30 replicate beads. The randomly assembled beads are decoded prior to shipment.[16] Once received, users are free to use the BeadArray™ in the same manner as standard microarrays are used.

1.2.3 Encoded microparticles and spectral encoding

1.2.3.1 Introduction to encoded particles

High density microarrays are ideal for large scale multiplexing experiments, like those discussed in the beginning of the chapter. However, there is demand for more flexible, low level multiplexing systems.[15] Additionally, encoded particles provide better solution kinetics than microarrays, delivering faster and more sensitive assay results.[17] It takes more money and time to design and manufacture micorarrays with custom probe panels, than it does to create a custom probe panel with sets of encoded microparticles. This is because the customer can order large sets of encoded particles with each particle type/probe packaged separately and combine them into sets as they see fit. This is ideal for applications in the growing molecular diagnostics market.[15] There have been many types of multiplexing systems demonstrated, using encoded particles. Some systems are based on beads doped with fluorescence dyes[18], quantum dots[19, 20], and upconverting materials.[21] Other systems are based on making particles that have unique arrangements of metallic layers that define the code by the spatial pattern.[22] Additionally, some encoding schemes have been based on diffraction gratings[17] and photonic structures[23]. There are however, only two systems that have been successfully commercialized to date: the Luminex Xmap™ system[18] and Illumina's VeraCode™ system[15, 17, 24].

1.2.3.2 Commercial encoded particle multiplexing systems

1.2.3.2.1 Xmap™

With the Xmap™ multiplexing system, particles are encoded by impregnation of multiple types of dyes at different concentrations.[18] The particle's code and assay

results are readout using the multiple fluorescence channels of a customized flow cytometer system. The codes are defined by the unique fluorescence intensity ratio exhibited by each particle type. Up to 100 codes are possible, qualifying this system as a low level multiplexing system. Sets of particles can be functionalized with oligonucleotide probes, peptides, and antibodies.

1.2.3.2.2 VeraCode™

The VeraCode system, by Illumina, utilizes microscale diffraction gratings as the encoding element. The marketing brochure describes a cylinder 28 μm in diameter and 240 μm in length, whose encoding element is made by halolithography.[15] In a patent application, it's stated that the outer shell of the particle is made of silica glass or any other material that is suitable.[17] It's also stated that the center of the particle, containing the encoding element, can be doped with Boron and/or Germanium.[17]

The pool of particles, in which multiplexing levels can reach up to 384 (number of codes)[15], is reacted with the sample in fluid suspension, after which they are washed and assembled onto a substrate that is composed of grooves.[24] The grooves allow for the cylindrical particles to align in the orientation needed for optical readout.

The reader's functions are described as "…a dual-color laser detection system to identify the unique holographic code inscribed in each VeraCode microbead and to detect the signal intensity associated with each bead."[15] By "signal intensity" they are referring to the fluorescence signal of the bound, labeled analyte. The website goes on to describe that the halographic image encoded into the particle's core, diffracts the incident laser light into multiple components (a.k.a. a diffraction spectrum) which is then

projected onto a CCD camera. In a patent application, Moon et al. describe a readout system with both a 532 nm laser and a 632 nm laser. However, they also leave the door open to a source that can emit a "plurality of wavelengths."[17]

1.3 PROJECT GOALS

The high level goal of this project was to demonstrate that porous silicon photonic crystal particles, containing spectral barcodes, can function as a multiplexing platform. The underlying goals were (1) the development of a high capacity encoding method, (2) the development of instrumentation and methods for high-throughput decoding, (3) the development of a microfabrication method, (4) the demonstration of chemical stability, as evidenced by the maintenance of photonic codes and retention of chemical probes through biological assay conditions, and (5) the validation of the photonic encoding method by comparison to an independent encoding method based on oligonucleotides, while demonstrating multiplexed DNA detection.

1.4 PROJECT OVERVIEW

Figure 1 gives a general overview of how the system works. First, separate batches of microfabricated porous silicon photonic crystal particles, each containing a unique spectral barcode, are thermally oxidized to porous silica. Each particle type is then functionalized with a different oligonucleotide probe. Second, the particle types are pooled together and fluorescently labeled oligonucleotide targets are added to the mixture and allowed to react. Each target is specific to one of the probes. Third, the particles are assembled onto a surface and fluorescence images are acquired. Finally, in order to

determine if a specific probe/target interaction has occurred, the spectral identity of each particle is decoded and related to its fluorescent value. The details of how this is accomplished are discussed in this work.

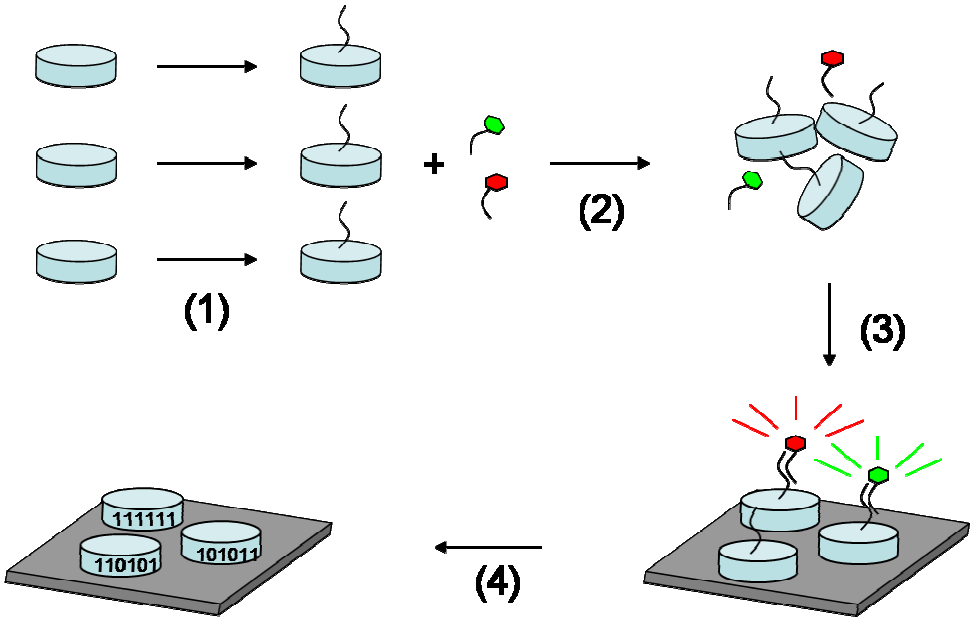

Figure 1 Experimental summary. (1) Three particles types, each exhibiting a different spectral barcode are each functionalized with a different DNA probe. (2) The particles are pooled together and fluorescently labeled targets are added to the mixture and allowed to react. (3) The particle suspension is washed, assembled onto a surface and fluorescence images are acquired. (4) Without moving the particle assembly relative to the detector, the particles are then decoded.

1.5 REFERENCES

1. Engle, L.J., C.L. Simpson, and J.E. Landers, *Using high-throughput SNP technologies to study cancer.* Oncogene, 2006. **25**: p. 1594–1601.

2. Fan, J.B., M.S. Chee, and K.L. Gunderson, *Highly parallel genomic assays.* Nature Reviews Genetics, 2006. **7**(8): p. 632-644.

3. Lockhart, D. J., Dong, H. L., Byrne, M. C., Follettie, M. T., Gallo, M. V., Chee, M. S., Mittmann, M., Wang, C. W., Kobayashi, M., Horton, H., Brown, E. L., *Expression monitoring by hybridization to high-density oligonucleotide arrays.* Nature Biotechnology, 1996. **14**(13): p. 1675-1680.

4. T. R. Golub, D. K. Slonim, P. Tamayo, C. Huard, M. Gaasenbeek, J. P. Mesirov, H. Coller, M. L. Loh, J. R. Downing, M. A. Caligiuri, C. D. Bloomfield, E. S. Lander, *Molecular Classification of Cancer: Class Discovery and Class Prediction by Gene Expression Monitoring.* Science. **236**: p. 531-537.

5. Syvanen, A.C., *Accessing Genetic Variation: Genotyping Single Nucleotide Polymorphisms.* Nature Reviews Genetics, 2001. **2**: p. 930-942.

6. Syvanen, A.C., *Toward genome-wide SNP genotyping.* Nature Genetics, 2005. **37**: p. S5-S10.

7. *Human Epigenome Project, http://www.epigenome.org/.*

8. Fodor, S. P. A., Read, J. L., Pirrung, M. C., Stryer, L., Lu, A. T., Solas, D., *Light-Directed, Spatially Addressable Parallel Chemical Synthesis.* Science, 1991. **251**(4995): p. 767-773.

9. *http://www.affymetrix.com.*

10. Schena, M., D. Shalon, R. W. Davis, P. O. Brown, *Quantitative Monitoring of Gene Expression Patterns With a Complementary DNA Microarray.* Science, 1995. **270**: p. 467-470.

11. Kucho, K.. Yoneda, Hidekatsu, Harada, Manabu, Ishiura, Masahiro, *Determinants of sensitivity and specificity in spotted DNA microarrays with unmodified oligonucleotides.* Genes & Genetic Systems, 2004. **79**(4): p. 189-197.

12. Heller, M.J., *An active microelectronics device for multiplex DNA analysis.* IEEE Engineering in Med. and Bio., 1996. **15**(2): p. 100-104.

13. Heller, M.J., *DNA Microarray Technology: Devices, Systems, and Applications.* Annu. Rev. Biomed. Eng., 2002. **4**: p. 129-153.

14. Ferguson, J.A., F.J. Steemers, and D.R. Walt, *High-Density Fiber-Optic DNA Random Microsphere Array.* Analytical Chemistry, 2000. **72**(22): p. 5618-5624.

15. *http://www.Illumina.com.*

16. Gunderson, K.L., Kruglyak, S., Graige, M. S., Garcia, F., Kermani, B. G., Zhao, C. F., Che, D. P., Dickinson, T., Wickham, E., Bierle, J., Doucet, D., Milewski, M.,Yang, R., Siegmund, C., Haas, J., Zhou, L. X., Oliphant, A., Fan, J. B., Barnard, S., Chee, M. S., *Decoding randomly ordered DNA arrays.* Genome Research, 2004. **14**(5): p. 870-877.

17. Moon, John A., Putnam, Martin A., *Diffraction grating-based encoded articles for multiplexed experiments*. United States Patent Application 20040075907

18. *http://www.luminexcorp.com/.*

19. Chan, W.C.W. and S. Nie, *Quantum dot bioconjugates for ultrasensitive nonisotopic detection.* Science, 1998. **281**: p. 2016-2018.

20. Bruchez, M., Moronne, M., Gin, P., Weiss, S., Alivisatos, A. P., *Semiconductor nanocrystals as fluorescent biological labels.* Science, 1998. **281**(5385): p. 2013-2016.

21. Haushalter, R.C., *Methods for optically encoding an object with upconverting materials and compositions used therein*. United States Patent Application 2005136486

22. Nicewarner-Peña, S.R., Freeman, R. G., Reiss, B.D., He, L., Peña, D. J., Walton, I. D., Cromer, R., Keating, C. D., Natan, M. J., *Submicrometer metallic barcodes.* Science, 2001. **294**(5540): p. 137-141.

23. Cunin, Frederique, Thomas, Schmedake A., Link, Jamie R., Li, Yang Yang Koh, Jennifer, Bhatia, Sangeeta N., Sailor, Michael J., *Biomolecular screening with encoded porous silicon photonic crystals.* Nature Mater., 2002. **1**: p. 39-41.

24. Putnam, M.A., J.A. Moon, and T. Li, *Diffraction grating-based encoded microparticle multiplexed assay stick*. United States Patent Application 200600772177

CHAPTER 2

Photonic encoding of porous silicon

2.1 ABSTRACT

This chapter introduces a method of producing one dimensional photonic structures that exhibit optical reflectivity spectra with multiple peaks. The height of a given peak can be modulated, or the peak can be deleted all together. The technique, referred to as rugate encoding, involves electrochemically etching a current-time waveform of superimposed sine waves into a silicon wafer. The porous nanostructure that results exhibits a reflection spectrum that represents an approximation of the Fourier transform of the porosity gradient defined by the electrochemical etch. The resultant spectral peaks can be used as a spectral barcode, where the number of codes possible is the number of resolvable peak intensity levels (states) raised to the maximum number of wavelength resolved peaks (bits) present in the spectral code. The capacity to encode over 1 million codes has been demonstrated using the method. Additionally, the development of a computer controlled etching system is presented in this chapter.

2.2 INTRODUCTION

The algorithm used to prepare encoded porous silicon films is summarized in Figure 2.1. Bovard et al. reviews the concepts used here in a work discussing rugate filter theory.[1] The method presented here involves creating a refractive index variation in a material whose spatial distribution consists of the sum of several sine waves. The reflection spectrum (intensity versus wavelength) that results from such a structure represents an approximation of a Fourier transform of the spatial distribution of the refractive index (refractive index versus distance) in the material. Berger et al. first demonstrated the application of this concept to the design of rugate filters fabricated from porous silicon.[2] The waveform used in the present work involves a superposition of n sine waves of different frequencies, where each individual sine component is represented by Equation 2.1 (Fig. 2.1a).

$$y_i = A_i[\sin(k_i t - \phi_i) + 1] + A_{i,min} \qquad \text{(Eq. 2.1)}$$

In equation 2.1 y_i represents a sine wave of amplitude, A_i; frequency, k_i; time, t; phase offset, ϕ_i, and amplitude offset, $A_{i,min}$. The variable A_i for each component follows Equation 2.2:

$$A_i = (A_{i,max} - A_{i,min})/2 \qquad \text{(Eq. 2.2)}$$

In equation 2.2 $A_{i,max}$ is the maximum amplitude of the sine component i and $A_{i,min}$ is the minimum amplitude of the sine component i. $A_{i,min}$ is equivalent in both Equation 2.1 and Equation 2.2. The individual sine components are summed together to form a composite waveform, Equation 2.3:

$$y_{comp} = (y_1 + y_2 + \ldots + y_n)/n \qquad \text{(Eq. 2.3)}$$

The encoding information contained in Equation 2.3, is converted to an analog current-time waveform (Fig. 2.1b) and a crystalline silicon wafer is etched using a computer-controlled galvanostatic power supply. The porous silicon film that results displays a porosity gradient that maps directly to the current-time profile, or encoded waveform, used in the etch (Fig. 2.1b). The height and spectral position of each of the main peaks in the reflection spectrum (Fig. 2.1d) depend on the amplitude and frequency of the corresponding sine components of the composite waveform (Fig. 2.1b). Therefore, the reflectivity spectrum (Fig. 2.1d) represents an approximation of a Fourier transform of the composite current-time waveform (Fig. 2.1b). The resultant spectral peaks can then be used as the bits of a spectral barcode. The number of codes possible is determined by the number of discernable peak heights (states) raised to the maximum number of peaks (bits) present in the spectral code.[3, 4]

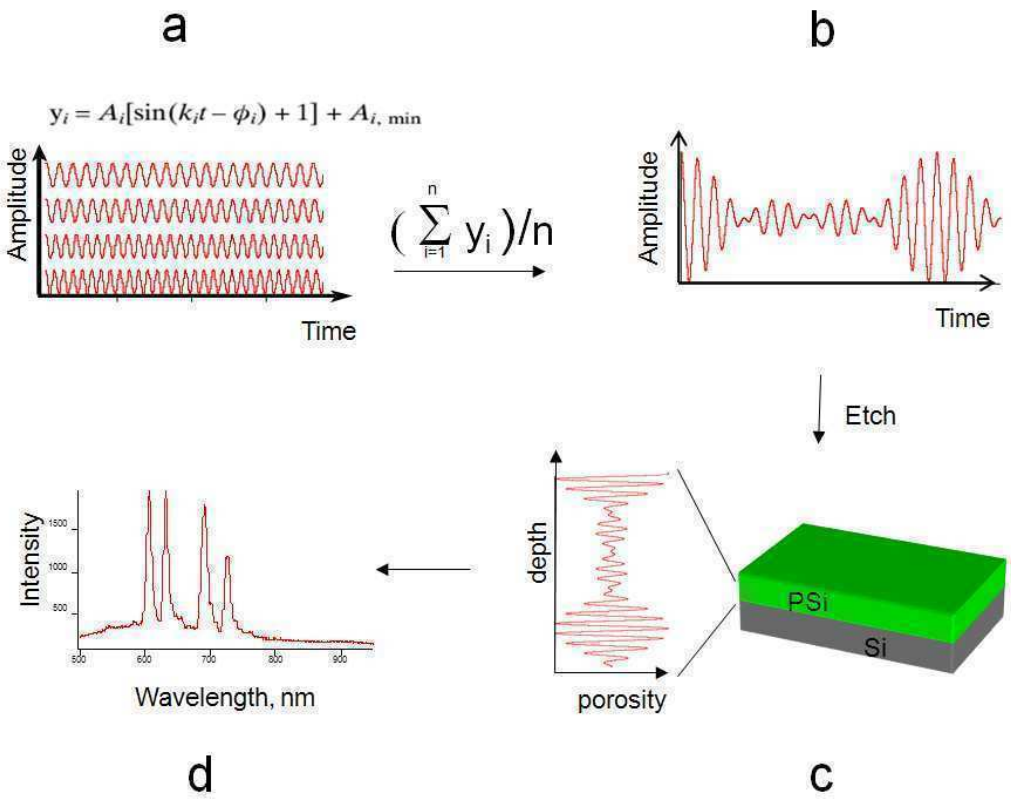

Figure 2.1 First, a set of sine waves varying in frequency and amplitude is created and set to desired levels. A composite waveform is then made by summing together the sine waves and divided by a scaling factor (number of sine waves in the set), to counteract the increase in amplitude due to the summation. The composite waveform is then used to run an anodic galvanostatic etch on a highly doped P-type silicon wafer using an ethanolic hydrofluoric acid solution. When optimized, the resulting porous matrix can exhibit a reflection spectrum like the one shown here. A peak's spectral position and height depends on the corresponding sine wave's frequency and amplitude, respectively.

2.3 INSTRUMENTATION

2.3.1 Background

In order to demonstrate the method described above, a computer controlled system for the electrochemical etching of silicon was developed. The system described in this work will be referred to as the "2nd generation etch rig" and was based on an earlier rig that sent out the current-time waves in the form of audio signals. The aim of the "2nd generation etch rig" was to reduce the electrical noise present in the original instrument.

2.3.2 Etch System

The improvement of "2nd generation etch rig" over the first etch rig was achieved by replacing the computer's audio source as the signal generator, with a data acquisition (DAQ) card featuring analog output channels. In general, a computer controlled/DAQ etch rig has several major components (Fig 2.2). One of which is the waveform writer software - a program that allows the user to create a text file (.txt) that contains the composite waveform defined by Equation 2.3. Figure 2.3 shows an example of a waveform writer, containing the algorithm described above, written in IGOR script (Wavemetrics). Note that k_i, in the scripted algorithm is not the same as k_i of Eq. 2.1 (the actual frequency in Hz). Instead, the k variable in the scripted algorithm is a frequency multiplier of the base frequency, which can be calculated using the length of the wave (in both data points and # of periods) and the voltage update rate of the etch rig's DAQ card. Using values listed in the scripted algorithm (Fig. 2.3) the calculation is as follows:

- Length of wave in terms of # of data points, **N** = 128000 (Fig. 2.3)
- The scale is set to run from 0 to 30*2π, therefore the number of periods is 30 (Fig. 2.3).
- Voltage update rate of system, **r (pts/s)** = 500
- Length of wave in terms of time (s), $\mathbf{N_T = N/ r}$ (Eq. 2.4)
- Period (s) in terms of number of points and number of periods, $\mathbf{T = N_T/(\#\ of\ periods)}$ (Eq. 2.5)
- Frequency in Hz, $\mathbf{k = 1/T}$ (Eq. 2.6)

Substituting the values in of **N, r** into Eq. 2.4, the values of $\mathbf{N_T}$ and the number of periods into Eq. 2.5, and substituting the calculated value of T into Eq. 2.6 yields the frequency in Hz, **k = 0.117 Hz**

The next piece of software, critical to the process, is the system control software (Fig. 2.4), whose function is to read the text file, extract the numbers into binary data, which is then sent out through the analog output channel of the DAQ card (Fig. 2.2). Figure 2.4 shows an example of the etch system control software written in LabView 6.0 code. The function of the DAQ card is to read the binary signal from the computer and translate it to an analog voltage signal. The voltage signal is then transmitted from the analog output channel of the DAQ card to the power supply (Fig. 2.2). The function of the power supply is to translate the voltage signal into a galvanostatic current signal which is used to etch the sample. The power supply can be wired directly to the DAQ

card or a junction board can be inserted in between (Fig. 2.2); making the DAQ card's other functions more accessible.

Details of electrochemical cells and their use have been discussed in great detail by others.[5] The pieces of the cell relevant to the electronic system are the electrode or the silicon sample itself (Fig. 2.2), the electrolyte solution (Fig. 2.2) and the counter electrode (Fig. 2.2). The counter electrode in this system is made of platinum, because of the metal's resistance to the corrosive hydrofluoric acid electrolyte. For large samples (~ 2.7 cm in diameter) a spiral Platinum electrode is preferred (Fig. 2.2 B). Table 2.1 lists a bill of materials for the "2nd generation etch rig." The items listed are dated and have since been updated by other workers, but the list provides a basis for building a system from scratch.

a

b

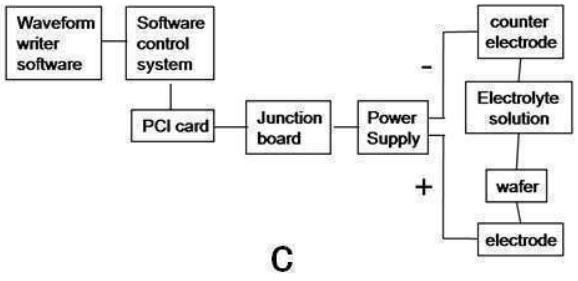

c

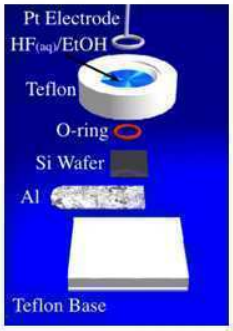

d

Figure 2.2 (a) Image of computer controlled etch rig. (b) Spiral, platinum counter electrode (c) System diagram for computer controlled etch rig. (d) The ubiquitous Sailor group diagram of an etch cell (graphic courtesy of Prof. Michael J. Sailor).

```
#pragma rtGlobals=1        // Use modern global access method.

Function waveforms()

    variable k1,k2,k3,k4,k5,k6,k7,k8,k9,k10,k11
    variable Amax1, Amax2,Amax3,Amax4,Amax5,Amax6,Amin
    variable A1,A2,A3,A4,A5,A6
    killwaves wave1, wave2,wave3, wave4,wave5,wave6,compwave
    Make/N=128000 wave1, wave2,wave3, wave4,wave5,wave6,compwave
    SetScale/I x 0,30*2*pi,"", wave1, wave2,wave3, wave4,wave5,wave6,compwave

    //Set frequency values
    k1 = 2.1
    k2 = 2.0
    k3 = 1.9
    k4 = 1.8
    k5 = 1.7
    k6 = 1.6

    //Set max and min amplitude values
    Amax1 =875
    Amax2 =875
    Amax3 =875
    Amax4 =875
    Amax5 =875
    Amax6 =875

    Amin = 50

    //Amplitude transform
    A1 = (Amax1 - Amin)/2
    A2 = (Amax2 - Amin)/2
    A3 = (Amax3 - Amin)/2
    A4 = (Amax4 - Amin)/2
    A5 = (Amax5 - Amin)/2
    A6 = (Amax6 - Amin)/2

    //Write each sine wave bound between Amin and Amax
    wave1 = A1*((sin(k1*x + 1/2*pi) + 1)) + Amin
    wave2 = A2*((sin(k2*x + 1/2*pi) + 1)) + Amin
    wave3 = A3*((sin(k3*x + 1/2*pi) + 1)) + Amin
    wave4 = A4*((sin(k4*x + 1/2*pi) + 1)) + Amin
    wave5 = A5*((sin(k5*x + 1/2*pi) + 1)) + Amin
    wave6 = A6*((sin(k6*x + 1/2*pi) + 1)) + Amin

    //compwave = (wave1 + wave2 + wave3 + wave4 + wave5 + wave6 )/6  //all peaks
    //compwave = (wave1 + wave3 + wave5 + wave6 )/4  //wave2 and wave4 deleted
    compwave = (wave1 + wave2 + wave4 + wave6 )/4  //wave3 and wave5 deleted

    Display compwave // create a graph of waves

    Save/G  compwave as "C:\New Rig Group Data\Shawn\SM9_99\wf_1049.txt"

End
```

Figure 2.3 IGOR code for writing multipeak, grayscale rugate waveforms. Note that ki, in this algorithm is not the same as k_i of Eq. 2.1 (the actual frequency in Hz). Instead, the k variable in this scripted algorithm is a frequency multiplier of the base frequency. Please see the discussion in section 2.3.2.

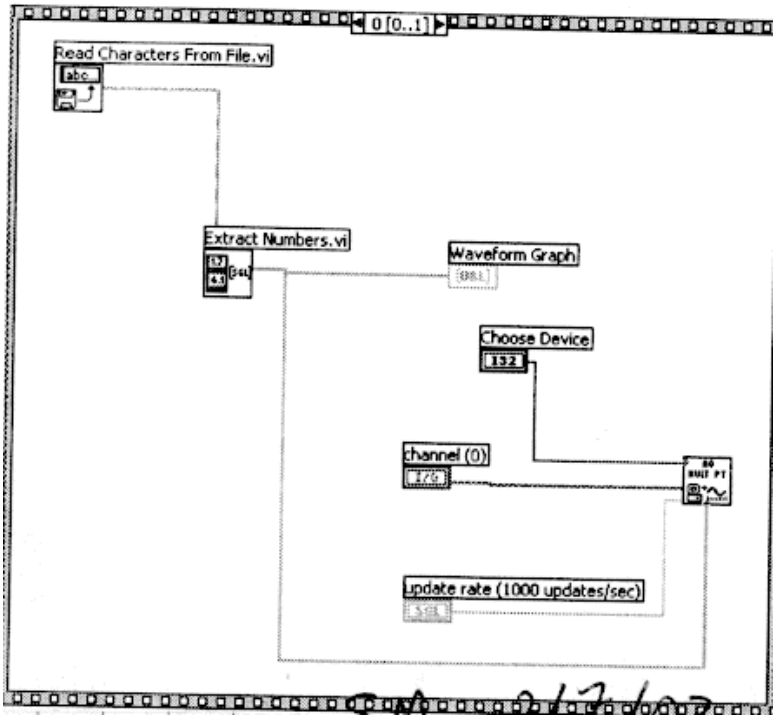

Figure 2.4 Etch system control software in LabView 6.0. Skeletal version showing only major components (VI's) needed to drive the etch rig.

Table 2.1 Bill of materials (BOM) for 2nd generation etch system.

2nd Generation etch system			
Item	**Description**	**Vendor**	**Part Number**
1	NI PCI-6024E Low-Cost Multi.I/O & NI-DAQ for Win2000/NT/Me/9x/MAC	National Instruments	PCI-6024E
2	R6868 Ribbon Cable, 1 m	National Instruments	182482-01
3	CB-68LP I/O Connector Block	National Instruments	CB-68LP
4	LabVIEW Base Package for Windows 2000/NT/XP/Me/98 (English)	National Instruments	776671-03
5	Model 363 Potentiostat/Galvanostat*	Princeton Instruments	363
6	Etch Cell	SIO machine shop	Custom
7	Platinum electrode	Alfa-Aesar	Custom

2.4 EXPERIMENTAL SECTION

2.4.1 General protocol for the preparation of porous silicon

P-type, B-doped, (100)-oriented silicon wafers, with resistivities between 0.5 – 1.2 mΩ*cm (Siltronix, inc.) were used in this study. Immediately before the electrochemical etch, the silicon chips were cleaned by rinsing with 1 M NaOH (aq). After assembly of the electrochemical cell (Fig. 2.5) an electrolyte solution composed of 48 % aqueous HF:ethanol (3:1 by volume) was added. See the study section for example waveforms. During the etch process, the solution was mixed with a pipet, ensuring that a single position was not held for more than a few seconds (Fig. 2.5). The mixing eliminates spots, or regions of electropolishing that form on the film when hydrogen gas bubbles build up on the surface and are not removed. Also, uniform mixing is important so that porosity gradients (of the x,y sample plane) do not form. Following etching, the cell was rinsed with ethanol, dried and the sample was removed from the cell. The sample was rinsed again with ethanol to remove any electrolyte that may have crashed out on the surface.

If desired, the porous silicon films can be lifted off of the surface of the silicon wafer by electropolishing.[5] In cases where this was necessary, films were lifted off by the following conditions: a solution of 48% HF:ethanol (1:14.5 by volume), a current density of ~ 4 mA/cm^2, at a duration of ~ 200 s.

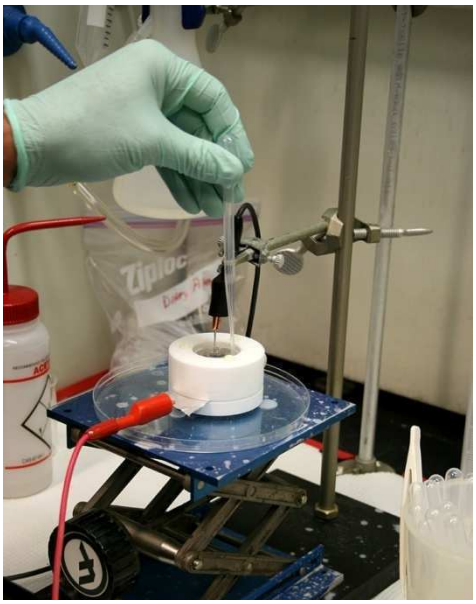

Figure 2.5 At high current densities, mixing is critical in maintaining uniform porosity across the surface of the porous silicon sample. Mixing can be achieved with a pipette, holding it in the manner shown, while continuously moving it across the surface - not holding the same position for more than a few seconds for the entire duration of the etch.

2.4.2 Multipeak, binary rugate encoding

As a demonstration of binary encoding, this study was designed to show the complete deletion of a peak, while holding the positions and heights of the remainder peaks constant. The presence or absence of a spectral peak, or bit, is recognized as an on state, 1, or an off state, 0, respectively. A waveform containing ten separate sine components was investigated by entering the following parameters into the equations 2.1, 2.2 and 2.3: the values of k_i (from Eq. 2.1) for each of the sine components were varied from 0.275 to 0.163 Hz, with a spacing of 0.0125 Hz between each sine component. The phase offset angle φ_i (from Eq. 2.1) was set to 3/2 π for all components. The maximum and minimum amplitude of the sine components 1-4 and 6-10 used in the waveform were 115 and 9 mA/cm^2, respectively.

2.4.3 Mulitpeak, grayscale rugate encoding

More than just binary information ("on" versus "off" states) can be incorporated in the reflection spectrum by varying the amplitudes of the sine components that correspond to the spectral peak heights. The number of combinations, or codes, in the spectrum is defined by the number of discernable peak intensities (i.e. gray levels, grays states, etc…) raised to the number of wavelength-resolved peaks, or bits, (# of codes = states ^ bits). To demonstrate intensity encoding, four waveforms were created and etched into samples (with three replicate samples per waveform). The amplitude of the sine component corresponding to one of the spectral peaks (A_5 in Eq. 2.1) was set at different values for each of the four samples (Table 2.2).

Table 2.2 Parameters used in Eq. 2.1 to generate four different levels for the height of peak five (peak at ca. 650 nm in Fig. 2.7). Listed for each target amplitude level are the maximum current amplitude, $A_{5,max}$, in units of amperes, for peak number five, and for the remainder peaks. The k_i values (from Eq. 2.1) for each of the sine components were varied from 0.275 to 0.163 Hz, with a spacing of 0.0125 Hz between each sine component. The phase offset angle ϕi (from Eq. 1) was set to 3/2 π for all components. The maximum and minimum amplitude of the sine components 1-4 and 6-10 used in the waveform were 115 and 9 mA/cm^2, respectively. The resistivity of the silicon wafers used was 1.45 mΩ cm.

Relative amplitude for peak # 5	$A_{5,max}$ (mA/cm^2)	$A_{1\text{-}4,6\text{-}10,\ max}$ (mA/cm^2)
4	146	111
3	115	115
2	93	118
1	57	121

2.4.4 Correcting the instrument response function, check bits and spectra of freestanding films

As seen in the results section, the heights of all the peaks (Figs. 2.7) of a reflection spectrum are not the same even though each of the sine component's amplitudes is the same. This results from the instrument response function of the CCD/spectrometer system. The effect can be counteracted in the design of the waveform by modulating the amplitudes of the individual sine waves (A_i in Eq. 2.1). Eleven sine components, y_i, were incorporated into this waveform to show that 10 ratiometric bits (defined by the distance of a given peak to the check bit) are possible. Additionally, the film was lifted off the substrate to show that the spectrum is not detrimentally affected by the electropolishing process.

2.4.5 Phase offset angle (Cosine waves)

After the above studies were completed, it was found that the phase offset angle, φi, of Equation 2.1, has a large impact on the spectral quality of the codes. In this study four waveforms were created, each with six sine components, varying in the values of the phase offset angle, φi, (Table 2.3). The values of k_i (from Eq. 2.1) for each of the sine components were varied from 0.288 to 0.213 Hz (400K pts, 1000pts/sec, 50 periods) with a spacing of 0.013 Hz between each sine component. The A_{max} and A_{min} of the all the sine components used in all the waveform was 157 and 9 mA/cm^2, respectively.

Table 2.3. When multiplied by π, the values listed in the table show the phase offest angles, φi of Equation 2.1, used in each waveform.

Peak	Wave 1	Wave 2	Wave 3	Wave 4
1	3/2	3/2	3/2	1/2
2	3/2	½	1/2	1/2
3	3/2	1	3/2	1/2
4	3/2	0	1/2	1/2
5	3/2	¾	3/2	1/2
6	3/2	5/4	1/2	1/2

2.5 RESULTS AND DISCUSSION

2.5.1 Multibit, binary rugate encoding

In figure 2.6 the spectral peaks are divided up into bins with the bit representation shown above each bin. The presence or absence of a spectral peak, or bit is recognized as an on state (1) or an off state (0), respectively. The top spectrum represents a sample with bit number 5 deleted, while the lower spectrum represents a sample with all ten bits in the "on" state. Using binary encoding the number of codes possible would be 2^10 or 1024 codes.

2.5.2 Multipeak, grayscale rugate encoding

The normalized intensity of the spectral peaks (Fig. 2.7) can be resolved (within three standard deviations) to four different amplitudes (Fig. 2.7). Therefore, the total possible number of codes demonstrated here are 4^{10}, or 1,048,576. Of course, one might point out that due to the instrument response function, not all the peaks can allow for the same number of intensity levels as do peaks 5 and 6. This question was the motivation for the next study.

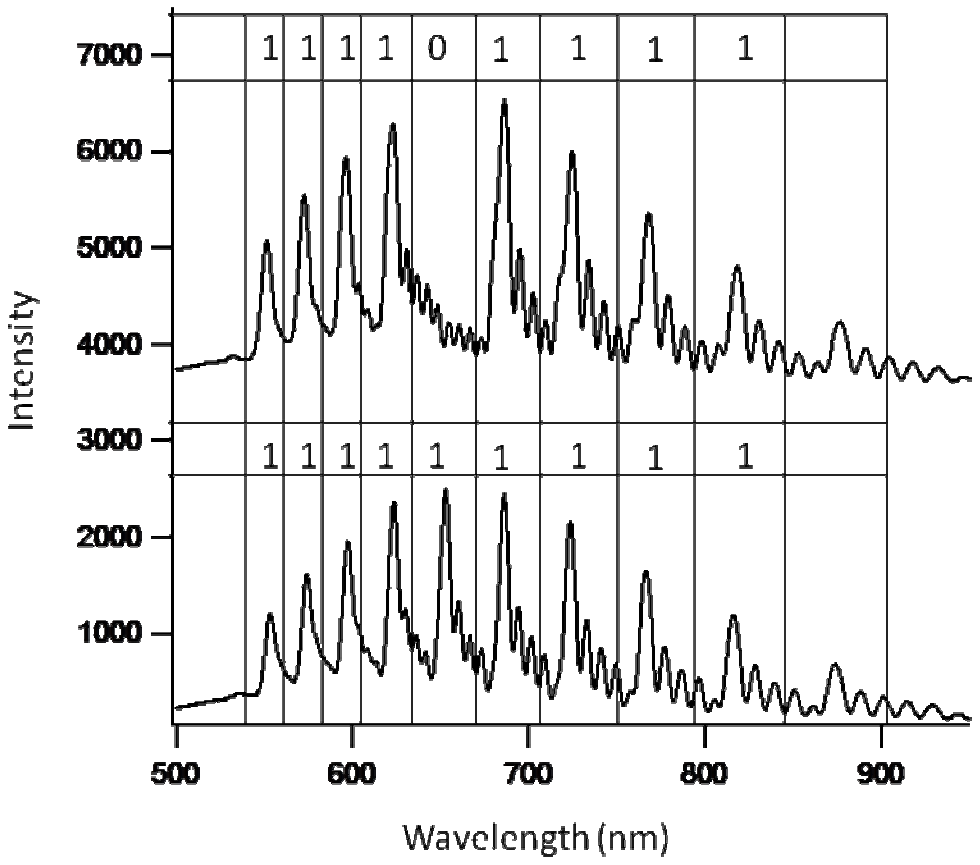

Figure 2.6 Reflectance spectra of two encoded porous silicon samples prepared according to the parameters provided in section 2.4.2, showing multibit, binary encoding. The spectra shown are divided up into bins, and the bit representation of each peak in the spectrum is superimposed over each bin. The presence or absence of a spectral peak, or bit, is recognized as an off state (0) or an on state (1), respectively. The bottom spectrum represents a sample with all ten bits in the "on" state; bit number 5 (counting from the blue end of the spectrum) is deleted in the sample represented by the upper spectrum.

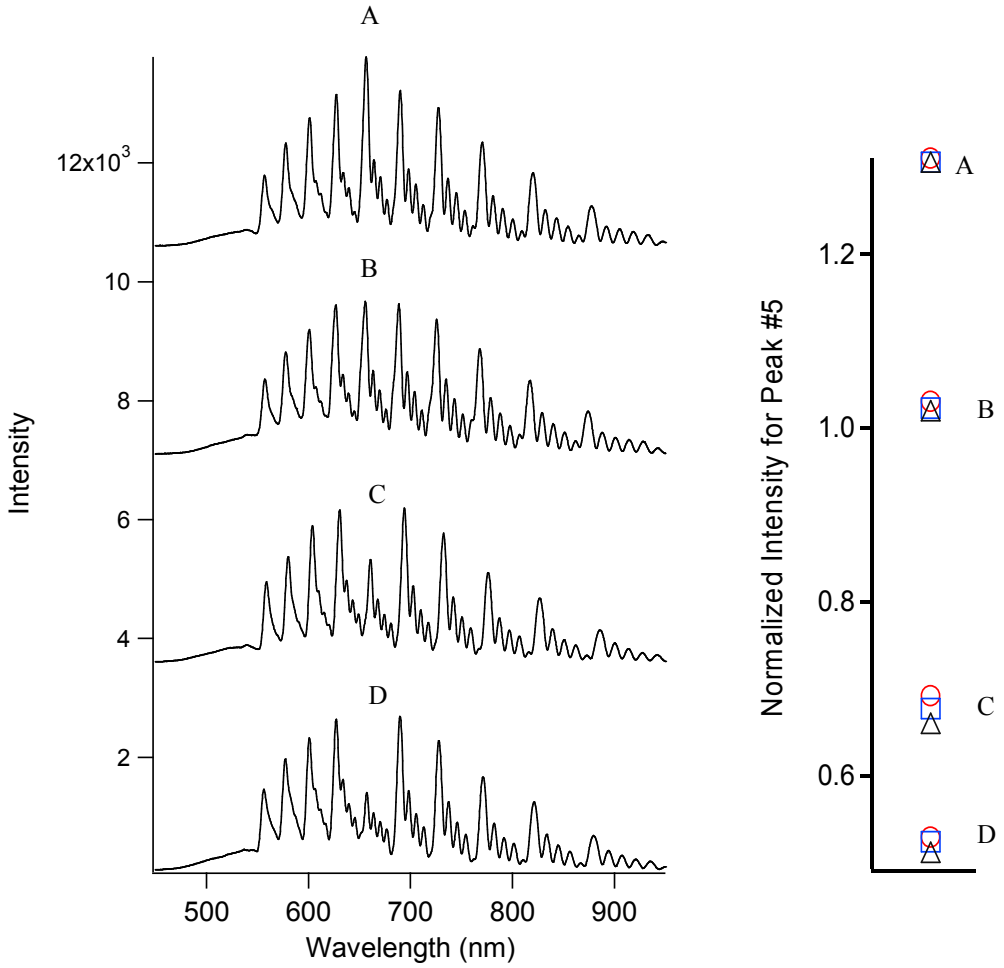

Figure 2.7 Demonstration of grayscale encoding. The left plot displays four spectra of porous Si samples prepared using the parameters displayed in Table 2.2, in which peak #5 in the spectrum (labeled, at approx. 650 nm) is varied over four discrete intensity values (A-D) relative to the rest of the spectral peaks. The plot at the right shows the normalized intensity of peak #5 (relative to peak #6) for each of the four sample types A-D, as indicated. Three replicate samples were prepared for each of the four waveforms. Four discrete gray levels, or four states per bit, are displayed.

2.5.3 Correcting for the instrument response function, check bits and the spectra freestanding films

Spectrum A of figure 2.8 shows that it's possible to encode at least eleven peaks, still allowing for 10 bits, if one peak is used as a check bit. In this case each bit would be defined not as the presence or absence of a spectral peak, but as the distance between the peak in question and the check bit. Spectrum A (Fig. 2.8) was acquired from the freestanding film of the same sample placed on glass, while spectrum B was acquired from the film-on-wafer sample. The absence of the large index break between porous silicon layer and the crystalline silicon layer allows for the reduction in ringing observed in spectrum A as compared to spectrum B.

2.5.4 Effect of varying the phase offset angle on spectral quality (cosine waves)

The effect of varying the phase offset angle from $3/2\pi$ to $1/2\pi$ (Cosine), on the spectral quality is dramatic (Fig 2.9). The major effects were an increase in peak to valley ratio and the removal of the interference peak seen between 810 and 815 nm in the spectra of samples etched with wave 1 and 3.

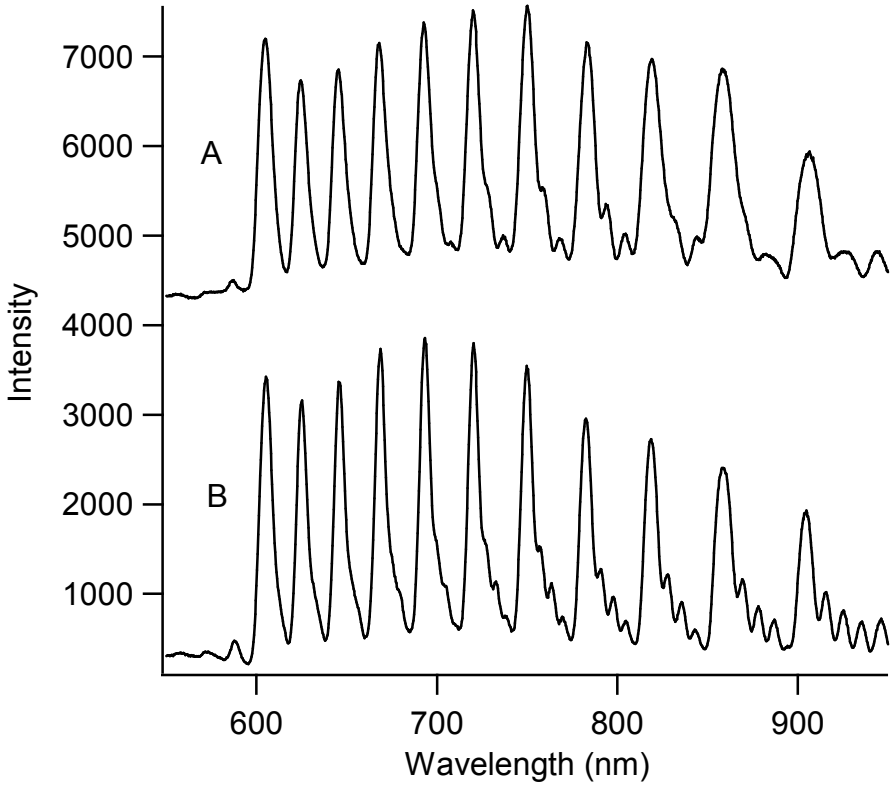

Figure 2.8 (A) Reflection spectrum of the film after liftoff, encoded with eleven peaks. This demonstrated that even 10 ratiometric bits are possible, while using one peak as a check bit. (B) Reflection spectrum of film still attached to wafer. This figure also demonstrates that the peak heights can be artificially increased to counter the instrument response function.

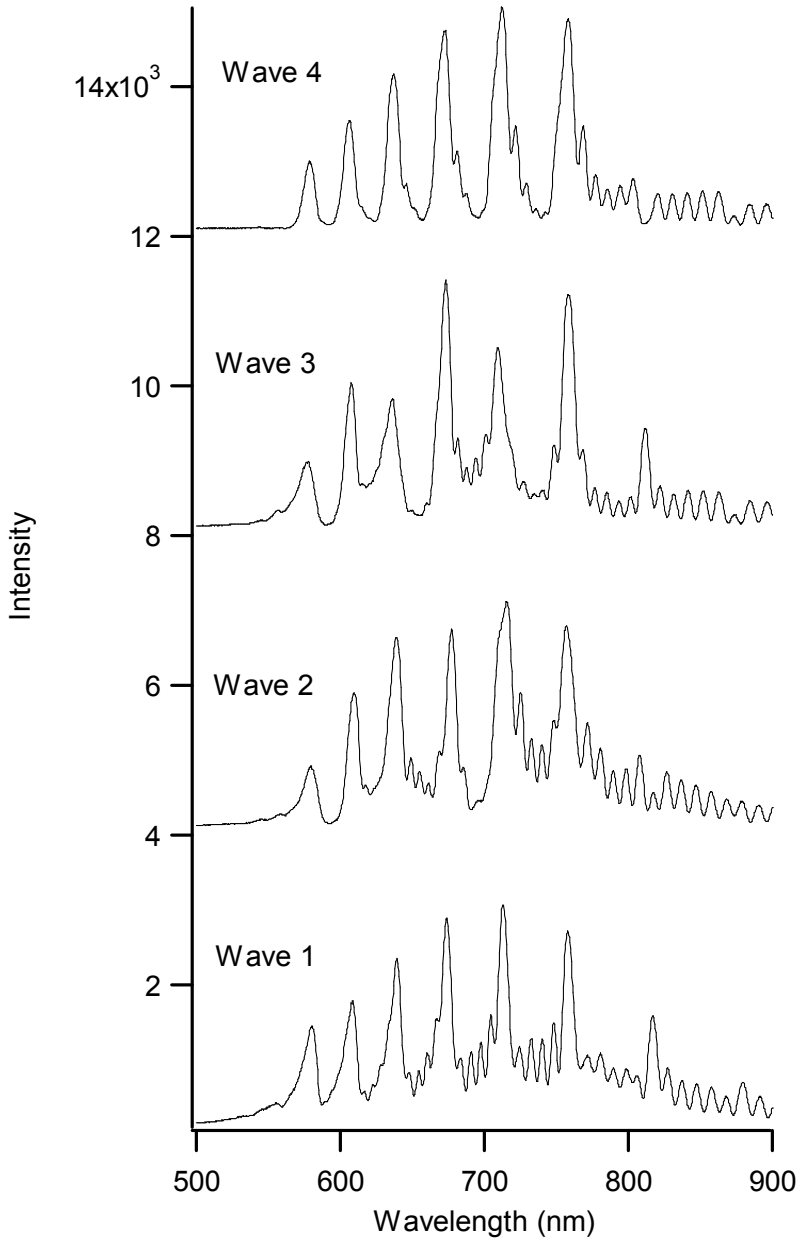

Figure 2.9 The reflection spectra of the four waveforms where the phase offset angle was varied from one code to the next (values listed in Table 2.3).

2.6 BUILDING A CODE LIBRARY

2.6.1 Objectives

The objective this protocol is to create a library of encoded porous silicon (film-on-chip) samples. The library consists of three, binary codes: one containing six peaks (111111) and the other two containing four peaks that have the 2nd and 4th peaks deleted (101011) and 3rd and 5th peaks deleted (110101), respectively. The target spectral position of the 1st peak (located at the shorter wavelength end of the spectrum) was 630 +/- 10 nm, while the target position of the 6th peak was approximately 800 nm.

2.6.2 Background

To create a library of encoded porous silicon samples, the wafer must first be calibrated before accurately encoded samples can be made. Calibration of the wafer makes up for spectral variation resulting from differences in resisitivity from one wafer to the next. The calibration process consists of a series of etches that are carried out on one chip from the wafer by varying the $A_{i,max}$ (Eq. 2.1; set to the same value for all i sine components; now be referred to as A_{max}) until the target wavelength is hit or at least three data points have been acquired. In general, an increase in amplitude of the waveform, will red shift the peaks and a decrease in amplitude will blue shift the peaks. Decreasing the frequency, k_i (Equation 2.1), will also red shift the peaks and increasing the frequency will cause a blue shift. However, calibrating the peak position by k (Eq. 2.1) is less effective, because the linear adjustment range is smaller. Once at least three data points have been acquired (where the 1st peak of one of the samples is bracketed within the

dataset) then a plot of A_{max} versus reciprocal wavelength of the 1st peak's position can be made. A linear equation fitted to the data set of this plot can then be used to predict the A_{max} value needed.

2.6.3 Wafer calibration

Wafers used in this section met the parameters listed in section 2.4. First a composite waveform was written having the parameters listed in the scripted IGOR file shown in Fig 2.3. The etch process protocol outlined in section 2.4.1 was followed. The spectrum of the sample was acquired using a USB 4000 CCD/Spectrometer (Ocean Optics). Three more consecutive etches, increasing at increments of 4 mA/cm^2 for A_{max} (of IGOR script), were run before the target was hit. It should be noted that in the IGOR program, Amax is current, not current density. The area of the sample used was 5.72 cm^2, so the actual increase in the IGOR parameter Amax would be 25 mA. Since the third and fourth etch were so close to the target peak position, a calibration plot was not necessary. However, for description purposes one is shown (Fig. 2.10c). The table below (Fig. 2.10b) shows the extracted peak positions of the 1st peak of each spectrum (Fig. 2.10a).

(1)

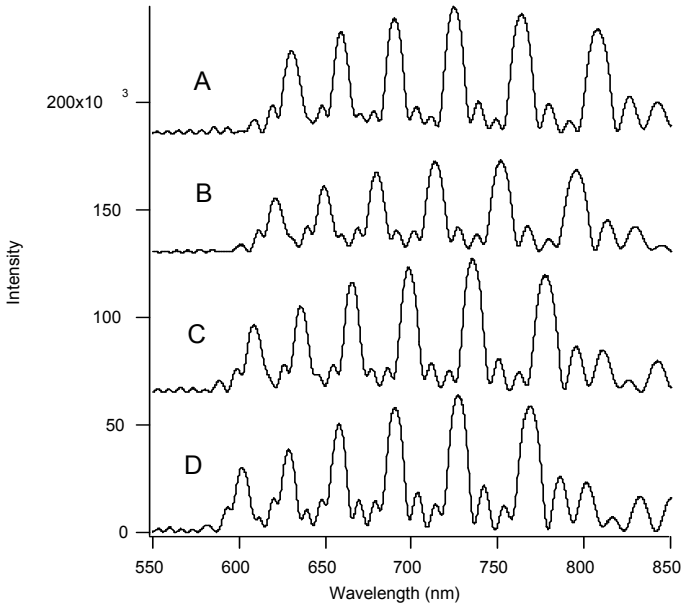

(2)

Spectra	Amax	Wavelength (nm)
A	875	630
B	850	621
C	825	608
D	800	602

(3)

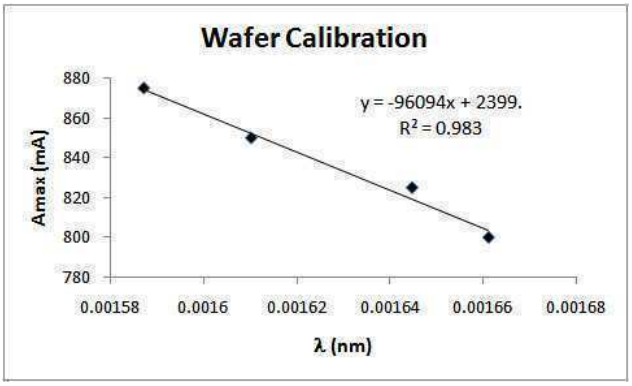

Figure 2.10 Wafer calibration using the parameter A_{max}. (1) Spectra of four samples each etched with different A_{max} values. (2) Table of A_{max} values and measured wavelengths of peak 1. (3) Plot of extracted position for peak 1 versus reciprocal wavelength. The A_{max} value was held constant for all peaks. The linear equation fitted to the data can be used to predict desired peak placement.

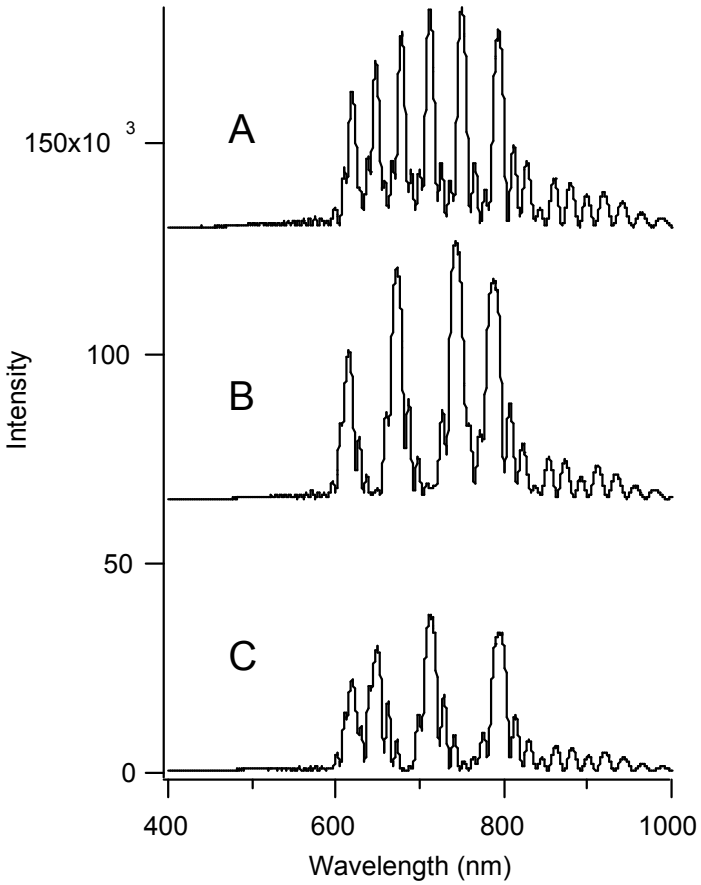

Figure 2.11 Reflection spectra of the three codes that compose the spectral library. Spectrum A has all six peaks present. Spectra B and C have peaks 2 and 4 deleted and 3 and 5 deleted, respectively. All samples are film-on-wafer samples, which causes the spectral ringing, or side lobes.

2.6.3 Building the rest of the library

After the target peak position for the 1st peak of 111111 was reached the rest of the code library was made. For reasons discussed in chapter 4, the micrfabrication process requires that all samples have flat surfaces. Reused samples have a recess from the previous liftoffs. So a replicate waveform of code 111111 was made along with the other two codes, 101011 and 110101 using new chips. The waveforms of the codes 101011 and 110101 were generated by deleting the y_2 and y_4 sine components and the y_3 and y_5 sine components, respectively. For both 101011 and 110101, n = 4 (Eq. 2.3) instead of n = 6. The spectra of all the samples met the peak position criteria needed for the downstream experiments described in the following chapters (Fig. 2.11).

2.7 CHAPTER SUMMARY

A method used to prepare photonically encoded porous silicon exhibiting multibit, grayscale codes has been demonstrated. Considering four states per bit and ten-ratiometric bits per particle, this method has the capability to create encoded libraries of over one million different codes. Porous silicon photonic crystals can be constructed that display spectral peaks spanning the visible, near infrared, and infrared region of the spectrum, allowing the possibility of a much larger number of codes than demonstrated in the present work. This work demonstrates the first example of a single material that can be used to construct an encoded library covering such a broad wavelength range. Finally, a computer controlled etch rig was developed and used to carry out the experiments discussed in this work.

2.8 REFERENCES

1. Bovard, B.G., *Rugate filter theory: an overview.* Appl. Optics, 1993. **32**(28): p. 5427-5442.
2. Berger, M. G., Arens-Fischer, R., Thoenissen, M., Krueger, M., Billat, S. Lueth, H., Hilbrich, S., Theiss, W., Grosse, P., *Dielectric filters made of porous silicon: advanced performance by oxidation and new layer structures.* Thin Sol. Films, 1997. **297**(1-2): p. 237-240.
3. Sailor, M.J. and S. Meade, *United States Patent 20070051815: Optically encoded particles with grey scale spectra* United States.
4. Meade, S.O., Yoon, M.S., Ahn, K.H., Sailor, M.J. , *Porous silicon photonic crystals as encoded microcarriers.* Adv. Mater., 2004. **16**(20): p. 1811-1814.
5. Lehmann, V., *Electrochemistry of Silicon*. 2002, Weinheim, Germany: Wiley-VCH. 51-75.

CHAPTER 3

Instrumentation and Methods for Decoding and Assay Readout

3.1 ABSTRACT

This chapter describes the development of instrumentation and methods for high-throughput decoding and assay readout of spectrally encoded photonic crystal particles. The system is comprised of a fluorescence microscope modified for high resolution spectral imaging. Assay readout requires the detection of fluorescence labeled targets (see chapter 5) and is accomplished through the use of standard fluorescence microscopy. However, accurate decoding of the particle's spectral identity requires that the fluorescence microscope be modified for high resolution spectral imaging. This was accomplished by coupling a computer controlled monochrometer to the microscope. In addition to instrument development, this chapter covers the decoding method, which identifies codes based on the number of spectral peaks present, the distance between neighbor peaks and thresholds of the peak intensities. Data acquired and processed using the instrumentation and methods introduced in this chapter will be presented in the following chapters.

3.2 INTRODUCTION

The project goal, addressed in this chapter, was to develop a system capable of decoding the spectral code and fluorescence signal of many particles, in a high-throughput manner. The method of readout involves the assembly of particles onto a flat surface after the hybridization and rinsing steps introduced in chapter 1 (Fig. 1) have been completed. This is also similar to the BeadArrayTM [1-3] approach discussed in chapter 1 as well, except that there are no defined areas where the particles are intended to assemble. Assembly onto a flat surface opened the door to using a modified fluorescence microscope as the reader. In fact, the first attempt at decoding the particles in a high throughput manner used only components that come standard with a fluorescence microscope. The method, coined "bandpass decoding," along with a proof of principle experiment are presented and discussed in detail in appendix B. In short, band pass filter decoding was not chosen because it required that the spectral peaks be accurately placed in order to identify the code. Currently such accuracy is difficult achieve due to the variability of the encoding process. However, in a controlled manufacturing setting variability could be reduced. To get around the problem of accurate peak placement, a method based on a peak's position relative to a check bit (another peak present in the spectrum) is easier to implement. However, knowing a spectral peak's position with respect to one of its neighbors requires a high resolution spectral scan of the photonic crystal particle's spectrum. This type of measurement is easily acquired using a CCD/spectrometer like the one used in chapter 1. However, such instruments only collect data one spot at a time. Therefore, if more than one particle is present in the spectral acquisition spot, then multiple codes will be readout in one channel, making it extremely difficult to separate out all the codes present, while

determining which particle types exhibit the fluorescence signal of a hit. What was needed was a system that could separately readout the spectral code and fluorescence signal of many objects in parallel. The latter requirement is easy to achieve with a fluorescence microscope. However, the former requirement calls for a system capable of classifying the spectral characteristics of multiple objects within the field of view of a digital imager. [4] Systems designed to readout both the fluorescence signal and spectral code of many encoded particles assembled onto a flat surface within the field of a digital imager have been constructed and demonstrated previously. [5, 6]

3.3 INSTRUMENTATION

Both decoding and assay readout were performed with one instrument, consisting of a Nikon LV-150 fluorescence microscope coupled with a computer controlled SpectraPro 275 monochrometer (Princeton-Acton). The system is shown in figure 3.1. Assay results were readout in upright, fluorescence mode while decoding was accomplished in hyperspectral mode – both are described below (Fig. 3.2). The system uses two light sources, a 100W mercury source for fluorescence (# 2, in Fig. 3.1 and 3.2) and a 100W halogen source for the monochrometer (#4, Fig 3.1 and 3.2). An IR/heat filter (not shown in diagram) rests between the monochrometer (#3 Fig. 3.1 and 3.2) and halogen source (#4 Fig. 3.1 and 3.2). Both sources interface to the scope body, through the same c-mount opening via a t-mount adapter that contains an adjustable diverter mirror (#8, Fig. 3.1 and 3.2) to switch between sources. In fluorescence mode standard filter cubes, containing the desired dichroic, and excitation and emission filters (#5, 7, and 6, respectively in figure 3.2), are placed in the optical path. In figure 3.1 the arrow pointing from the set of labels 5, 6, 7 and 11 indicates the general area where the filter wheel is located. In spectral mode a filter cube containing a 50/50 mirror (#11 Fig. 3.2) is placed in the optical path. The detector is a CoolSnap HQ2 (Photometrics) 14 bit, monochromatic camera (#1 Fig 3.1 and 3.2). Metamorph software (Molecular Devices) is used to create an automated routine to run both the camera and monochrometer in synchronization generating the spectral image stacks. The software is written as a Metamorph "Journal" in which commands (specified in the SpectraPro 275 manual) are strung together and sent to the monochrometer through a serial port connection. The actual connection is made between the serial port of the computer and an external control

device (the device with the small keyboard on it, to the left of the microscope - Fig. 3.1) which in turn is connected to the monochrometer. In summary, this system allows for fluorescence images to be registered to the spectral image stack, so that the reflection spectrum of the object can be compared to its fluorescence value on a pixel by pixel basis. This will be demonstrated in chapter 6.

1	CCD	7	Excitation filter
2	Mercury source	8	Mirror from T-mount adapter
3	Monochrometer	11	50/50 mirror
4	Halogen source		
5	Dichroic		
6	Emission filter		

Figure 3.1 Imaging system with critical components numbered in red.

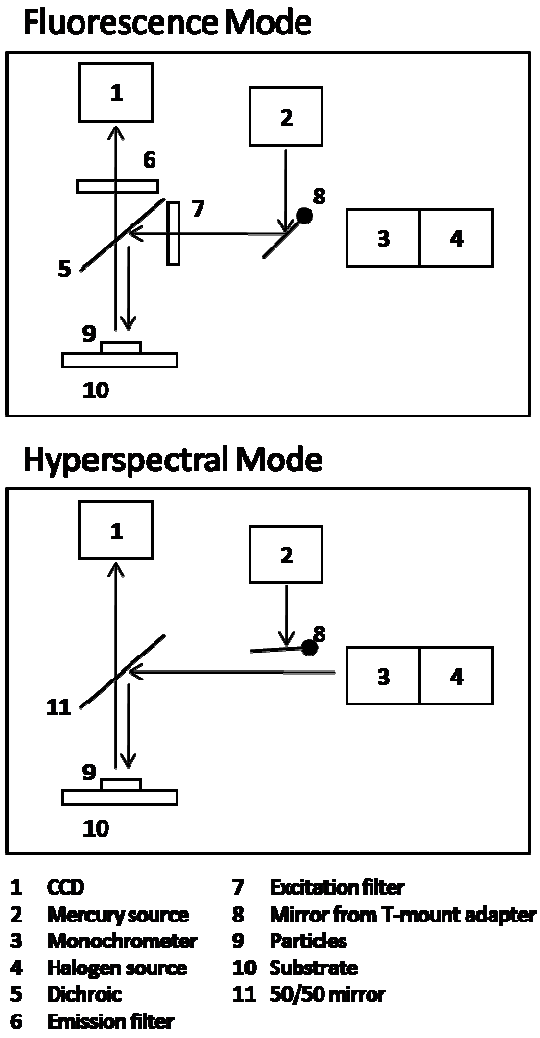

Figure 3.2 Block diagram of imaging system in both (a) fluorescence and (b) spectral modes.

3.4 DECODING AND ASSAY READOUT PROCESS

3.4.1 Data acquisition

First, a fluorescence image is acquired (Fig. 3.3) of the dry assembled particle array (Fig 1). More than one fluorescence channel can be used depending on the number of dyes used in the assay. Then the imaging system is put in spectral mode (Fig. 3.1) and a sequence of images is acquired while scanning over the desired spectral range. This results in a spectral image stack, where each pixel contains the entire reflection spectrum of the object that it corresponds to (Fig 3.3). For specifics on instrument settings, such as the magnification of the objective, exposure times, filters used, etc…, please see the following chapters where data is presented.

3.4.2 Data analysis

The fluorescence image(s) (Fig 3.3) and spectral image stack (Fig. 3.3) are read into a decoding program and for every pixel it executes the following commands: (1) Find the position and intensity of each peak of the reflection spectrum. (2) Calculate the distance between each peak. (3) Compare the relative peak distances and peak intensities to a set of predetermined values assigned to a particular code. If the pixel meets the criteria for a particular code then it is identified as that code. If the pixel does not meet any codes predetermined criteria, then the pixel is termed invalid and thrown out of the experiment. Finally, a list is comprised that contains each pixel's photonic code and corresponding fluorescence value(s), or assay result (Fig 3.3). For a detailed description of the algorithm please see figures 3.4.1 and 3.4.2, which display the Matlab script and associated comments.

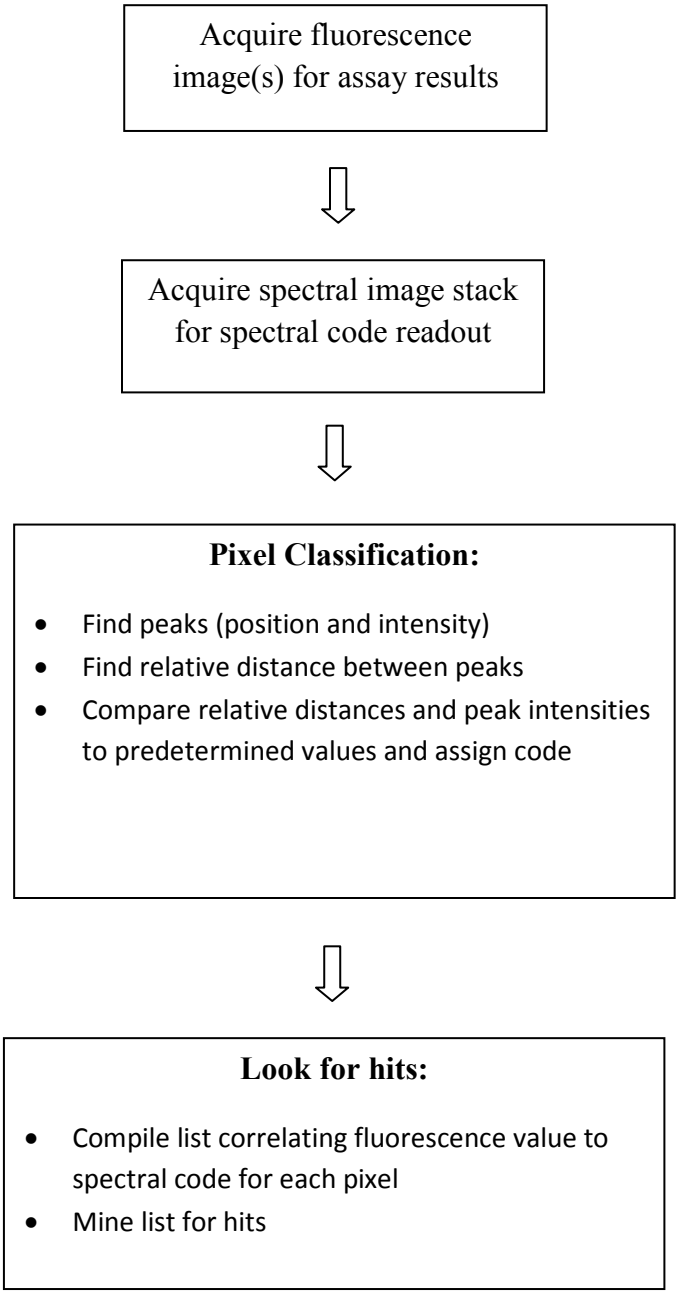

Figure 3.3 Overview of decoding and assay readout process.

```
%Decode 9
% Shawn Meade and Michelle Chen
% 10/14/07

%In general, this program extracts the spectrum and assigns a corresponding code to each pixel in a hyperspectral data set (image %stack). The program then compares the decoding result of that pixel to the its corresponding value from an image(s) taken in the %fluorescence channel.

%The program is arbitrarily broken up into 8 modules.  Module 1 reads the image stack, stored in the working directory and %creates "data."  The user can define a cropped area of the original image frame.  Module 2, for visual display purposes only, %plots out a composite image of the "data" where the maximum value of the spectrum of each hyperspectral pixel is displayed as a %color of a heat map.  Module 2 also plots out a spectrum of a selected pixel and plots the cropped regions of the image(s) taken %in the fluorescence channels. Note: the fluorescence images (AF555 and AF680 in this case) need to be imported into the %workspace before execution of the m file. Module 3 runs a peak finding routine, using a function called "lmax.m" on each pixel. %See documentation of lmax for def. of "filt."  The output of module 3 are the cell arrays Max and Ind.  Each element of Max %contains the intensity and each element of Ind contains the index of each peak, found in each hyperspectral pixel.  Module 4 %finds the distance between each peak using a function called Relative distance storing it in "reldispeak."  Module 5 is the code %recognition portion of the program. In it reldispeak is and Max are scanned and compared against predetermined values of peak %separation and intensity thresholds assigned to each code. From thesis criteria, the classes of 111111, 101011, 110101, or %invalid are assigned.  Module 6 is a collection of analysis and display functions.


%Module 1: Read image stack in working directory.
wl_ind = 1001:1:1326; %create the spectral axis vector, wl.
base = 'SCAN_10xB2FC15ms_';

for k = 1:length(wl_ind)
    fn = [base, num2str(wl_ind(k))];
    x = imread(fn, 'tif');
    x2 = imcrop(x,[20 20 480 480]);  %Cropped region
    data(:, :, k) = x2;
end


%Module 2: Plot composite max image, sample spectrum and cropped
%fluorescence images
wl=400:1:725;[mx, ind] = max(data, [], 3);
figure;imagesc(wl(ind));colorbar

%Plot spectrum
spectrum = squeeze(data(10,35,:));    %(row,col), not (x,y)
figure;plot(wl,spectrum)
xlabel('Wavelength(nm)')
ylabel('Intensity')
title('Spectrum of pixel 10,35 of crop [20 20 480 480]')


%Plot fluorescence image 1
AF555Crop = imcrop(AF555,[20 20 480 480]);
AF555Crop = double(AF555Crop);
figure;imagesc(AF555Crop);
title('AF555')


%Plot fluorescence image 2
AF680Crop = imcrop(AF680,[20 20 480 480]);
AF680Crop = double(AF680Crop);
figure;imagesc(AF680Crop);
title('AF680')


%Module 3: Run peak finding algorithm on every hyperspectral pixel in
%"data"

filt = 60;    %Set number of averages to be used in "lmax"
x = 480;    %Set x,y to dimensions of image
y = 480;

Max = cell(x,y);    %Set dimensions of Max to match image dimensions
Ind = cell(x,y);    %Set dimensions of Ind to match image dimensions
Decode = ones(x,y);  %Set dimensions of Decode to match image dimensions,
                %Decode displays each class of decoded pixel as a
                %    false color

for i = 1:x;
   for j = 1:y;
      spectra = squeeze(data(i,j,:));  %Extract spectrum from data for
                                %the i,jth pixel
      spectra2 = double(spectra);     %must convert to double integer
                                %for lmax to work
      [lmval,indd]=lmax(spectra2,filt);  %peak finding algorithm
      Max(i,j) = {lmval};
      Ind(i,j) = {indd};

   end
end
```

Figure 3.4.1 First page of Matlab decoding program

```
%Module 4: find distances between peaks

relPeakDis=RelativeDistance(Ind);


%Module 5: Code recognition algorithm

invalid = [];
code_111111 = [];
code_101011 = [];
code_110101 = [];
code_111111_AF555 =[];
code_111111_AF680 =[];
code_101011_AF555 =[];
code_101011_AF680 =[];
code_110101_AF555 =[];
code_110101_AF680 =[];
code =[];

for i = 1:x;
   for j = 1:y;
      rb = relPeakDis{i,j}; %rb = ratiometric bit
      bi = Max{i,j};  %bi = bit intensity
      numPeaks = size(rb);
      numRB = numPeaks (2);
      if (numRB ~= 3 & numRB ~= 5)
         invalid = [invalid;i,j];
         Decode(i,j) = 1;
      elseif numRB == 3
         if(21 <= rb(1) & rb(1) <= 27 & 52 <= rb(2) & rb(2)<= 58 & 63<= rb(3) & rb(3)<=72)
            if(1500 <= bi(1) & 1500 <= bi(2) & 1500 <= bi(3))
               code_110101 = [code_110101; i,j,AF555Crop(i,j),AF680Crop(i,j)];
               code_110101_AF555 = [code_110101_AF555; AF555Crop(i,j)];
               code_110101_AF680 = [code_110101_AF680; AF680Crop(i,j)];
               code = [code; AF555Crop(i,j),AF680Crop(i,j),110101];
               Decode(i,j) = 4;
            else
               invalid = [invalid;i,j];
               Decode(i,j) = 1;
            end
         elseif( 45 <= rb(1) & rb(1) <= 55 & 55 <= rb(2) & rb(2)<= 65 & 33 <= rb(3) & rb(3)<=40)
            if(1500 <= bi(1) & 1500 <= bi(2) & 1500 <= bi(3))
               code_101011 = [code_101011; i,j,AF555Crop(i,j),AF680Crop(i,j)];
               code_101011_AF555 = [code_101011_AF555; AF555Crop(i,j)];
               code_101011_AF680 = [code_101011_AF680; AF680Crop(i,j)];
               code = [code; AF555Crop(i,j),AF680Crop(i,j),101011];
               Decode(i,j) = 3;
             else
               invalid = [invalid;i,j];
               Decode(i,j) = 1;
            end
         else
            invalid = [invalid;i,j];
            Decode(i,j) = 1;
         end
      elseif(20 <= rb(1) & rb(1) <= 28 & 23 <= rb(2) & rb(2)<= 30 & 28 <= rb(3) & rb(3)<=32 & 29 <= rb(4) & rb(4) <= 35 & 33… …<= rb(5) & rb(5)<= 41)
         if(1200 <= bi(1) & 1200 <= bi(2) & 1200 <= bi(3)& 1200 <= bi(4)& 1200 <= bi(5) & 1000 <= bi(6))
            code_111111 = [code_111111; i,j,AF555Crop(i,j),AF680Crop(i,j)];
            code_111111_AF555 = [code_111111_AF555; AF555Crop(i,j)];
            code_111111_AF680 = [code_111111_AF680; AF680Crop(i,j)];
            code = [code; AF555Crop(i,j),AF680Crop(i,j),111111];
            Decode(i,j)= 2;
         else
            invalid = [invalid;i,j];
            Decode(i,j) = 1;
         end
      else
         invalid = [invalid;i,j];
         Decode(i,j) = 1;
      end
   end
end

%Module 6: Scatter plot
figure;gscatter(code(:,1),code(:,2),code(:,3),'rkg','xos');
xlabel('AF555')
ylabel('AF680')
title('SM9-99 Vial 4; Array1; Decode 1 of crop [20 20 480 480]')
```

Figure 3.4.2 Second page of Matlab decoding program

3.4.3 Room for improvement

As will be demonstrated in the following chapters, the system outlined above worked very well for proof of principle experiments. However, there is room for improvement. For example, the current algorithm processes every pixel in the image, regardless of whether it corresponds to a particle, resulting in a very slow execution. To get around this problem, a white light image of all the particles could be acquired and an object recognition algorithm could designate only the pixels corresponding to particles for decoding. This step would also allow for individual particle statics. Additionally, the algorithm does not allow for an estimated miscall rate. In this work, we will present empirical evidence for decoding accuracy by comparison to an independent method (Chapter 6). An example of an error checking procedure for a decoding process, run on a commercial multiplexing platform, is outlined in the work by Gunderson and Krugliak et al.[1] However, even this advanced signal processing procedure only determines an estimation of the miscall rate - not an actual error rate.

3.5 CHAPTER SUMMARY

Instrumentation and methods for high-throughput decoding and assay readout of spectrally encoded photonic crystal particles have been developed. The system described is comprised of a fluorescence microscope modified for high resolution spectral imaging. The decoding method that was developed identifies the photonic codes based on the number of peaks present, the relative distances between neighbors and thresholds of peak intensity. Data acquired and processed using the instrumentation and methods introduced in this chapter will be presented and discussed in the following chapters.

3.6 ACKNOWLEDGMENTS

Chapter 3, in part is a reprint of the material as it will appear upon submission of the manuscript in progress: Meade, S.O., Chen, M., Sailor, M.J. “A bioassay multiplexing system utilizing porous silica photonic crystal particles containing spectral barcodes” (2008).

3.7 REFEERENCES

1. Gunderson, K.L., et al., *Decoding randomly ordered DNA arrays.* Genome Research, 2004. **14**(5): p. 870-877.

2. Ferguson, J.A., F.J. Steemers, and D.R. Walt, *High-Density Fiber-Optic DNA Random Microsphere Array.* Analytical Chemistry, 2000. **72**(22): p. 5618-5624.

3. *http://www.Illumina.com.*

4. Dickinson, M.E., et al., *Multi-Spectral Imaging and Linear Unmixing Add a Whole New Dimension to Laser Scanning Fluorescence Microscopy.* BioTechniques, 2001. **31**(6): p. 1272-1278.

5. Empedocles, S.A. and A.R. Watson, *Two-Dimensional Spectral Imaging System*. 2004, Quantum Dot Corporation: United States.

6. Cunin, F., et al., *Biomolecular screening with encoded porous silicon photonic crystals.* Nature Mater., 2002. **1**: p. 39-41.

CHAPTER 4

Microfabrication of encoded porous silica particles

4.1 ABSTRACT

This chapter introduces a method for the microfabrication of freestanding encoded porous silica particles. The method utilizes photolithography and plasma etching to define the particle dimensions in the x- and y- coordinates of a premade encoded porous silicon film. Following microfabrication and liftoff, the freestanding encoded porous silicon particles are then thermally oxidized to porous silica. Oxidation does have an effect on the spectral codes, but it is predictable and can therefore be factored into the encoding process. Once fully oxidized, the encoded porous silica particles are ready for the probe immobilization and assay processes discussed in the next chapter.

4.2 INTRODUCTION

4.2.1 Requirements for encoded particles in multiplexing systems

Multiplexing systems based on encoded particles require particles that are microscale in dimension, uniform in size and able to be encoded with spectral information. Dimensions on the order of a few to tens of microns are important because more particles, and thus more particle types, can be mixed with the patient sample. This in turn allows for higher levels of multiplexing. Assuming uniform immobilization chemistry, uniform size distribution allows for similar numbers of probes per particle, which in turn reduces the noise of the assay. For multiplexing systems that use flow cytometry[1] (read out the particle as one data point) a uniform number of probes per particle and therefore uniform size, is critically important. However, in our system this is not necessarily the case, as will be demonstrated in the next chapter. Finally, high quality and uniform spectra (similar to the results presented in chapter 2) are important because they allow for easier decoding.

4.2.2 Prior methods

Several methods for making microscale encoded porous silicon particles preceded this work. The most widely used method in our own research group is the fractionation of freestanding porous silicon films using ultrasonication.[2, 3] The results of the cited works show that it's possible to create batches of particles with high quality spectral characteristics. However, the size distribution for this method is quite high. Typically the size of particles, made by fractionation, range from hundreds of microns all the way

down to submicron dimensions. It is true that size exclusion filtering methods can reduce size variability. Yet, as with most size exclusion filtering methods on non-uniform populations, increasing the uniformity decreases the yield. Another method used to make microscale encoded porous silicon particles entails photopatterning before porous silicon formation.[2] This method can produce particles uniform in size. However, not all of an individual particle is spectrally uniform within its x- and y-dimensions. This is due to the isotropic nature of the formation of porous silicon when p-type wafers are used.[4] The dry removal soft lithography method developed by Burrato and coworkers [5] was tried but we were unable to reproduce the effect on our encoded films. Additionally, a novel method for the fabrication of microscale photonic crystal particles, utilizing microdroplets of polymer solution to replicate encoded photonic structures, was considered.[6] The method can produce microscale particles. However, the method was not chosen due to the fact that the size distribution is inherently large. Additionally, and most important, no spectral data was acquired from freestanding replicate particles. A method based on the microdroplet method discussed above, called bead patterning, was devised and investigated as an alternative to microfabricating the porous silicon. However, we were unable to obtain reflection spectra from freestanding particles made by the method. This work can be reviewed in appendix D and a recent publication.[7]

4.2.3 Overview of photopatterning after porous silicon formation

The situation described above led us to develop a method, after the work of Arens-Fischer et al. that utilized photolithography and plasma etching to define the

dimensions in the x- and y- coordinates of an existing encoded porous silicon film.[8] As discussed in the last chapter and in a previous publication, the z-coordinate contains the encoding information, defined using a current-time waveform during the electrochemical etch.[9] Figure 4.1 summarizes the process. First, an aluminum layer is sputter coated onto the surface of the porous silicon (Fig 4.1, step 1). The aluminum acts as a capping/release layer for the photoresist. In step 2, the substrate (Fig. 4.1b) is spin-coated with photoresist (Fig. 4.1c). Steps 3, 4 and 5 involve the exposure, post exposure bake and development of the resist (Fig. 4.1d). In step 6, the unprotected regions of the substrate are then removed all the way down to the crystalline silicon by plasma etching (Fig. 4.1e). In step 7 the substrate is immersed in a dilute solution of hydrofluoric acid, dissolving the aluminum and removing the photoresist mask features (Fig. 4.1f). Next, in step 8, the microfabricated porous silicon features are lifted off of the silicon substrate by electropolishing (Fig. 4.1g). Finally, in step 9, the freestanding particles are thermally oxidized to form porous silica (Fig. 4.1h).

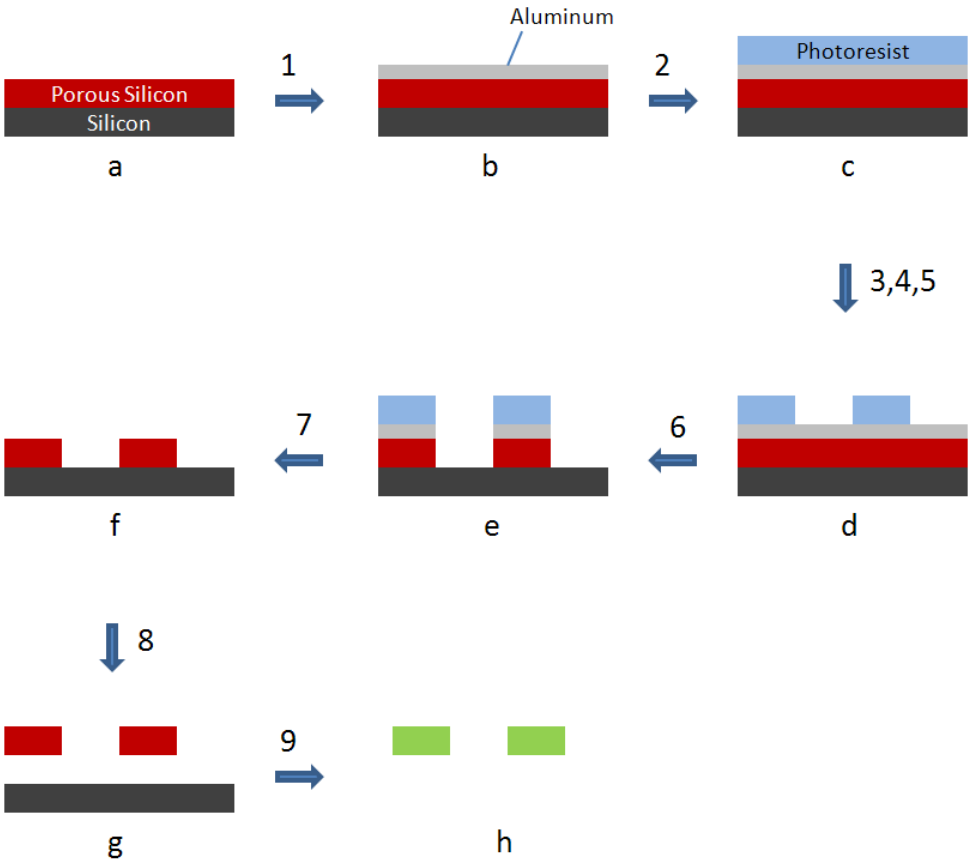

Figure 4.1 Summary of the procedure used to prepare mircoparticles from a spectrally encoded porous silicon film: (1) aluminum deposition; (2) pretreatment and resist application; (3) exposure, (4) post exposure bake (5) photoresist development; (6) plasma etch; (7) dissolution of aluminum and liftoff of photoresist mask features; (8) particle isolation by electropolishing liftoff; and (9) thermal oxidation of the porous silicon to form porous silica. The change in color represents the blue shift that occurs in the particle's reflection spectrum.

4.3 EXPERIMENTAL SECTION

Step 1: Aluminum deposition

A Discovery 18 sputtering system (Denton) was used to coat the porous silicon samples (Fig 4.1a, Fig 4.2a) with aluminum. The sputterer power was set to 400 W, with an Argon gas flow rate of 35 sccm, resulting in a sputter pressure of 3.2 mTorr, and the temperature was set to 25 ºC. The samples were sputtered at these conditions for 6 min. This resulted in substrates coated with approximately a 40 nm thick layer of aluminum (Fig. 4.1b, Fig 4.2b).

Step 2: Pretreatment and resist application

The substrates (Fig. 4.1b) were then heated for 5 minutes at 200 ºC to anneal the aluminum to the surface of the porous silicon. The aluminum coated substrates were then sealed, with a layer of OmniCoat (Microchem), which was spin-coated on at 3000 rpm for 30 s followed by heating at 200 ºC for 1 minute. SU8-25 photoresist was then spin-coated on at 2250 rpm for 45 s, producing a ~ 20 μm-thick film. The substrate was soft-baked on a hot plate in two steps: 65 ºC for 3 min followed by 95 ºC for 7 min (Fig. 4.1c).

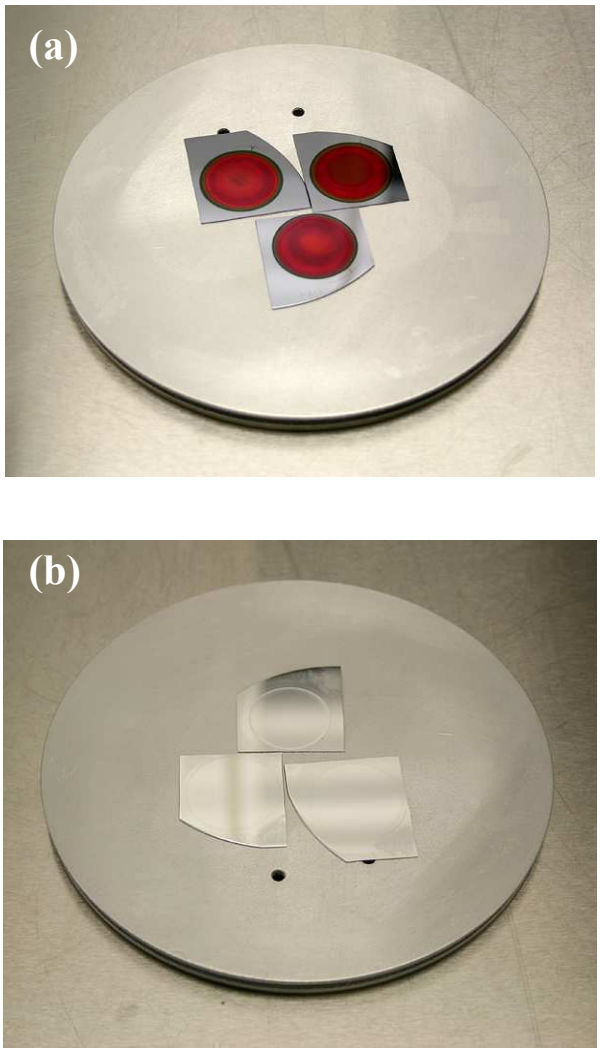

Figure 4.2 (a) Porous silicon samples prepared in Chapter 2, section 2.6. (Fig. 3.1a); (b) Porous silicon samples after aluminum sputter deposition (Fig. 3.1b). The samples are seen resting on the 6" base plate of the sputterer. Images by L. Gu.

Step 3: Exposure

First a contact mask (HTA Photomask) made with four different arrays (Fig 4.3a; 2.5 inches by 2.5 inches in total dimension) was adhered to a 5 inch plate of glass (Fig. 4.3a). This was done so that it could be used in a mask aligner made (Quintel) to hold 5 inch masks. The sub-array used consisted of an 404 by 404 square array of circles, each 25 μm in diameter with a pitch of 35 μm which was aligned to the center of porous silicon sample. Windows in the mask were used to allow for alignment (Fig. 4.3b). The photoresist-covered substrate was then exposed (λ = 365-405 nm, 170 W, 11.5 mW/cm^2) for 6 s through the contact mask.

Step 4: Post exposure bake

The exposed sample was baked on a hot plate at 65 ºC for 1 min and then transferred directly to another hotplate set at 95 ºC for 1 min.

Step 5: Photoresist development

The substrates were submerged in SU8 Developer (Microchem) while mixing for 4 min (Fig. 4.4a). At this point the sample consisted of an array of SU8 feature, 25 μm in diameter, bonded to an aluminum surface (Fig. 4.1d, Fig. 4.4b).

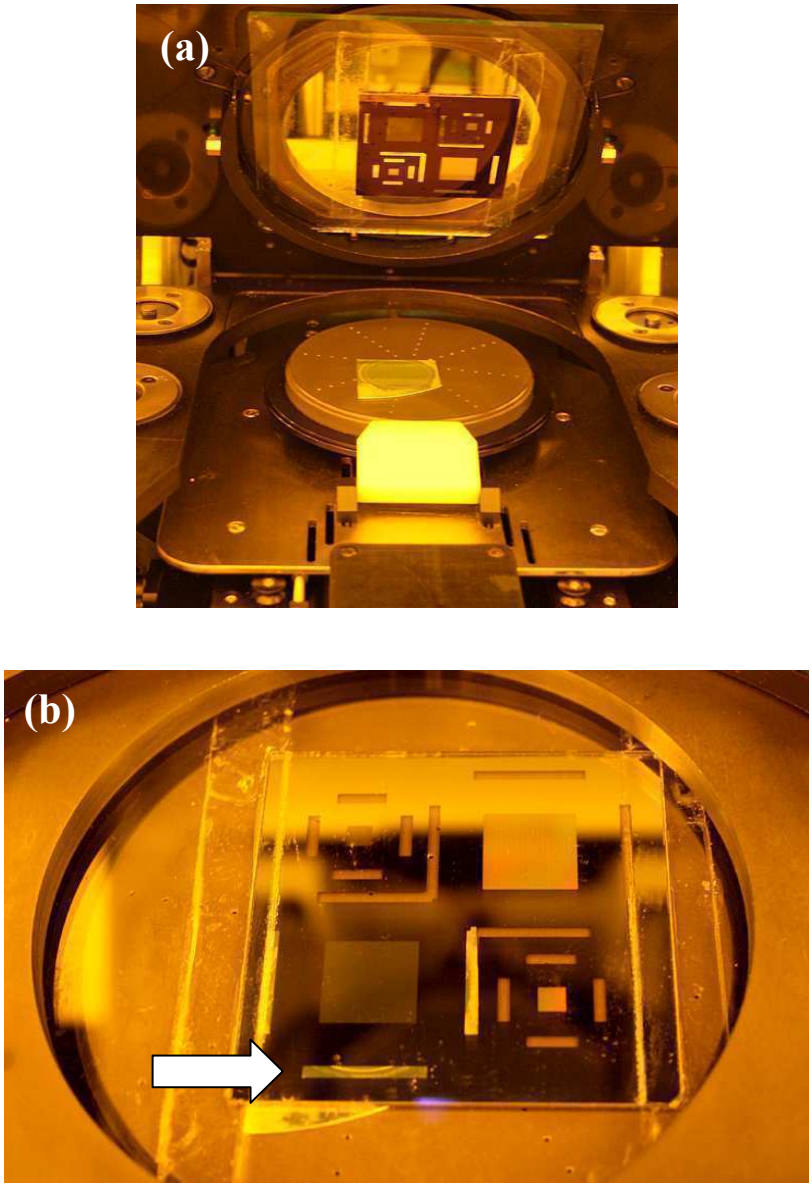

Figure 4.3 (a) Image of aluminum coated porous silicon sample (Fig. 3.1b) on the sample stage of the mask aligner, before the mask is brought down and aligned. (b) After the mask has been lowered onto sample. The arrow points to one of the four windows that surround the array of features allowing the user to align the array to the center of the sample. Images by L. Gu.

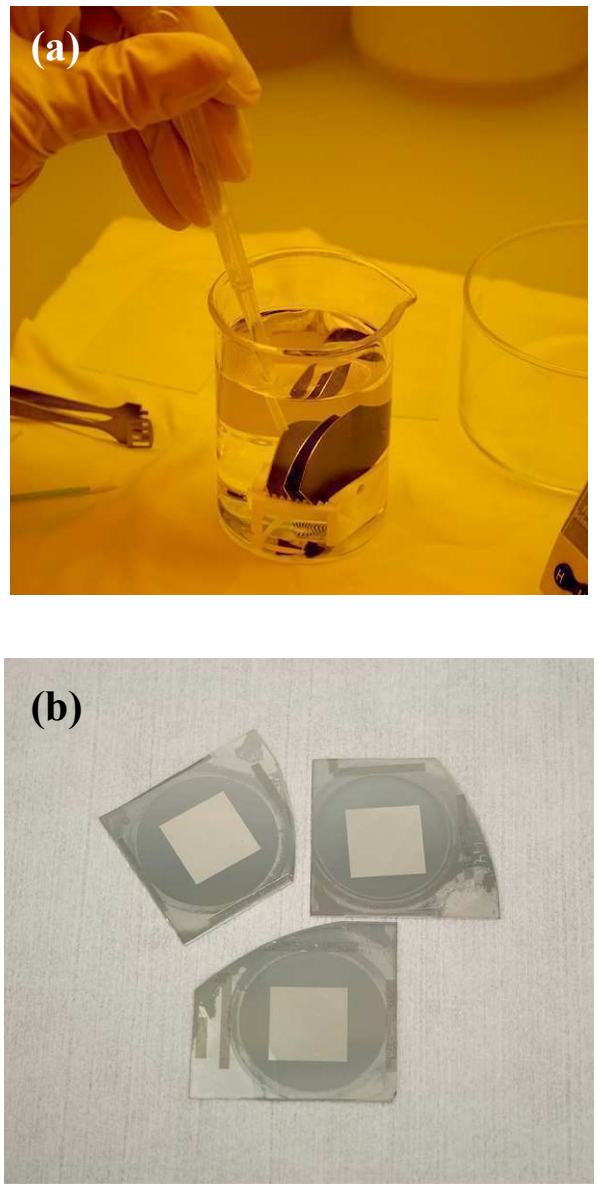

Figure 4.4 (a) The samples are placed on a rack, submerged in SU8 developer and mixed with a pipet for 4 minutes. (b) Samples after development (Fig. 3.1d). Images by L. Gu.

Step 6: Plasma etch

The unprotected regions of aluminum and porous silicon are then removed with a three step reactive ion etch (Fig. 4.1f). In the first step, the aluminum-coated and photopatterned substrate is exposed to argon plasma supplied at a rate of 30 sccm for 100 seconds at 200 W of RIE power under a pressure of 180 mTorr at 25 ºC. In the second step, without breaking the seal, the substrate is exposed to a mixture of Cl_2, BCl_3, and CH_4, supplied at 30, 30, and 3 sccm, respectively, for 30 sec at 300 W of RIE power under a pressure of 180 mTorr at 25 ºC. In some cases it was necessary to run for more than 30 s. In the third step, again without breaking the seal, the pressure is reduced to 15 mTorr, the gas flow rates are held constant, and the RIE power is raised to 350 W for 300 sec. During this process the substrates were observed through the viewport of the reactor chamber (Fig4.5b) to verify removal of the unprotected regions (Fig. 4.5c).

Step 7: Aluminum dissolution and removal of resist mask features

The aluminum layer along with the cured SU8-25 mask features were removed by first wetting the substrate with ethanol and then submerging it in a solution of 48% aqueous HF:ethanol (1:14.5 by volume) for 5-10 min, while mixing (Fig. 4.1f, Fig. 4.6a). This method was similar to the method shown in figure 4.4 a, except that a plastic beaker was used.

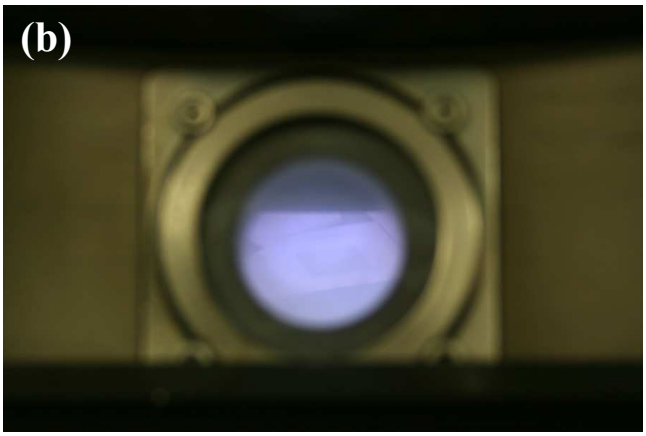

Figure 4.5 (a) Samples being loaded into the plasma etch rig. (b) A sample seen through the viewport during the etch process. The viewport allows for real-time monitoring of the process. (c) Samples after the plasma etch (Fig. 3.1 e). Images by L. Gu.

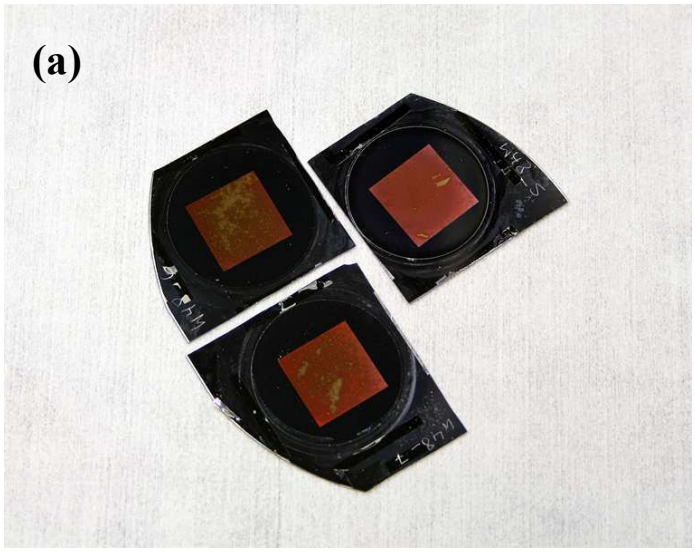

Figure 4.6 (a) Samples after the dissolution of the aluminum layer and subsequent liftoff of the SU8 mask features. This process is similar to the one shown in Fig. 4.4a, except that a plastic beaker is used because of the high solubility of glass in hydrofluoric acid. (b) The setup of the electrochemical cell is similar to the setup for the formation of porous silicon (Fig. 2.5) except that a smaller electrode (Platinum mesh, 1.5 cm in diameter) is used and held close to the surface (~ 5 mm). This reduces the amount of hydrofluoric solution that needs to be filtered off the samples. Images by L. Gu.

Step 8: Particle isolation by electropolishing liftoff

Finally, the microfabricated porous silicon disks were lifted off the crystalline silicon substrate by electropolishing with a current of 4mA/cm^2 and a solution composed of the 48% aqueous HF:ethanol (1:14.5 by volume) (Fig. 4.1g). The setup of the electrochemical cell is similar to the setup for the formation of porous silicon except that a smaller electrode (Platinum mesh, 1.5 cm in diameter) is used and held close to the surface (~ 5 mm) (Fig. 4.6b). The electrolyte solution was then rinsed off and the particles were further rinsed with ethanol using the filter component of an Ultrafree Cl centrifuge filter, 0.2 μm PVDF membrane (Millipore) (Fig. 4.7a). Vacuum was used instead of centrifugal force because the filtrate did not need to be reclaimed. The freestanding porous silicon particles were transferred to a microcentrifuge tube and centrifuged to form a pellet. Most of the ethanol was decanted off and the remainder of the ethanol suspension of particles was transferred to a nickel crucible (Fig. 4.7 b) - each code in a different crucible. The crucibles were heated at ~ 75 ºC for ~ 10 minutes, evaporating off the ethanol.

Step 9: Thermal oxidation

The separate batches of freestanding microfabricated porous silicon particles, loaded into separate nickel crucibles, as described above, were all placed in an alumina combustion boat (Fig. 4.7b). The boat was then placed in the tube furnace at 500 ºC, ramped up to 950 ºC at a rate of 50 ºC /min, held at 950 ºC for thirty minutes, cooled

back to 500 ºC and removed from the furnace. After oxidation, the particles were annealed to the surface of the crucible and to each other. Soaking the particles in 0.05% HCl (aq) liberated the particles from each other and somewhat from the surface of the nickel crucible. The liberated particles were then transferred to a microcentrifuge tube and washed with ethanol.

Figure 4.7 (a) Suction filtration apparatus used for the filtration of the hydrofluoric acid from the freestanding microfabricated porous silicon particles. (b) Nickel crucibles, each containing a separate particle type after the ethanol wash solution has been evaporated away.

4.4 RESULTS AND DISCUSSION

4.4.1 SEM characterization of encoded particles

The microfabricated encoded porous silicon particles were sputter coated with an approximately 20 nm thick layer of gold and imaged using an a scanning electron microscope. It should also be noted that the particles displayed in figures 4.8 and 4.9 were from an earlier batch as the ones discussed throughout the chapters of this work. Figures 4.8 a and b show the freestanding particles on a nylon filter viewed at an angle 45º from the surface normal. The images were taken at 96 x and 3245 x magnification, respectively. Figure 4.8 a shows evidence for a uniform sized population, while figure 4.8 b shows the smooth, flat top surface which provides for uniform reflectivity. Figure 4.9 clearly shows the mapping of the current-time waveform (used to etch the photonic code) to the porosity gradient in the porous silicon film. It should be noted that in these images the particles were not filtered and then transferred to a nickel crucible for evaporation, but were filtered out onto a porous nylon filter (Osmonics, MagnaGraph, Nylon transfer membrane, 0.45 μm), washed with ethanol and allowed to dry. The filter appears to be rougher than 0.45 μm because it was damaged by the hydrofluoric acid during filtration. This method was used before the optimized method, presented earlier was developed.

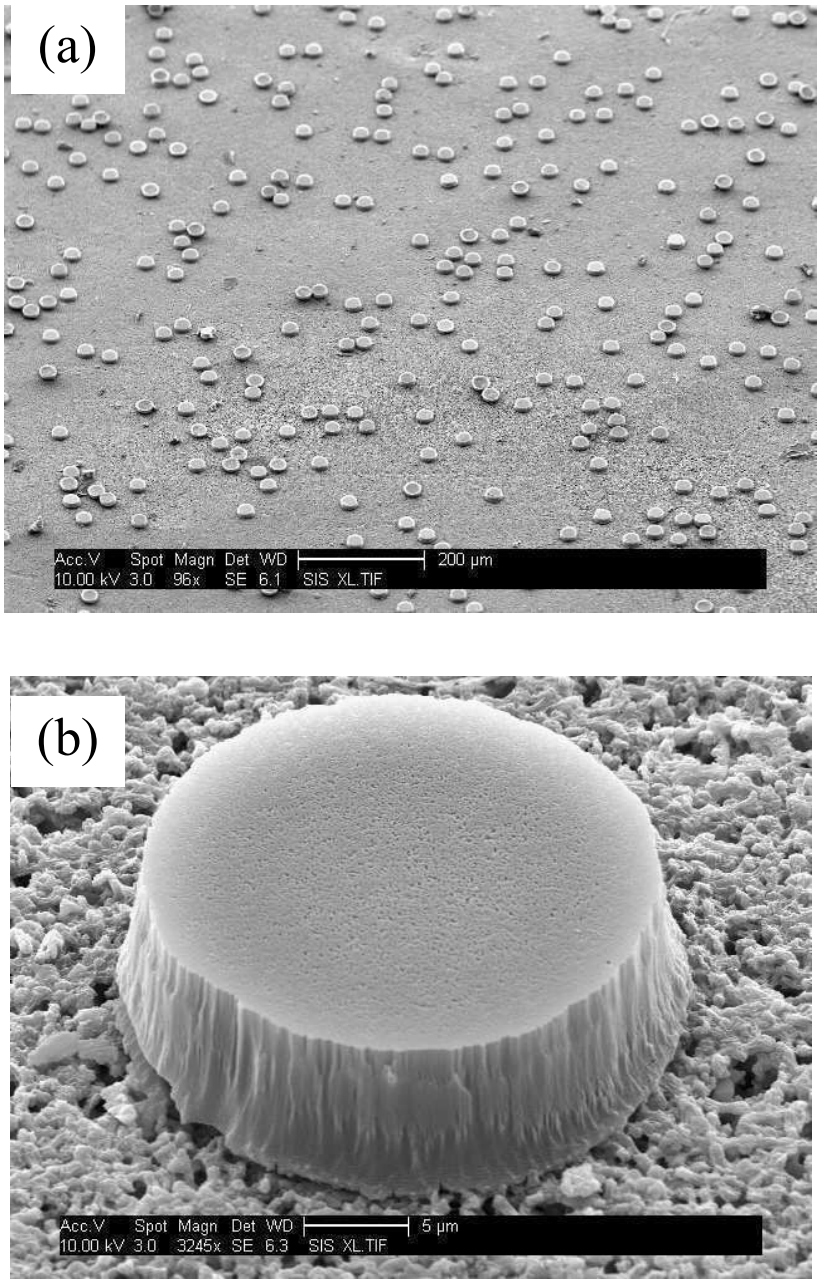

Figure 4.8 Scanning electron microscope (SEM) images of the freestanding particles assembled onto a nylon filter, viewed at an angle of 45º from the surface normal: (a) 96 x magnification; (b) close up view of a particle at 3245 x magnification. The samples were sputtered with a ~ 20 nm layer of gold in preparation for SEM imaging.

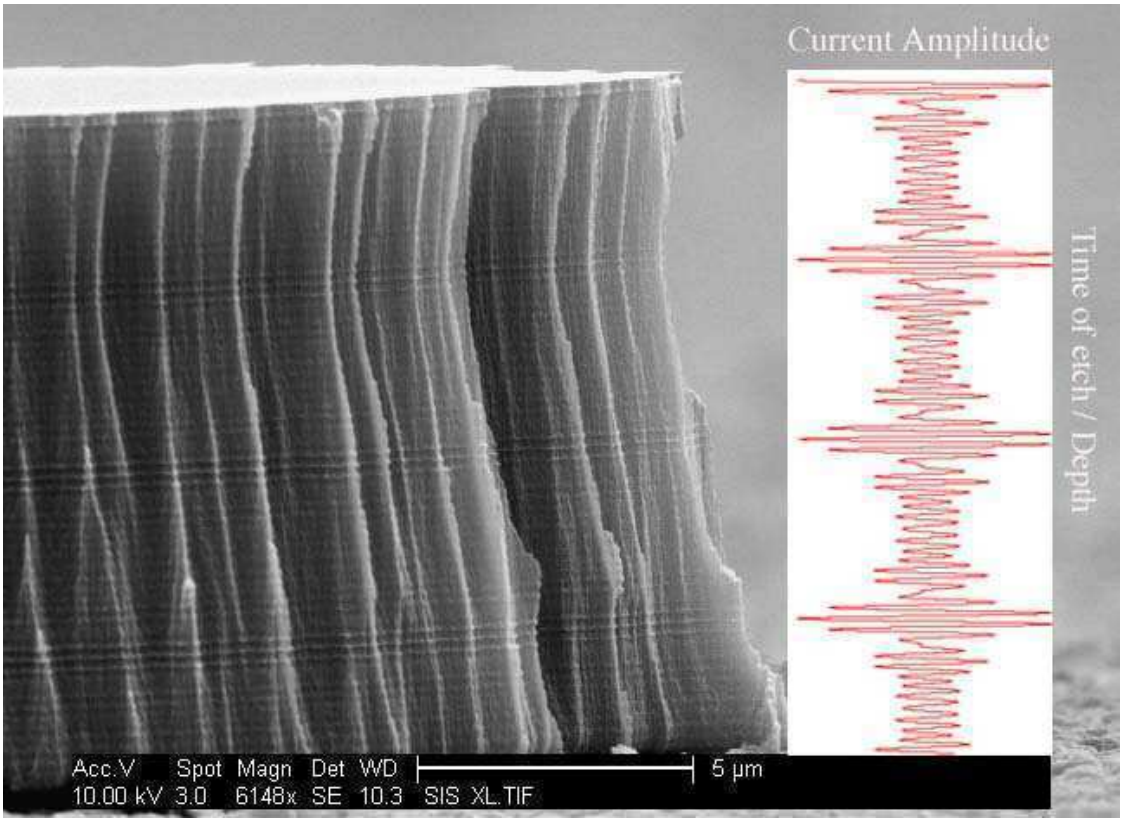

Figure 4.9 Cross-sectional SEM image clearly showing the mapping of the current-time waveform to the porosity gradient of the encoded porous silicon particle. The sample in this image was sputtered with a ~ 20 nm layer of gold in preparation for SEM imaging.

4.4.2 Spectra of freestanding encoded porous silica microparticles

Figure 4.10a shows the spectrum of the porous silicon film, still attached to the wafer. While, figure 4.10b shows the spectrum of a freestanding, microfabricated porous silica particle (after thermal oxidation) acquired using the spectral imaging system described in chapter 3. Figure 4.10c plots the amount of shift due to oxidation from the initial peak position. The amount of shift depends linearly on the initial peak position. Figure 4.10b demonstrates that the process can produce microscale particles (~ 25 μm in diameter and ~ 12 μm in height) that exhibit highly resolved spectral peaks – a key requirement for encoded microparticles.

4.4.3 Image evidence for the conversion to porous silica

As evidence for the conversion to porous silica, images of the particles before (Fig. 4.11a) and after oxidation (Fig. 4.11b) are displayed. An inspection of the particles that lay on their sides (allowing the color of the bulk material to be seen without interference from the rugate colors) shows a transition from an amber color to a translucent appearance. This indicates the conversion from porous silicon to porous silica. The oxidized particles do appear pale. However, as Figure 4.10b proves, the spectral codes are preserved through the oxidation process.

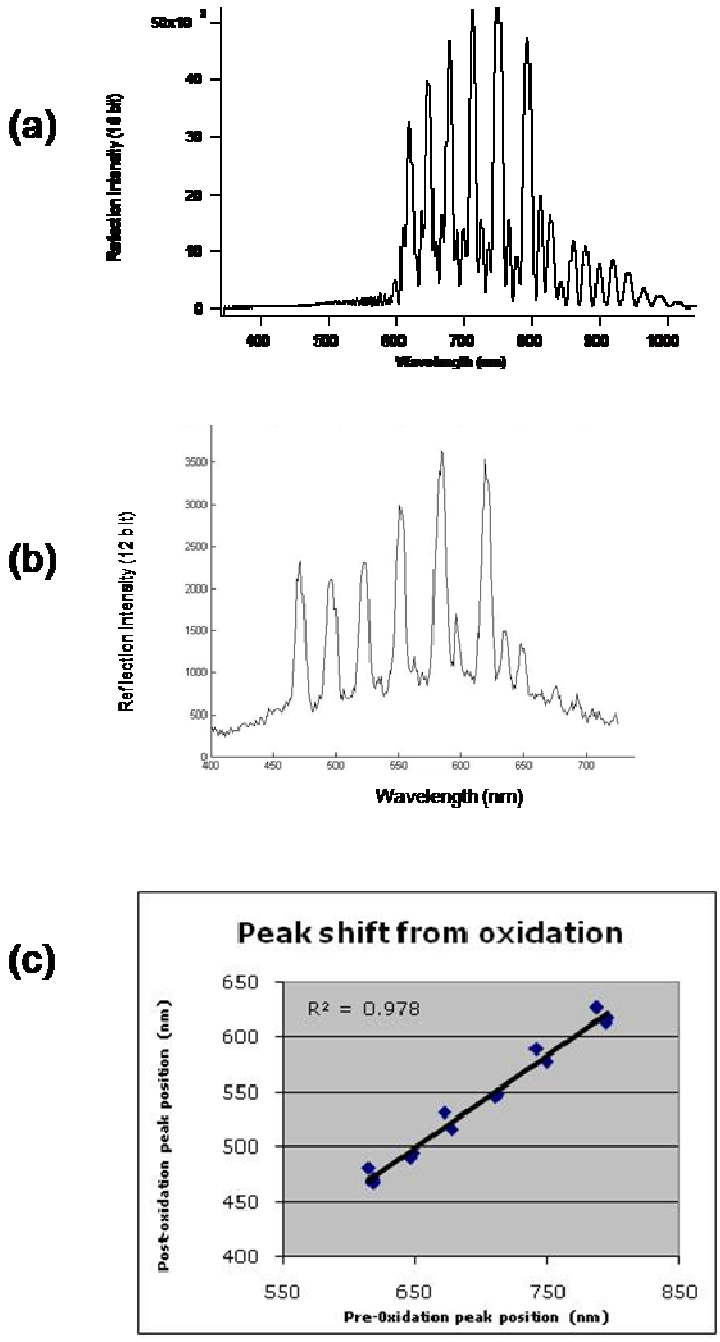

Figure 4.10 (a) Reflection spectrum of pre-oxidized porous silicon photonic crystal film, still attached to the wafer. (b) Reflection spectrum of an oxidized porous silica photonic crystal particle acquired with the spectral imaging system (chapter 3). The particle came from the same film shown in (a). (c) Amount of shift in the spectral peak positions due to oxidation plotted versus the initial peak positions. The data set is composed of three, six peak samples.

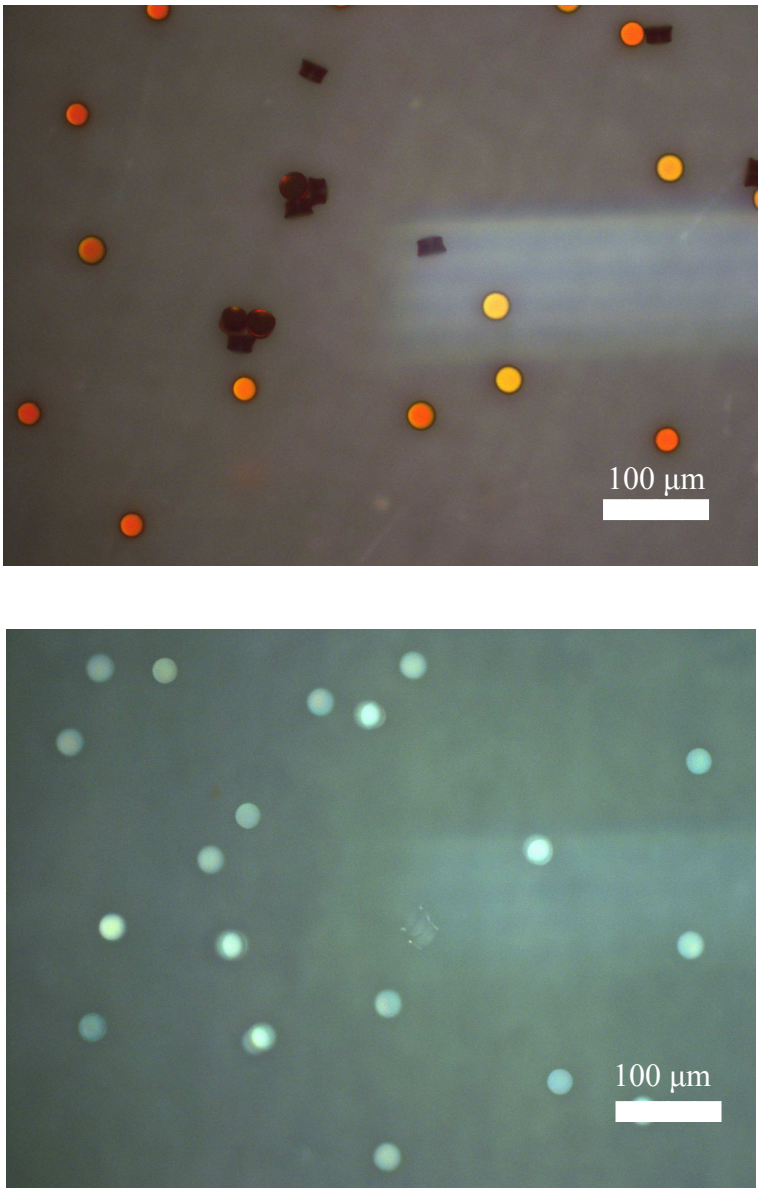

Figure 4.11. (a) Image of pre-oxidized microfabricated porous silicon photonic crystal particles. (b) Image of oxidized porous silica photonic crystal particles. Note the change in transparency of the particles (on their sides) between the pictures. The oxidized particles appear pale, however, as Figure 4.10b proves, the spectral codes are preserved through the oxidation process.

4.4.4 Purpose of the aluminum layer

The function of the aluminum layer is to allow for clean removal of the photoresist from the porous silicon particles at the end of the process. While, the function of the Omnicoat is to seal any openings that allow gas to escape from the pores during the soft back, causing air bubbles in the resist that pucker up and in turn cause the image of the contact mask to be out of focus.

4.4.5 Reasoning for the elimination of film edge from fabrication

Fabrication at only the center of the porous silicon film reduces the variability of the particle's spectral codes by eliminating the edges of the film from the microfabrication process. The porosity at the edges of the film decreases due to the restricted electrolyte diffusion and non-uniform current density in the region of the o-ring seal, during the formation of the porous silicon. See figure 4.2a for an example of this.

4.4.6 Electropolishing at low current densities

Electropolishing at low current densities is possible if the concentration of the hydrofluoric acid in the electrolyte is low. These conditions reduce the disintegration of the porous silicon film, which occurs when electropolishing is carried out at high current densities.

4.5 CHAPTER SUMMARY

In summary, encoded porous silicon films can be converted into monodisperse populations of micron-sized encoded particles. The codes can be read using the spectral imaging system discussed in chapter 3. Excluding the dwell time of the thermal oxidation, the entire process can be accomplished in under four hours and is highly scalable. Conversion of the porous silicon particles to porous silica does not harm the spectral quality of the reflection spectra-based codes. Additionally, since the material has been transformed to porous silica the particles can now be functionalized with biomolecular probes using standard silane chemisty. Finally, transformation of the porous silicon to porous silica creates a particle that's chemically stable in biological buffers. The latter two claims will be demonstrated in chapter 5.

4.6 ACKNOWLEDGMENTS

Chapter 4, in part is a reprint of the material as it will appear upon submission of the manuscript in progress: Meade, S.O., Chen, M., Sailor, M.J. “A bioassay multiplexing system utilizing porous silica photonic crystal particles containing spectral barcodes” (2008).

4.7 REFERENCES

1. *Luminex inc.,* http://www.luminexcorp.com/.

2. Cunin, Frederique, Thomas, Schmedake A., Link, Jamie R., Li, Yang Yang Koh, Jennifer, Bhatia, Sangeeta N., Sailor, Michael J., *Biomolecular screening with encoded porous silicon photonic crystals.* Nature Mater., 2002. **1**: p. 39-41.

3. Meade, S.O., Yoon, M.S., Ahn, K.H., Sailor, M.J. , *Porous silicon photonic crystals as encoded microcarriers.* Adv. Mater., 2004. **16**(20): p. 1811-1814.

4. Lehmann, V., *Electrochemistry of Silicon*. 2002, Weinheim, Germany: Wiley-VCH. 51-75.

5. Gargas, D.J., Muresan, O., Sirbuly, D.J., Buratto, S.K. , *Micropatterned Porous-Silicon Bragg Mirrors by Dry-Removal Soft Lithography.* Advanced Materials, 2006. **18**: p. 3164-3168.

6. Li, Y.Y., Kollengode, V.S, Sailor, M.J., *Porous-Silicon/Polymer Nanocomposite Photonic Crystals Formed by Microdroplet Patterning.* Advanced Materials, 2005. **17**: p. 1249-1251.

7. Park, Jennifer S.; Meade, Shawn O.; Segal, Ester; Sailor, Michael J. Porous silicon-based polymer replicas formed by bead patterning. *Physica Status Solidi A: Applications and Materials Science* (2007), 204(5), 1383-1387.

8. Arens-Fischer, R.; Kruger, M.; Thonissen, M.; Ganse, V.; Hunkel, D.; Marso, M.; Luth, H. *Formation of porous silicon filter structures with different properties on small areas.* Journal of Porous Materials (2000), 7(1/2/3), 223-225.

9. Meade, S.O. and Sailor, M.J., *Microfabrication of freestanding porous silicon particles containing spectral barcodes.* Physica Status Solidi RRL: Rapid Research Letters, 2007. **1**(2): p. R71-R73.

CHAPTER 5

Multiplexed DNA detection and validation of photonic encoding

5.1 ABSTRACT

A model system multiplexed DNA assay based on 50-mer oligonucleotide probes and perfect match fluorescently labeled targets was used as a means to demonstrate multiplexed detection and act as a benchmark for the accuracy of the photonic encoding method. Each particle type, from the particle library described in chapters 2 and 4, was functionalized with a unique oligonucleotide probe, using silane immobilization chemistry. The particles were then pooled together and reacted with a sample containing two oligonucleotide target sequences. Each target sequence, designed to be a perfect compliment toward one of the probe sequences, was labeled with a different color dye. After washing, the particles were assembled onto a surface for decoding and assay readout using the instrumentation and methods described in chapter 3. The results agreed with the experimental design, thus demonstrating both multiplexed detection and the validation of the photonic encoding method. Finally, the successful decoding and assay readout demonstrated chemical stability of both the photonic codes and immobilized probes all the way through the assay.

5.2 INTRODUCTION

5.2.1 Review of project goals

The high level goal of this project was to demonstrate that encoded porous silicon photonic crystal particles can be utilized in a multiplexing system. The subordinate goals were (1) the development of a high capacity encoding method, (2) the development of instrumentation and methods for high-throughput decoding and assay readout, (3) the development of a microfabriction method, (4) the demonstration of chemical stability of both the photonic structures and immobilized probes and (5) the demonstration of a multiplexed DNA assay, while validating the accuracy of the photonic encoding method. The first three goals were discussed in chapters 2, 3, and 4, respectively. The last two goals will be addressed in this chapter.

A model system assay based on 50-mer oligonucleotide probes and perfect match fluorescently labeled targets was designed as a means to demonstrate multiplexed DNA detection and act as a benchmark for the accuracy of the photonic encoding method. A strong correlation between the decoding results of the photonic codes and the assay results, or independent fluorescence/oligonucleotide codes [1] signify success in this experiment. Along with the successful decoding and assay readout, the demonstration of chemical stability of both the photonic codes and the immobilized probes will also be demonstrated.

5.2.2 Experimental design

The experimental design is shown in figure 5.1. Particle type 1 exhibited a

reflection spectrum or photonic code consisting of six peaks, represented in binary fashion as 111111 (Fig. 5.1). The second and fourth peaks were deleted in particle type 2's photonic code, 101011, and the third and fifth peaks were deleted in particle type 3's code, 110101, (Fig. 5.1). Particle type 1 was functionalized with the probe sequence P1 (see Table 5.1 of the experimental section for the sequences P1-P3, T1 and T2), which acted as the oligonucleotide code. Particle types 2 and 3 were each separately functionalized with the probe sequences P2 and P3, respectively. The probe functionalized particles were then pooled and reacted with the targets sequences T1 and T2. The oligonucleotide selection process, immobilization chemistry, pooling, hybridization, particle assembly and data acquisition techniques are described in the experimental section below.

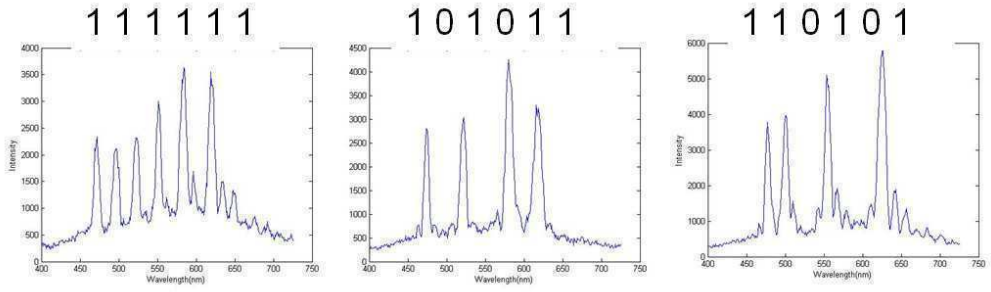

Photonic Code	Probe	Target	Target Label
111111	P1	T1	Alexa Fluor 555
101011	P2	T2	Alexa Fluor 680
110101	P3	none	no target

Figure 5.1 The reflection spectrum of each particle type is shown. The spectra were acquired after the hybridization step. The table at the bottom shows the experimental design and lists the probe sequence assigned to each particle type and the fluorescent label of the perfect match target for probes P1 and P2. No target was present for particle type 3, labeled with the probe P3, which was included as a nonspecific binding control, free from spectral bleed-through issues. See Table 5.1 for sequences.

5.3 EXPERIMENTAL SECTION

5.3.1 Oligonucleotide sequence design for the model system multiplexed DNA assay

Using the work of Kucho et al.[2], as a guide, a set of oligonucleotides was designed to act as a model system multiplexed DNA assay and as a benchmark for photonic encoding (Table 5.1). Two 50-mer probes, P1 and P2, were designed to be selective toward their perfect match compliments with melting temps of 85.4 and 83.4 ºC, respectively; free energies of –89.26 and –86.19 kcal/mol, respectively; and GC contents of 42 and 40%, respectively (Table 5.1a). A third sequence, P3, was included to act as a control for nonspecific binding. All three probes were modified with 5' amino C6 linkers (Operon) (Table 5.1a). Two target sequences, T1 and T2, were made to be perfect matches for P1 and P2, respectively (Table 5.1a). T1 was labeled with Alexa Fluor 555 and T2 was labeled with Alexa Fluor 680 (Operon) (Table 5.1a). In order to optimize the specificity of the model system assay, interactions between non-complimentary pairs and hairpins were reduced by designing the interactions to have free energies of –6.78 kcal/mol or smaller. See table 5.1b for all possible dimer free energy values. All calculations for melting temperatures and free energies assumed a salt concentration of 1 M, a temperature of 25 ºC and an oligonucleotide concentration of 500 nM.[3]

Table 5.1 (a) Probe and target sequences, designed for the multiplexed DNA detection and photonic encoding validation study. The GC content, melting temperature (T_m) and compliment, highest self dimer and max hairpin free energies (kcal/mol) are given. All calculations assumed a sodium concentration of 1 M, a temperature of 25 ºC, and an oligo conc. 500 nM. (b) The resultant free energy values and contiguous sequence identities for all possible dimer interactions.

(a)

Sequence name	Probe Sequence (5'--3')	GC content (%)	T_m	Comp-liment dG (kcal/ mol)	highest self dimer dG (kcal/ mol)	max hairpin dG (kcal/ mol)
P1	ACT GTG TGA TGA AGT TTG GTC AGT CGG CTT GTT ATT ATC TCG TGC TTG TA	42	85.4	-89.26	-4.89	-1.89
T1	TAC AAG CAC GAG ATA ATA ACA AGC CGA CTG ACC AAA CTT CAT CAC ACA GT					
P2	TCC TGT AAT GAT CCA GGT GAG TGA TAT GCC ATA CAT CCT AGA TCC TTA TA	40	83.4	-86.19	-6.62	-4.66
T2	TAT AAG GAT CTA GGA TGT ATG GCA TAT CAC TCA CCT GGA TCA TTA CAG GA					
P3	TCT GGA TAG TCA TAC GTC ACC CTC GCT TAG GAT CTA TAC TTA CTA TAC TA	40	82.4	-83.22	-6.3	-3.36

(b)

Seq 1	Seq 2	dG (kcal/ mol)	Cont. Seq Ident (bp)
P1	**T1**	**-89.26**	**50**
P1	T2	-6.35	5
P2	T1	-6.35	5
P2	**T2**	**-86.19**	**50**
P3	T1	-6.78	4
P3	T2	-5.73	5
T1	T2	-6.21	3
T1	T1	-4.89	4
T2	T2	-6.62	4

5.3.2 Immobilization of DNA to porous silica

After the work of Steinberg et al. [4], oligonucleotide probes were immobilized to the thermally oxidized microfabricated encoded particles. First, 1 mL of 0.5 % 3-aminopropyltriethoxysilane (Aldrich) in ethanol was added to approximately 100,000 photonically encoded porous silica particles and shaken for one hour (Fig. 5.2). The particles were then washed with ethanol three times, and once with acetonitrile, using a centrifugal filter (Pall). Next, 980 µL of acetonitrile and 20 µL of N,N diisopropylethylamine (Aldrich) were added to the particles, followed by an addition of 10 mg of cyanuric chloride and allowed to react for two hours while shaking (Fig 5.2). The particles were then washed with acetonitrile four times and transferred to a microcentrifuge tube in ethanol, spun down and the suspension was dectanted to a volume of approximately 25 uL. Next, a 1 mL solution of 500 nM 50-mer oligonucleotides (5' amino-C6 modified from Operon) in 0.05 M sodium borate buffer, 2 M NaCl, at pH 8.5 was added to the particles and shaken overnight (Fig. 5.2). The particles were washed four times with 0.05 M sodium borate buffer. In these high salt, high density conditions the centrifugal filter is absolutely necessary. Centrifugation alone can separate the porous silica particles from the wash solution. However, the speeds required (~12000 rpm) destroy the photonic structures.

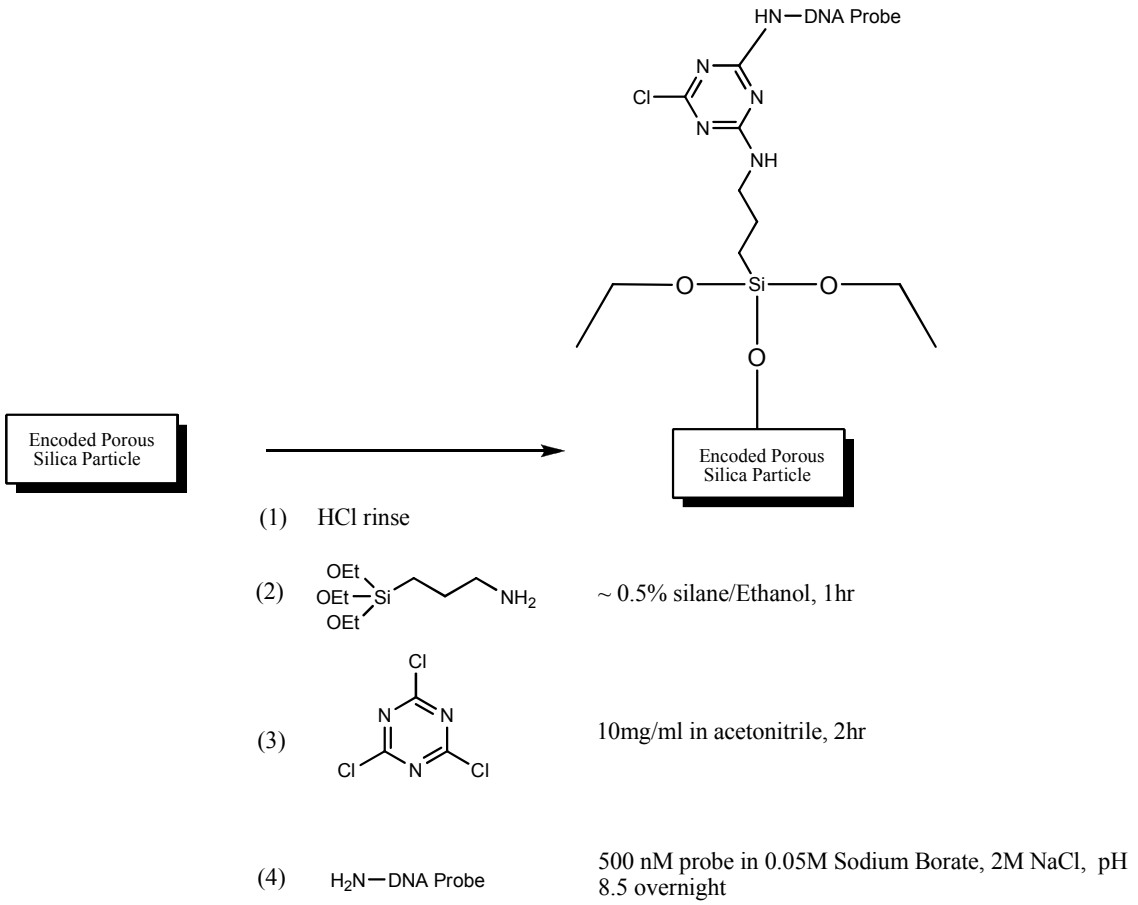

Figure 5.2 Immobilization chemistry. (1) The porous silica particles are rinsed in 0.05% HCl (aq). (2) After the work of Steinberg et al., the particles are reacted with 3-aminoproplytriethoxysilane, (3) followed by cyanuric chloride, (4) and finally with the amino-C6-oligonucleotide probe.

5.3.3 Pooling and hybridization

The three particle types were pooled together and the borate buffer was filtered using the centrifugal filter device. The oligonucleotide target sequences were added to the particles to achieve final the concentrations of 10 nM each in a total volume of 250 μL, when diluted with the hybridization buffer from Steinberg et al. (0.1 M potassium phosphate, 1 M sodium chloride, and 0.1 % Tween-20, and 5 % ethanol, set to a pH of 7.6).[4] The suspension was shaken for one hour after which the particles were washed three times with hybridization buffer, once with a 0.5 x dilution of hybridization buffer and once with an ethanol/water mixture. Following the last wash the particles were immediately suspended in 100% ethanol.

5.3.4 Particle assembly

The suspension of pooled, hybridized and washed particles was pipetted onto an Anodisc porous alumina filter (Whatman, 0.2 μm pores) under vacuum. A gasket made of PDMS was used to define a circular area, 5 mm in diameter, for assembly (Fig. 5.3a). The microcentrifuge tube was rinsed with several more milliliters of ethanol to collect any residual particles. A white light color microscopic image of the particle assembly can be seen in figure 5.3b.

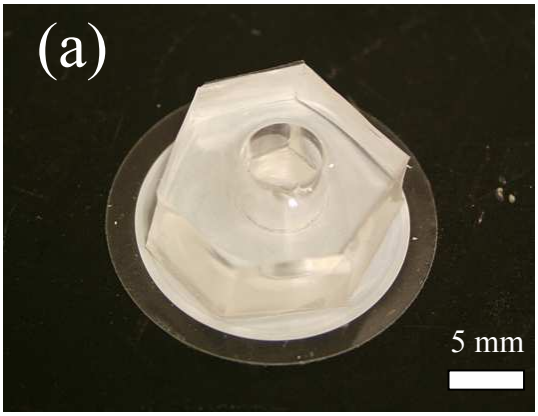

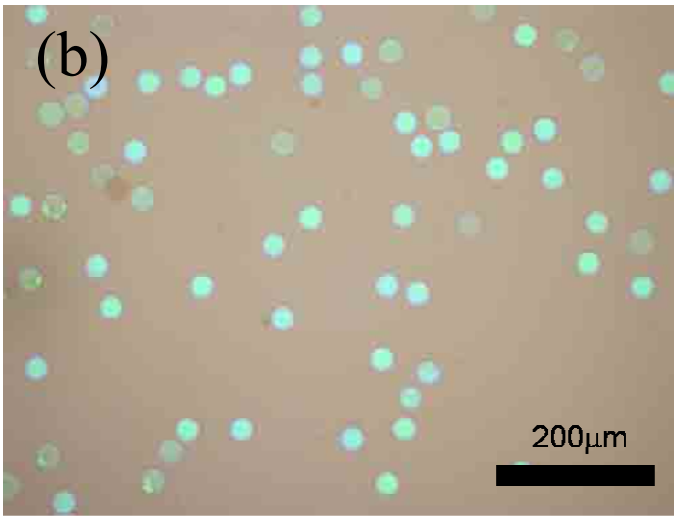

Figure 5.3 (a) Porous alumina Anodisc filter and PDMS gasket used to collect and assemble the particles for decoding and assay readout. (b) White light microscopic image of particles assembled onto the Anodisc filter.

5.3.5 Data acquisition

Using the imaging system described in chapter 3, images were acquired using a 10x objective with the detector set at a binning of 2, yielding an array, 520 by 696 pixels in size. For analysis, the image was cropped to a size of 480 by 480 pixels. The assembled particles were first imaged in the "Cy5.5" channel (excitation filter was centered at 650 nm with a 45 nm bandpass, the dichroic centered at 680 nm, and the emission filter was centered at 710 nm with a 50 nm bandpass) with an exposure time of 2 s. Next the particles were imaged in the "Cy3" channel (excitation filter was centered at 535nm with a 50 nm bandpass, the dichroic centered at 565 nm, and the emission filter was centered at 610 nm with a 75 nm bandpass) at an exposure time of 5 ms with a neutral density filter (ND4, or 25 % transmission) in place. Finally, the system was set to monochromatic scanning mode and the particles were scanned from 400 to 725 nm, stepping every 1 nm. The exposure time was 15 ms for each frame in the spectral image stack.

5.4 RESULTS AND DISCUSSION

5.4.1 Multiplexed DNA detection and validation of photonic encoding

A composite, false color image of both the "Cy3" and "Cy5.5" channels, displays the particles as green and red, respectively (Fig. 5.4a). Using the decoding method described in chapter 3 a false color image was constructed, displaying all the decoded pixels, where each code is assigned a color (Fig. 5.4b). Pixels decoded as 111111, 101011, 110101 and invalid are colored as white, red, blue and black, respectively. The number of pixels decoded as 111111, 101011, and 110101 were 769, 597, and 935, distributed over 12, 7, and 6 particles, respectively. The average number of pixels per particle was 79, 85, and 156 for codes 111111, 101011, and 110101, respectively. Codes 111111, 101011 and 110101 composed 0.33%, 0.25%, and 0.41% of the entire image, respectively. As seen in Fig. 5.4a, not all particles assembled with their photonic axis parallel with the detector. However, the pixels corresponding to these objects were decoded as invalid and were therefore thrown out of the experiment (Fig 5.4b). The large half moon shaped object present in the image is most likely residual SU8 or Omnicoat that flowed into the porous matrix during the photoresist pretreatment.

In Fig. 5.5a the decoded pixels are plotted against the intensity axes of each fluorescent channel and labeled according to their assigned photonic code. The resultant clusters are based on the oligonucleotide code. Again, the intensity scale is 14-bit, having a maximum value of 16383 counts. The average intensities, standard deviation, % CV are shown in Fig. 5b. In order to determine the selectivity of each probe-functionalized-particle-type for its assigned target, ROC analysis was performed between

the particle type pairs 111111/1101011 and 101011/1101011. No false positives were found to occur between either pair.

The scatter plot (Fig. 5.5a) demonstrates agreement between the photonic encoding method and the independent fluorescence/oligonucleotide based encoding method. Specifically, the 111111 code is highest in the "Cy3" channel and low in the "Cy5.5" channel (Fig. 5.5a). This is in line with expected results, because 111111 was functionalized with the sequence P1, whose complimentary target in solution was labeled with Alexa Fluor 555 dye (Fig 5.1). Correspondingly, 101011 was low in the "Cy3" channel and highest in the "Cy5.5" channel (Fig. 5.5a). This also in line with expected results because 101011 was functionalized with the sequence P2, whose complimentary target was labeled with Alexa Fluor 680 (Fig. 5.1). Code 110101 was labeled with the sequence P3 (Fig. 5.1), which had no fluorescently labeled compliment in solution. Fittingly, the intensity values of 110101 were lowest in both fluorescence channels (Fig. 5.5a). The non specific binding of the assay was low, as is evident by the clear separation of both the 101011/110101 and 111111/110101 pairs.

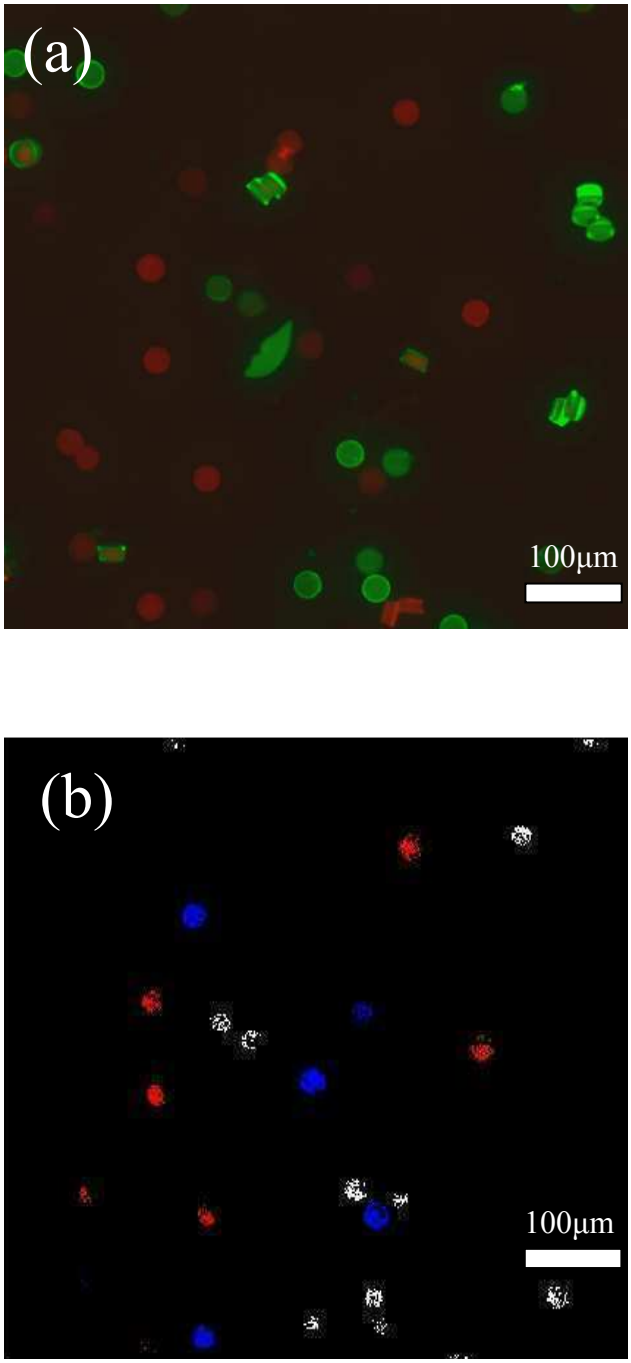

Figure 5.4 (a) False color, composite image of the Alexa Fluor 555 (AF555) and Alexa Fluor 680 (AF680) fluorescence images. (b) False color image of the decoded pixels. Pixels decoded as 111111, 110101, 101011 and invalid are colored as white, blue, red and black respectively.

(a)

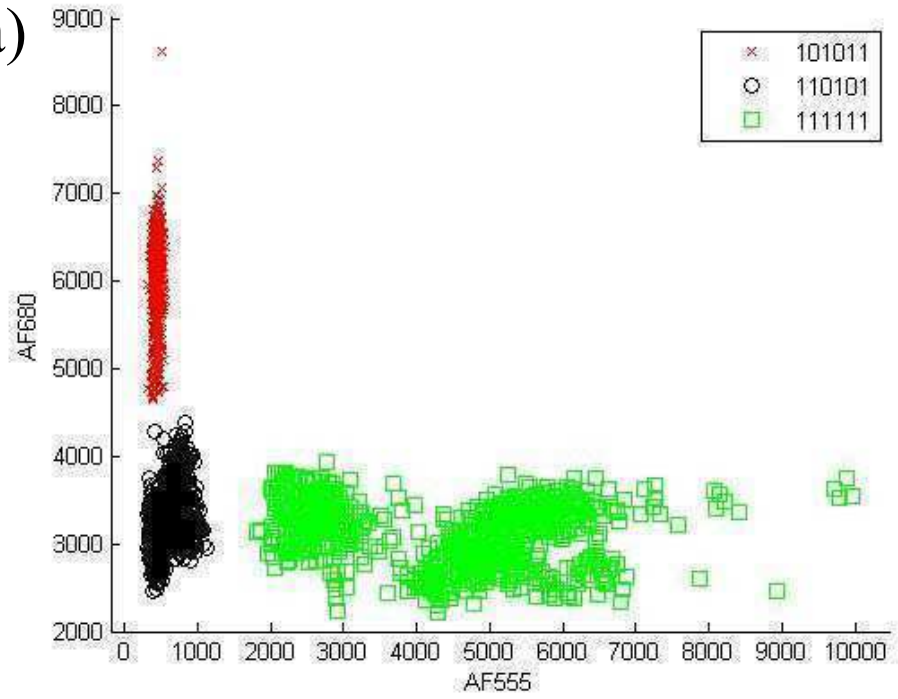

(b)

Code	Channel	Avg	Stdv	% CV
111111	555	4387	1512	34
111111	680	3111	355	11
101011	555	446	40	9
101011	680	5987	508	8
110101	555	588	182	31
110101	680	3239	355	11

Figure 5.5 (a) Decoded pixels are plotted with respect to their corresponding fluorescence intensity values in both the "Cy3" (AF555) and "Cy5.5" (AF680) channels. The number of pixels decoded as 111111, 101011, and 110101 were 769, 597, and 935, distributed over 12, 7, and 6 particles, respectively. (b) The average intensity (14-bit scale, max 16383), standard deviation and coefficient of variance as a percent (%CV) are shown.

5.4.2 Improving the packing density

The greatest area of concern in moving toward a medium to high-throughput multiplexing platform is the low percentage of the image that contained decoded pixels. In addition to the dye absorption effects on the reflection spectra, discussed below, the low percentage was due to difficulty in creating a high packing density in the particle assembly. Additionally, not all particles were assembled perpendicular to the detector; some were stacked on top of each other or on their sides.

5.4.3 Improving imaging conditions

Using lower magnification, at the full digital resolution of the detector, instead of the 10x objective with the detector set at a binning of 2, would greatly increase the number of particles per image. Lower magnification at high resolution was not used in this experiment because the decoding program was not able process such a large data set. Lower magnification with a binning of 2, did not allow enough pixels to represent each particle. However, if a 5x objective were used at full digital resolution and assuming the particles could be assembled into a square packed array with a 35 μm pitch, then approximately 1900 particles would be present in one image. This would allow for 76 particle types, with 25 replicates each. Of course, in randomly assembled arrays there is no set number of replicates. Gunderson et al. provide an interesting discussion on the problem.[1]

5.4.4 Chemical Stability

The spectra extracted from the spectral image stack (Fig. 5.1), were acquired after the assay procedure, demonstrating that the photonic structures are chemically stable throughout the probe immobilization and assay procedures. Additionally, the selective assay results demonstrate stability of the probe immobilization chemistry.

5.4.5 Effect of fluorescent dye on spectral code

The absorption characteristics of the fluorescent dyes have an effect on the reflection spectra, or photonic codes. This is evidenced in the modulated spectral envelope of the six peak spectrum to the left of Fig. 5.1. As the name suggests, Alexa Fluor 555, has its absorption maximum at around 555 nm - where the spectral envelope is at its minimum. This effect is only apparent at high concentrations of dye. Notice that the higher intensity particles (colored green in Fig. 5.4a) were classified as invalid (colored black in Fig. 5.4b). In these cases, it is speculated that the large amount of Alexa Fluor 555 molecules absorb most of the photons that would otherwise be reflected back to the detector during the spectral decoding process, thus reducing the intensity of the reflection spectra below the intensity thresholds set in the code recognition algorithm.

5.4.6 Contributions to assay noise

The noise of the fluorescence signal extracted from the photonic code 111111 in the AF555 channel at 34% CV, was quite high (Fig 5.5). In fact, its distribution is not only broad but bimodal as well. One possible source of this bimodality can be visualized through the use of intensity line profiles seen in figure 5.6. Interestingly, the particles with a higher overall signal, also exhibit a ring of elevated intensity around their

perimeter. This is true for both particles that lay flat and ones that lay on their sides (Fig. 5.6). One possible explanation is that there are more fluorophores on the surface of the particle than in the porous matrix of the particle. Therefore, more fluorophores would be present in the optical path of a pixel corresponding to an edge of a particle than that of a pixel completely over the porous matrix of a particle. An interesting observation can be seen in figure 5.6. Notice that the lower intensity particles do not exhibit the "edge effect" to the same degree that the higher intensity particles do. This could indicate that in the lower intensity particles, the targets are distributed uniformly throughout the both the porous matrix and surface of the particle. While in the higher intensity particles the fluorophore concentration is higher on the surface than in the porous matrix.

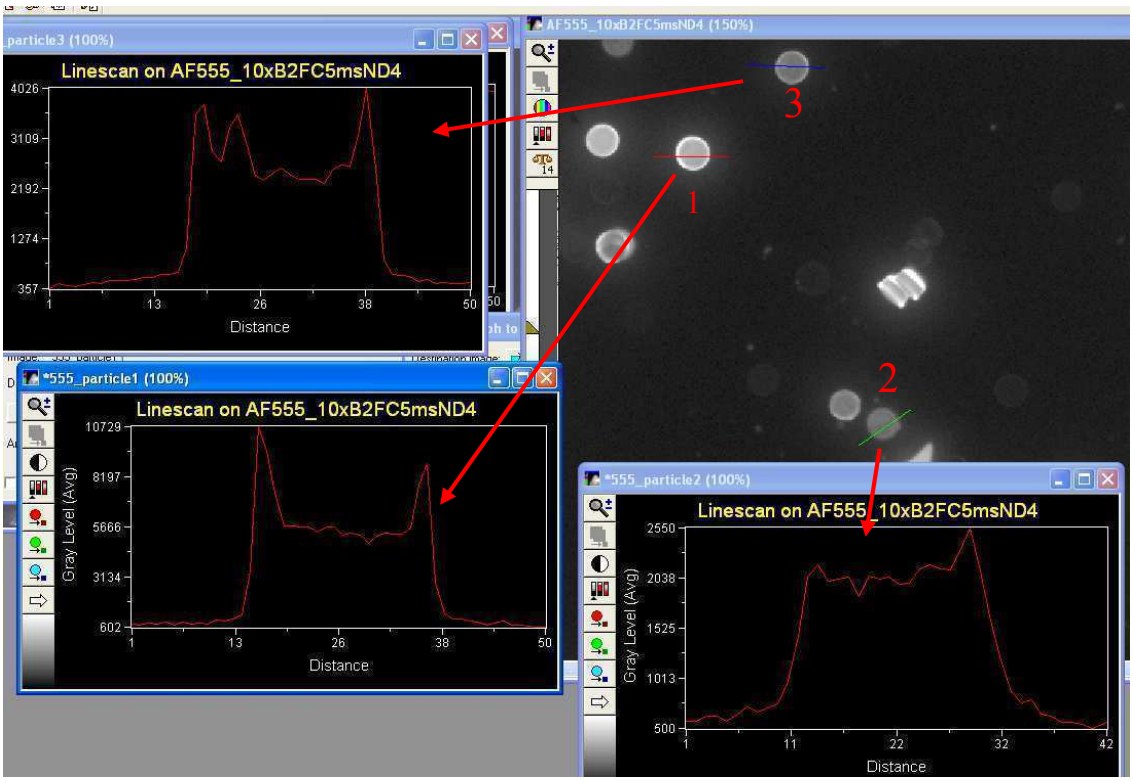

Figure 5.6 Intensity line profiles for three selected particles imaged in the AF555 fluorescence channel.

5.5 CHAPTER SUMMARY

In summary, it has been demonstrated that a system based on porous silica photonic crystal particles is capable of multiplexed DNA detection. Additionally, the photonic encoding method was found to be in agreement with the independent fluorescence/oligonucleotide encoding method. Furthermore, the photonic codes of thermally oxidized encoded porous silica particles as well as their chemical probes are stable in biological assay conditions. However, if the system were to be commercialized, several issues would need optimization, such as the particle assembly's low packing density and the assay noise.

5.6 ACKNOWLEDGMENTS

Chapters 5, in part is a reprint of the material as it will appear upon submission of the manuscript in progress: Meade, S.O., Chen, M., Sailor, M.J. “A bioassay multiplexing system utilizing porous silica photonic crystal particles containing spectral barcodes” (2008).

5.7 REFERENCES

1. Gunderson, Kevin L.; Kruglyak, Semyon; Graige, Michael S.; Garcia, Francisco; Kermani, Bahram G.; Zhao, Chanfeng; Che, Diping; Dickinson, Todd; Wickham, Eliza; Bierle, Jim; Doucet, Dennis; Milewski, Monika; Yang, Robert; Siegmund, Chris; Haas, Juergen; Zhou, Lixin; Oliphant, Arnold; Fan, Jian-Bing; Barnard, Steven; Chee, Mark S. *Decoding randomly ordered DNA arrays.* Genome Research (2004), 14(5), 870-877

2. Kucho, Ken-ichi; Yoneda, Hidekatsu; Harada, Manabu; Ishiura, Masahiro. *Determinants of sensitivity and specificity in spotted DNA microarrays with unmodified oligonucleotides.* Genes & Genetic Systems (2004), 79(4), 189-197.

3. http://www.idtdna.com.

4. Steinberg, Gali; Stromsborg, Katie; Thomas, Lynette; Barker, David; Zhao, Chanfeng. *Strategies for covalent attachment of DNA to beads.* Biopolymers (2004), 73(5), 597-605.

APPENDIX A

FFT Encoding

A.1 INTRODUCTION

In addition to rugate encoding, an alternate method, called FFT encoding, was investigated. The idea entails creating porous silicon samples with multiple layers that vary in porosity as a step function from one layer to the next, like a Bragg filter,[1] but without the photonic properties. The resultant sample would then exhibit complex Fabry Perot reflection spectra[1] from which encoded information could be decoded by taking the FFT of the interferogram in reciprocal wavelength space.[2]

A.2 EXPERIMENTAL SECTION

Figure A.1 shows the experimental design for a study that investigated the effects of varying the thicknesses of two discrete layers differing in porosity (refractive index) on the resultant spectra. In this experiment, five "double layer" waveforms were created where the first layer was etched at a current density of 13.3 mA/cm^2 and the second layer at 39.8 mA/cm^2, for the times shown in figure A.1. Two replicate samples for each waveform were fabricated. Please see chapter 2 for the general protocol on etching porous silicon.

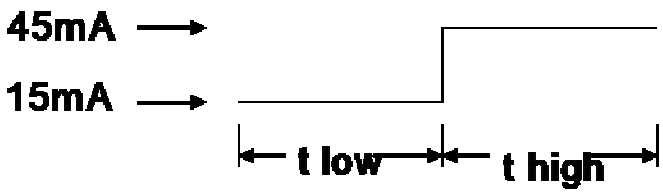

Code	t low (min)	t high (min)
1	0	8
2	2	6
3	4	4
4	6	2
5	8	0

Figure A.1 Experimental design for FFT encoding experiment.

A.3 RESULTS, DISCUSSION AND SUMMARY

The replicate spectra for each code are each plotted on the same plot to show reproducibility between replicate samples. A visual inspection from one code to the next does indeed reveal reproducibility in a qualitative sense. (Fig. A.2 and A.3). Specifically, the spectral envelopes and relative fringe heights of neighboring fringes, differ from one code to the next yet are similar between replicates of the same code. FFT analysis was not performed on this data set because the method was set aside once the Rugate method began showing great promise. The FFT method has since been taken up by other researchers and developed (manuscript in process).

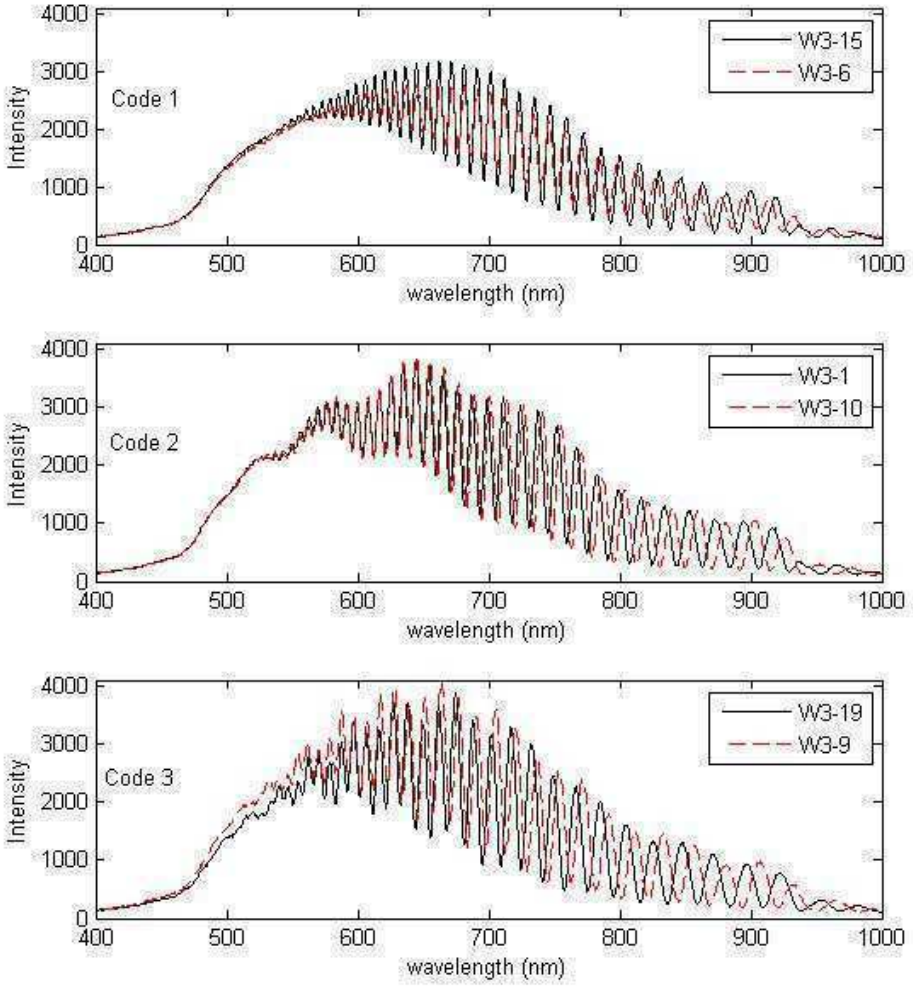

Figure A.2 Resultant Fabry-Perot spectra from the preliminary investigation on FFT encoding.

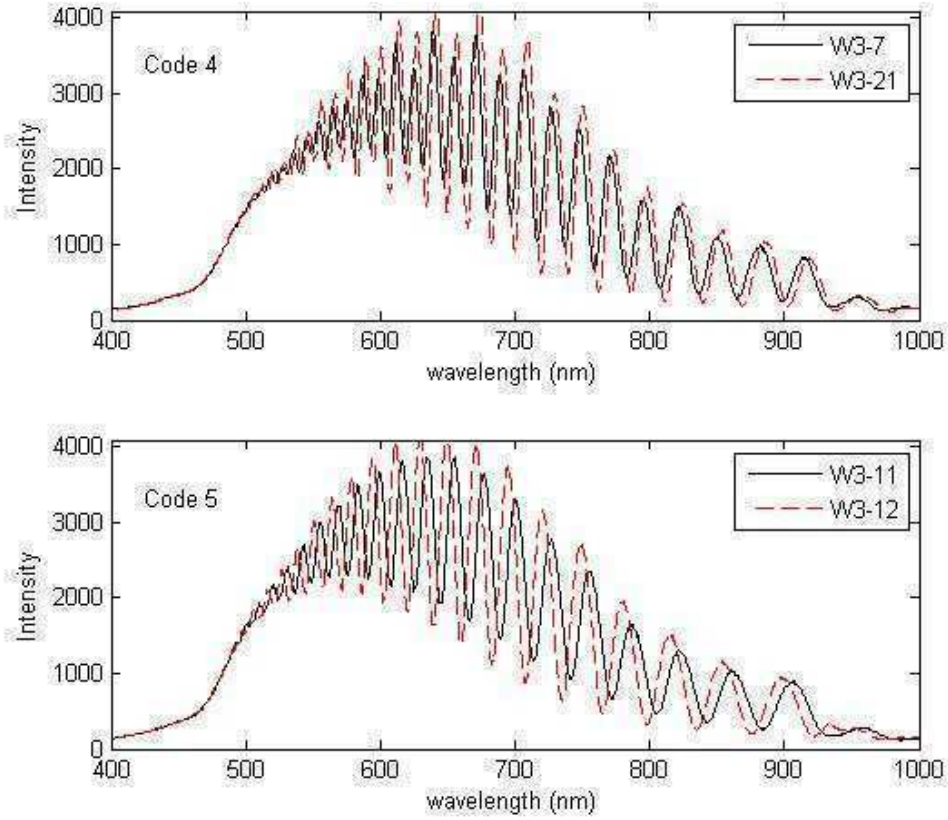

Figure A.3 More spectra from the preliminary investigation on FFT encoding.

A.4 REFERENCES

1. Pavesi, L. and P. Dubos, *Random porous silicon multilayers: application to distributed Bragg reflectors and interferential Fabry-Perot filters.* Semicon. Sci. Tech., 1997. **12**(5): p. 570-5.

2. Sailor, M.J. and S.O. Meade, *Optically Encoded Particles*, in *U.S. Patent Application # 10/503,217*. 2004, University of California, San Diego.

APPENDIX B

Decoding with Bandpass Filters and a Preliminary Assay

B.1 INTRODUCTION

The goal of this experiment was to decode the particle's spectral identity, using only components that are commonly available with a fluorescence microscope. As in chapter 5 the decoding results of the photonic codes would be compared against an independent encoding method utilizing oligonucleotide codes. Unfortunately, the decoding results were unsuccessful. However, in this experiment it was shown that thermally oxidized porous silicon photonic crystal particles (transformed to porous silica) could maintain spectral codes through thermal oxidation, probe immobilization and assay conditions - a major goal of the project. It's recommended that the reader is familiarized with the principles introduced in the 5 main chapters of this thesis before reading this appendix.

B.2 EXPERIMENTAL SECTION

B.2.1 Scheme for bandpass decoding

Figure B.1 describes the decoding process. As opposed to the decoding process described in chapter 3 that used high resolution spectral imaging, in this method, only sparse regions of the spectral code are sampled, by the use of bandpass filters. In this method the microscope is used in transmission mode, where white light is passed through the rugate encoded particles. The spectrum shows decreased intensity where the particle contains reflection maxima (peaks). The light then passes through a chosen emission

filter, acting as a bit. When the field of particles is imaged, the particles containing rugate peaks that align with the bandpass filter will appear dimmer than the background. So, each filter used acts as a bit and the amount of light blocked by the particle acts as the state (see chapter 2 for definitions of bits and states with respect to spectral codes). Theoretically, accurate encoding and narrow band pass filters could allow for gray scale encoding. The benefit of this decoding method is that the standard components of the fluorescence microscope can be used. The negative is that peak placement needs to be very accurate in relation to the filter's spectral window.

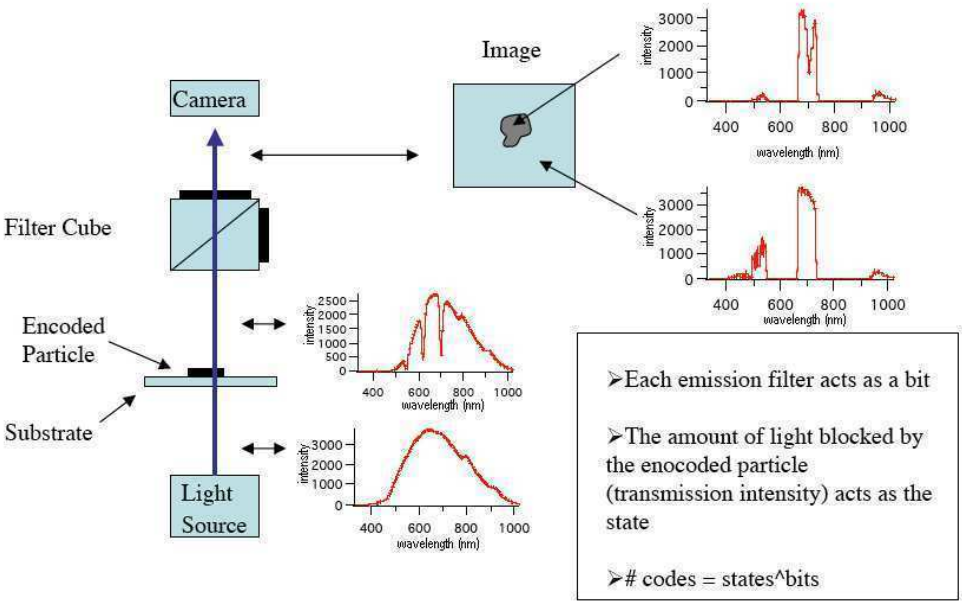

Figure B.1 Scheme for bandpass decoding.

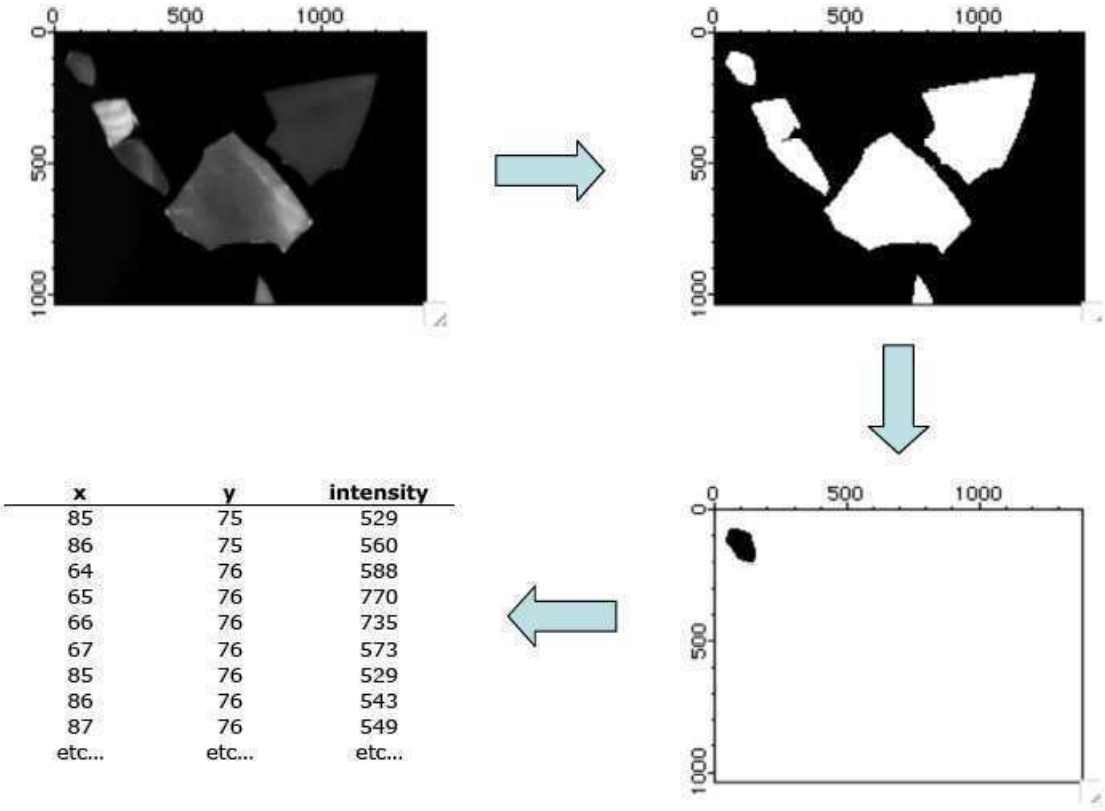

Figure B.2 Image processing. (a) Image of particles showing all particles. (b) Binary image created using an intensity threshold. (c) A map of one particle is made using a seed finding algorithm applied to a single pixel selected within a particle of interest. A map of pixel indices is created for each processed particle (d).

B.2.2 Probe functionalized encoded particle fabrication.

For an overview of the workflow of this experiment please see chapter 1. For encoding, oligo immobilization and hybridization methods please see chapters 2 and 5, respectively.

B.2.3 Experimental design

Table B.1a shows the experimental design. Two encoded particle types were made. The first particle type was encoded with a single rugate peak, represented in binary fashion as "10." The second particle type was encoded with a double rugate peak spectrum, represented in binary fashion as "11". Particle types "10" and "11" were both functionalized with the unique oligonucleotide probes, Probe1 and Probe2, respectively (Table B.1b). The hybridization solution was spiked with the Cy3 labeled oligonucleotide, Target1, which was a perfect-compliment of Probe1 (Table B.1b). Please note that in this experiment "1" indicates the presence of a peak in the spectral region of the emission filter acting as the bit. Again, this should make the particle go dark, in transmission mode. "0" indicates the absence of a peak. In this case the particle should be close to background in the image.

B.2.4 Image processing technique

A program was written to extract intensity data from each particle in each image. The process works as follows: first an image showing all the particles is acquired (Fig B.2a) and using an intensity threshold a binary image is created (Fig. B.2b). Second, a

pixel from a one particle is selected and an algorithm that identifies all neighboring pixels of the same value, 1 or 0 is employed. The single particle template (Fig B.2c) is then used to extract the intensity of each pixel of a given particle form the assay and decode images (Fig. B.2d). The process is repeated for all particles.

Table B.1 (a) Experimental design. (b) Filter setup and oligonucleotide sequences.

(a)

Code	Bit 1 State	Bit 2 State	Probe	Target
1	1	0	Probe1	Target1
2	1	1	Probe2	None

(b)

Bit1	CY3 emission filter
Bit2	CY5 emission filter
Fluorescence Readout	CY3 Cube
Oligo1(Target)	3'-GCCCGTAAACCTTCACGCCAATCAGCCGAA-CY3-5'
Oligo1(Probe)	5'-NH2-CGGGCATTTGGAAGTGCGGTTAGTCGGCTT-3'
Oligo2(Probe)	5'-NH2-GCGTTTAATATAGCAGGATATCGATATGGC-3'

B.3 RESULTS AND DISCUSSION

Spectra of the oxidized silica films (three replicates each) are compared to the filters acting as bit 1 and bit 2 (Fig B.3). Code 10 was taken in transmission and Code 11 was taken in reflection mode. This was done for convenience and is irrelevant to the experiment. What is important is the fact that each sample is contained within the boundaries of the filters.

In figure B.4, which displays the bit 1 decode image, several things are amiss. First, the particles were too big. The reason for this is that the freestanding films were oxidized prior to ultrasonication. To create fractionated particles that are smaller (< 100 μm) it is recommended that the freestanding porous silicon film be sonicated into particles before thermal oxidation. Particles, 25 μm in diameter, scattered across the entire field of the image would be ideal. The smaller the particle, the more types of probes are possible in one image, resulting in higher multiplexing levels. This is why the microfabrication method described in chapter 4 was invented and developed. Second, all the particles should be equally dark. Particles 4 and 5 were anomalously bright, probably due to the variability of the spectral peaks with respect to their alignment with the bandpass filter. The image of Bit 2 on the other hand showed a promising result (Fig. B.5). Some particles, namely particles 1 and 3 are much brighter than the rest - as one would expect for the “10” particle type.

All the particles in the Cy3-fluorescence image showed signal (Fig. B.6). Assuming that both particle types were present, a high signal across all particles would indicate a large amount of nonspecific binding of Target1 to particle type “11” labeled

with Probe2. Nonspecific binding would also explain the large amount of non-homogeneity in signal across a particle.

In Figure B.7 the average intensities are plotted for each particle. The error bars represent 1 standard deviation. The results are inconclusive. In order for the results to agree with the experimental design all the Bit 1 intensities would be equally suppressed and some of the Bit 2 decode particles be suppressed along with their respective intensities from the assay image. Since this was only a preliminary experiment and would not be carried further some cherry picking of the data was permitted. In figure B.8 particles 5 and 6 with anomalous brightness were thrown out. Results in ballpark agreement with the experimental design can now be seen. Similar extracted transmission intensities for all the particles can be seen in the bit 1 image data set. And, in the bit 2 image data set, the two particles with the highest transmission intensities also have the highest fluorescent signal.

Figure B.9 shows the only significant finding of the whole experiment: the particle's spectral code is retained after probe immobilization and hybridization, thus demonstrating chemical resistivity of encoded porous silica photonic crystals through biological assay conditions. Again the fact that the spectrum of the particle (before immobilization chemistry) is in transmission mode is irrelevant to experimental results. This was only done for convenience.

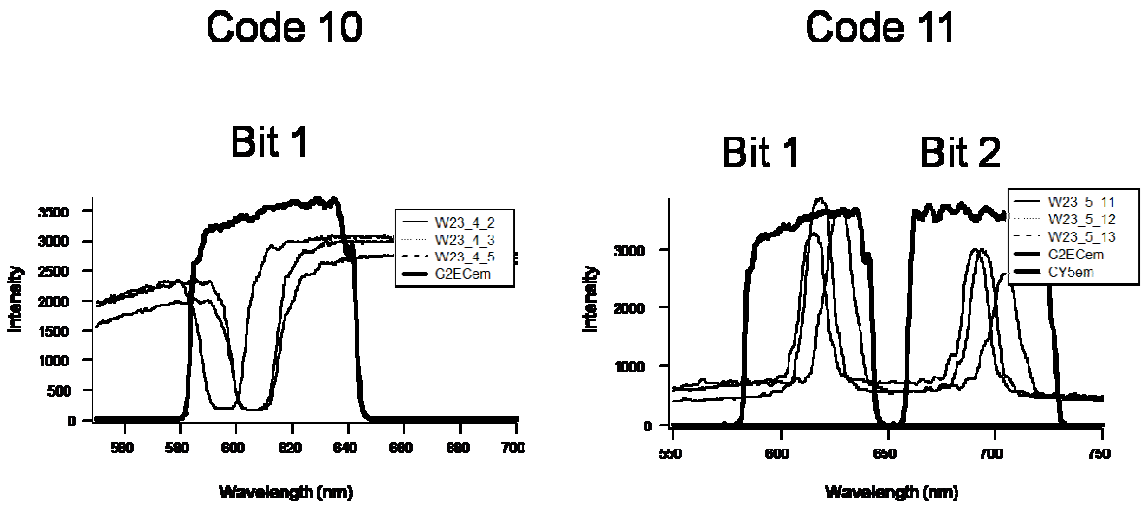

Figure B.3 Alignment of spectral codes and bandpass filters. The spectra shown to the left were taken in transmission mode and the spectra to the right were taken in reflection mode. This was only done for convenience and does not have any significance to the experiment.

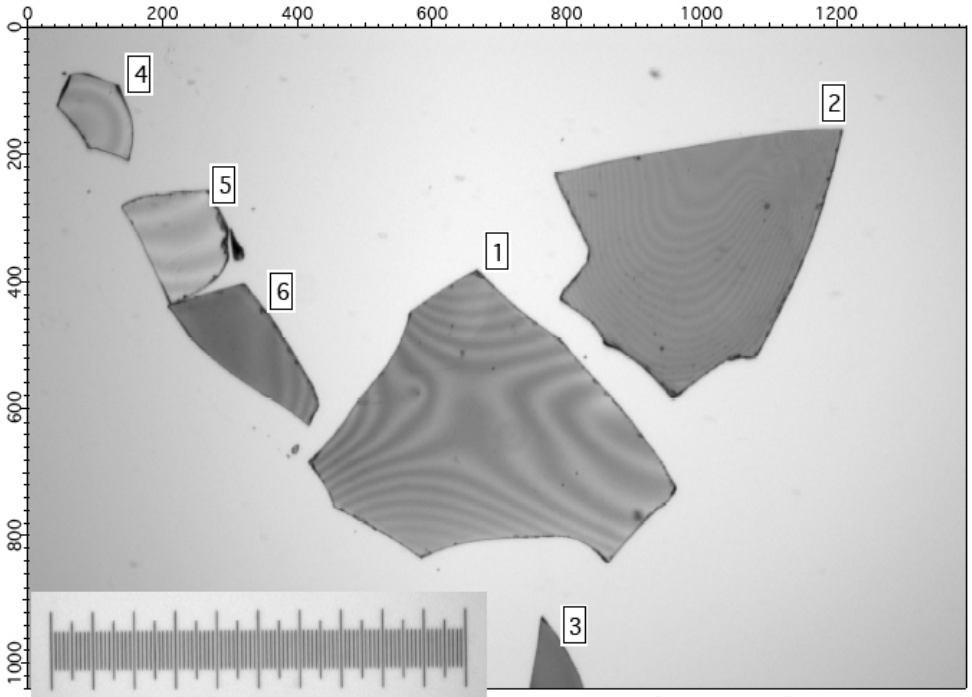

Code	Bit 1 State	Bit 2 State	Probe	Target
1	1	0	Probe1	Target1
2	1	1	Probe2	None

Figure B.4 Bit 1 decode image.

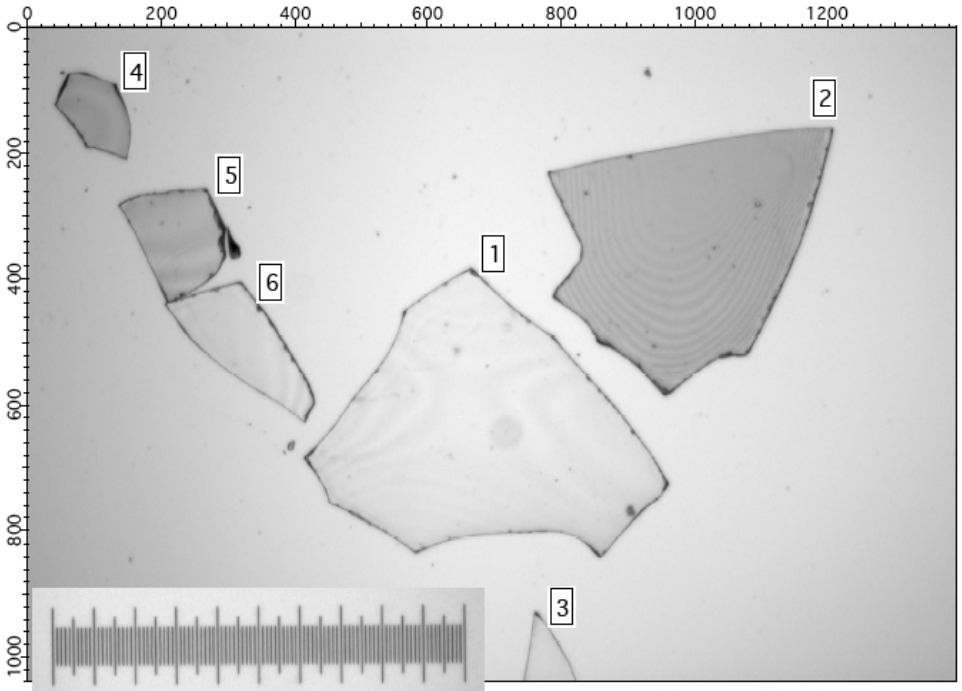

Code	Bit 1 State	Bit 2 State	Probe	Target
1	1	0	Probe1	Target1
2	1	1	Probe2	None

Figure B.5 Bit 2 decode image.

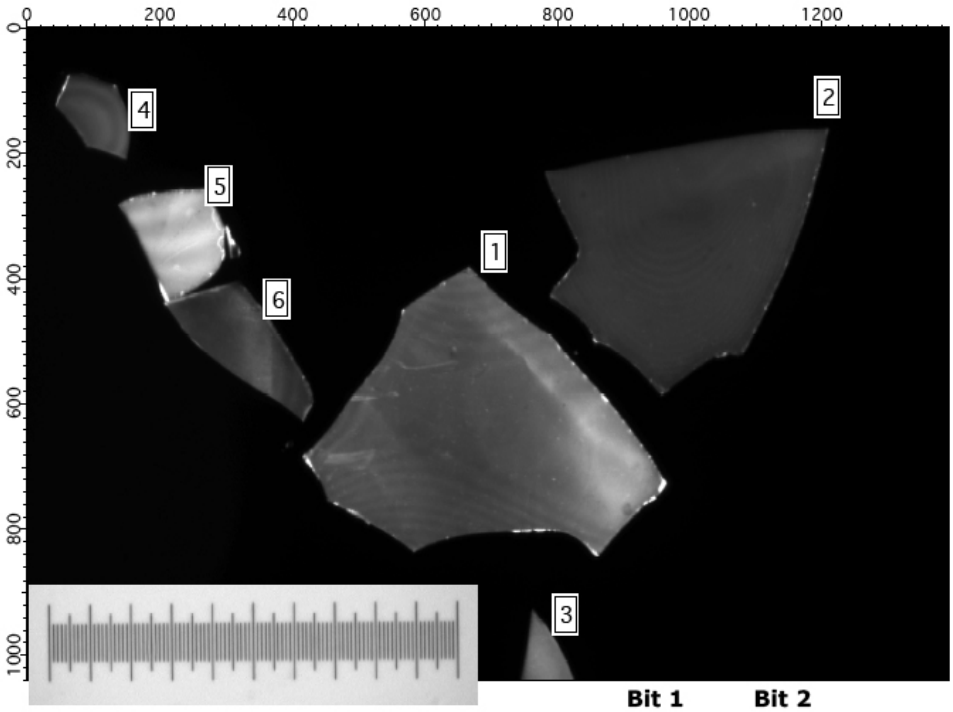

Code	Bit 1 State	Bit 2 State	Probe	Target
1	1	0	Probe1	Target1
2	1	1	Probe2	None

Figure B.6 Cy3 fluorescence image.

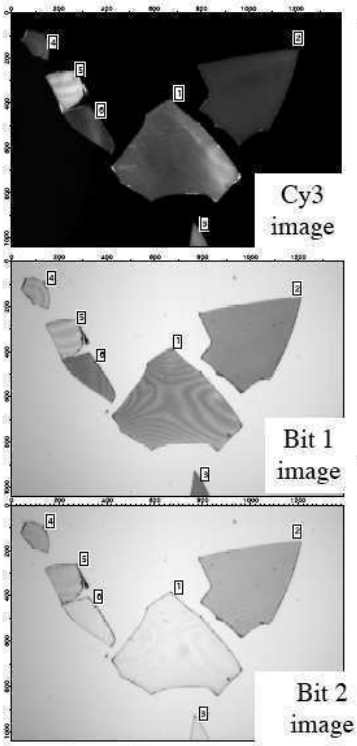

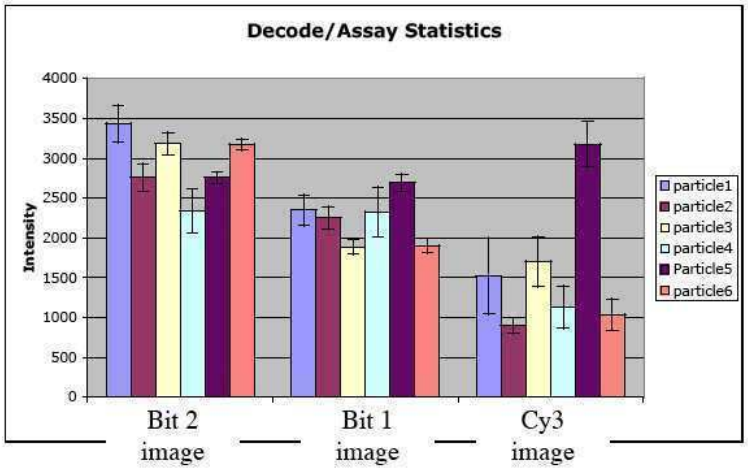

Code	Bit 1 State	Bit 2 State	Probe	Target
1	1	0	Probe1	Target1
2	1	1	Probe2	None

Figure B.7 Extracted data.

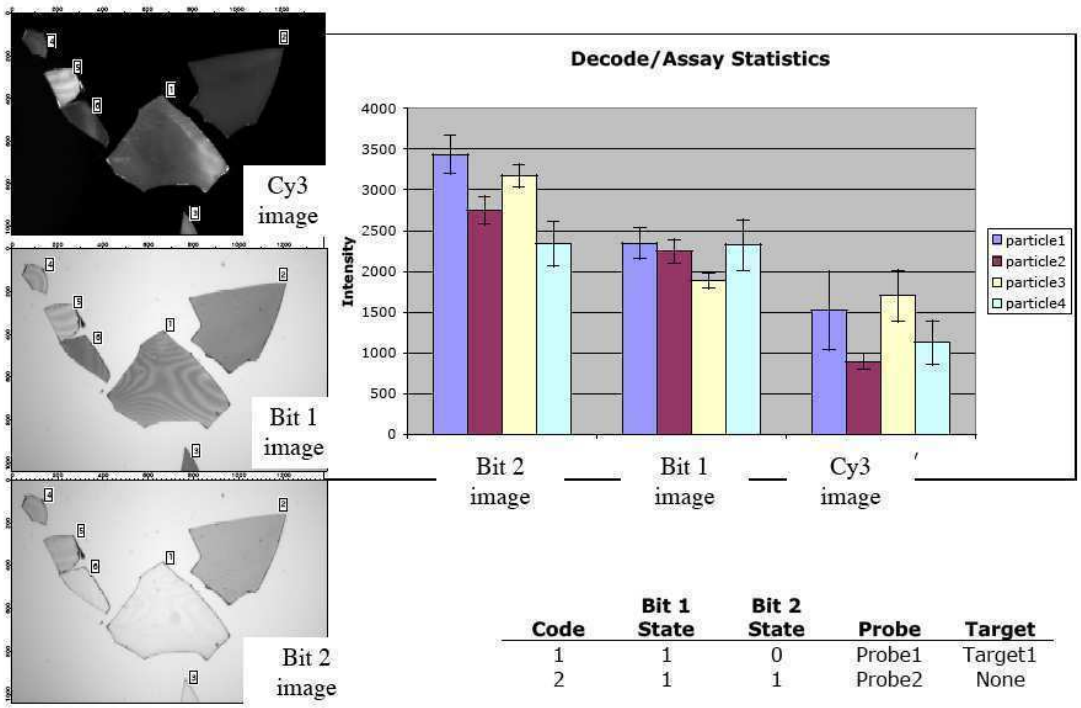

Code	Bit 1 State	Bit 2 State	Probe	Target
1	1	0	Probe1	Target1
2	1	1	Probe2	None

Figure B.8 Extracted data with the anomalous particles 5 and 6 thrown out.

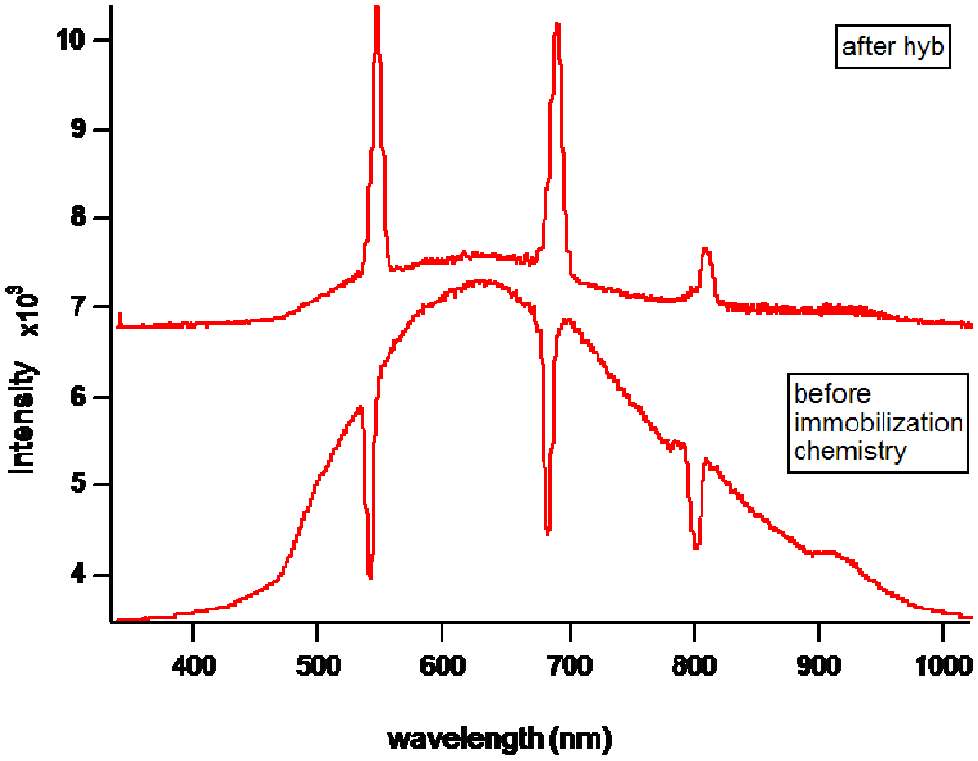

Figure B.9 Spectra of the selected particles before and after the probe immobilization and hybridization steps. The spectra taken before the probe immobilization steps were acquired in transmission mode for convenience only. There is no other significance to this.

B.4 SUMMARY

Bandpass, or low resolution decoding was unsuccessful. Therefore, the decoding method outlined in chapter 3 was developed. Spectrally encoded porous silica photonic crystal particles were demonstrated to be chemically stable throughout the probe immobilization and assay conditions described in chapter 5.

B.5 REFERENCES

Pertinent references can be found within the chapters that were referred to.

APPENDIX C

Stabilization of porous silicon by norbornylene metathesis

C.1 INTRODUCTION AND EXPERIMENTAL SECTION

In order to improve the chemical stability of the porous silicon particles, the films were broken into small particles and coated with polynorbornylene. The process begins by first, creating the encoded porous silicon film on wafer samples. The porous silicon film is lifted off of the crystalline silicon wafer using the electropolishing reaction and the freestanding film is then fractionated into particles by ultrasonication. See chapter 2 for techniques. A thin film of polynorbornylene is then grown on the surface of the particles by insitu polymerization of norbornylene using a ruthenium ring-opening metathesis polymerization catalyst.[1]

In order to test stability of the polymer-coated particles, they were exposed to a sodium carbonate/bicarbonate buffer solution (pH 10) for 30 min. As a control, a set of non-polymer-coated particles (porous silicon only) were exposed to the same conditions.

C.2 RESULTS, DISCUSSION AND SUMMARY

Due to the fact that the reflection spectra of the control set (Fig. C a) and the polymerized particles before exposure to the buffer (Fig. C b) are alike, it is presumed that the polymer does not penetrate the pores. Otherwise, the penetration of the polymer into the porous matrix would cause a red shift of the spectral peaks in response to the increase in refractive index of the polymer with respect to air. Also, it is assumed that the polymer coating is not continuous because the spectrum from both the uncoated and coated particles red-shift, upon immersion in ethanol. When exposed to pH 10 for 30 minutes the polymer-coated particles still display their spectral codes, while the control set releases bubbles and are dissolved away after 30 minutes. However, the polymer-

coated particles are blue shifted somewhat (~ 50 nm) after the base treatment. This can be attributed to the partial dissolution of the porous silicon under the polymer coating and shows the robustness of the encoding technique (discussed in chapter 2) due to the fact that the encoding information (photonic structure) is distributed throughout the porous silicon matrix. As discussed in chapter 3 a shift of the entire spectrum can be normalized using bits based on relative peak spacing.

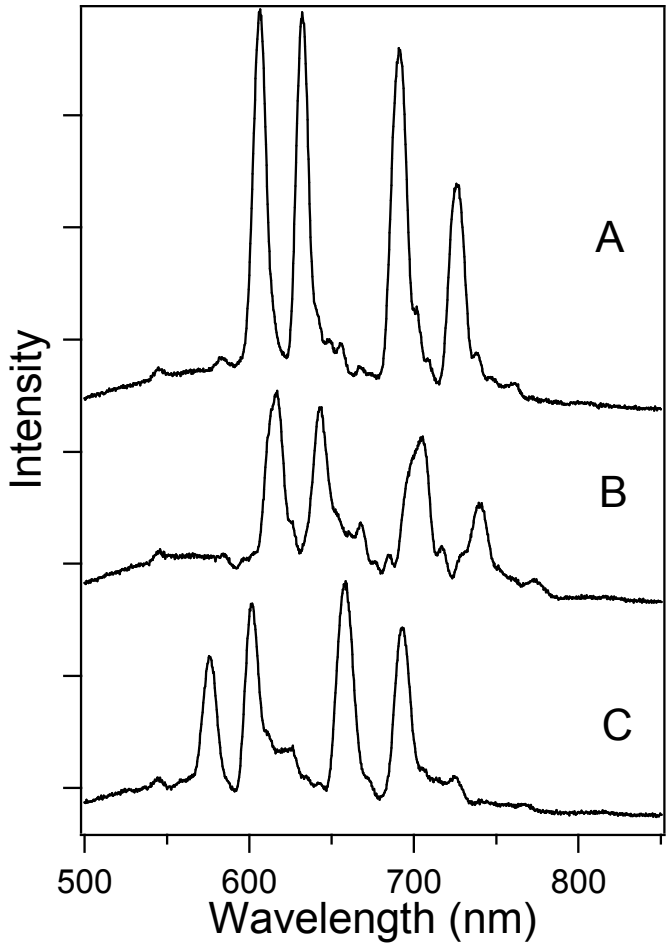

Figure C Reflection spectra of stabilized, encoded porous silicon particles. A) Spectrum of a fresh porous silicon particle. B) Spectrum of a polynorbornylene-treated porous silicon particle. C) Spectrum of a polynorbornylene-treated porous silicon particle after exposure to base. All spectra were obtained from particles assembled on the bottom of a dish filled with ethanol. Particles dimensions were approximately 250 μm on edge.

C.3 REFERENCES:

1. Yoon, Myeong Sik; Ahn, Kyo Han; Cheung, Ronnie W.; Sohn, Honglae; Link, Jamie R.; Cunin, Frederique; Sailor, Michael J., *Covalent Crosslinking of 1-D Photonic Crystals of Microporous Si by Hydrosilylation and Ring-Opening Metathesis Polymerization.* Chem. Commun., 2003: p. 680-681.

APPENDIX D

Bead Patterning

D.1 ABSTRACT

The method discussed in this appendix, called bead patterning, utilizes monodisperse populations of polymer beads as the starting material for polymer replicate photonic crystal microparticles. Unfortunately the goal of fabricating freestanding polymer replicate photonic crystal particles, exhibiting the original optical codes of the parent porous silicon film was not achieved. Once the microfabrication method discussed in chapter 4 began to show promise, the bead patterning method was put on hold and the findings were passed onto other workers, resulting in a publication.[1]

D.2 INTRODUCTION

Li et al. were first to show that polymer/silicon composites could be made of porous silicon photonic crystal films.[2, 3] In the first work, polymer/silicon composite photonic structures, the size of the original film were made for drug delivery experiments.[2] In the second work, Li et al. sprayed microdroplets of polymer solutions (polystyrene) onto the surface of a porous silicon film with the objective of creating freestanding polymer replicates. Unfortunately, the size distribution of the microdroplets is quite large.[3] To get around that problem, premade polymer beads, purchased in populations with very small size distributions, were used as the starting material for polymer replicates. The method is described below.

D.3 EXPERIMENTAL SECTION

The beads used in this experiment were polystyrene (non-crosslinked) with a mean diameter of 12.32 microns (Bangs Inc. Lot number PS07N/6674). Porous silicon samples were created according to the procedures outlined in chapter 2.

Step 1: Bead Washing/Solvent Transfer.

The stock vial of beads were vortexed until fully suspended (takes on a milky appearance). 100 μL of stock bead suspension was then transferred into a microcentrifuge tube by pipette and 400 μL of ethanol was added. The suspension was then vortexed for ~10 seconds, until all the beads were suspended. The suspension was then centrifuged and decanted. 500 μL of ethanol was added and the washing process was repeated two more times. The final volume was made to be 500 μL.

Step 2: Dispersion of beads onto surface of porous silicon sample.

Approximately 4 μL of the bead suspension (solid content unknown) were pipetted onto the surface of the porous silicon chip and allowed to dry. Once dry, the porous silicon sample was brushed until the beads were dispersed evenly across the surface of the silicon chip (Fig D.1 a). Any soft piece chemically inert of material will work. Mylar or PDMS work fine. Inspection with a microscope is necessary in this step. Beads resting on the outer ring (~ 2mm from the outer edge) of the porous silicon were removed with an ethanol wetted swab.

Step 3: Softening/Infiltration.

The substrate was then placed on a hotplate at ~ 75 deg ºC for 20 minutes. After which the temperature was raised to ~200 ºC for an additional hour (Fig. D.1 b). The substrate was then allowed to cool.

Step 4: Isolation of particles from porous silicon.

The porous silicon is then stripped away using an ethanolic solution of potassium hydroxide (Fig. D.1 c). First the substrate was placed in an etch cell, 200 μL of 3:1 0.5 M KOH(aq)/Ethanol was added and mixed with a pipet. Once the vigorous bubbling caused by the initial dissolution of the porous silicon subsided, 400 μL of 0.5 M KOH (aq) was added and mixed until all the porous silicon was dissolved away. The particle suspension was then transferred to a microcentrifuge tube and left to sit for one half hour to allow for the dissolution of any porous silicon still present within the porous matrix of the particles.

Step 5: Collection of particles.

The particle suspension was then filtered through an Anodisc filter (0.2 μm pores, Millipore) under vacuum and washed several times with DI water.

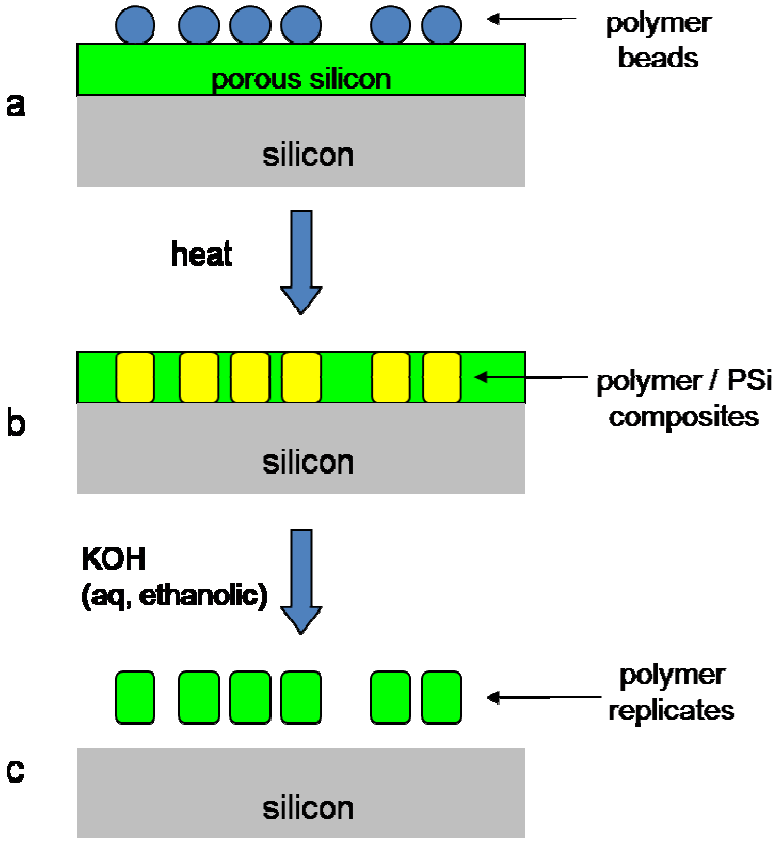

Figure D.1 In the bead patterning method polymer beads are distributed on the surface of the porous silicon. The substrate is then heated to hopefully infiltrate into the porous silicon matrix, thus replicating it. After infiltration the polymeric regions are freed by dissolving the porous silicon away with base.

D.4 RESULTS AND DISCUSSION

Figure D.2a shows the beads dispersed onto the surface of the porous silicon sample. Figure D.2b shows the same sample after the heating/infiltration step. The color change in the regions of the porous silicon, where beads coincide, is indicative of infiltration into the porous matrix due to the shift of refractive index. The freestanding polymer beads after base stripping step (Fig. D.2c) did not exhibit reflection spectra. The method was passed onto other workers for further investigation and can be reviewed in the cited publication.[1]

Sometimes art can result from a failed experiment (Fig D.3a,b). During a particular run, the base stripping process (particle isolation) was stopped midway through. Figure D.3a shows a field of what look like mushrooms. In figure D.3b a blow up shows a hemispherical cap which is the portion of the bead that did not infiltrate into the porous matrix. The midsection is the composite material of both polymer and silicon and the pedestal is the porous silicon matrix.

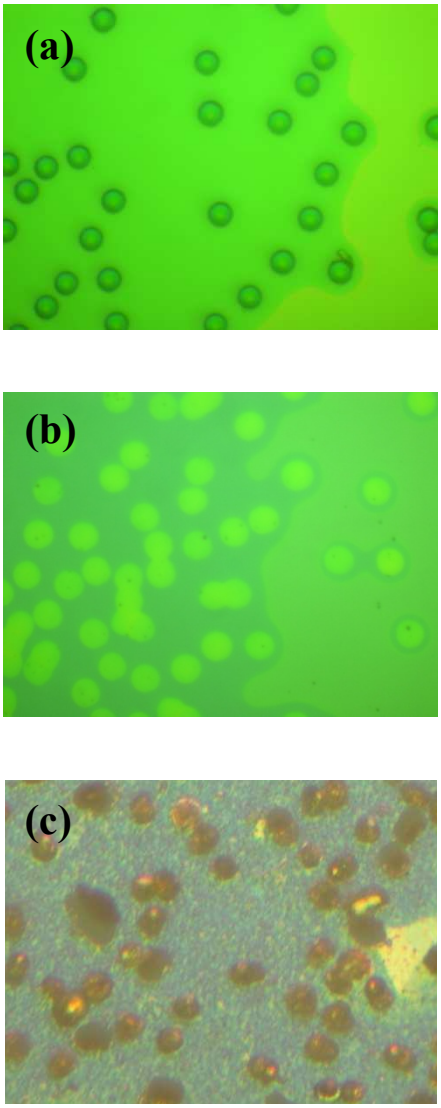

Figure D.2 Results of bead patterning experiment. (a) White light microscope image of particles dispersed onto porous silicon surface. (b) Substrate after heating. (c) Freestanding polymer "replicates" after being isolated from porous silicon matrix. Particles did not exhibit reflection spectra.

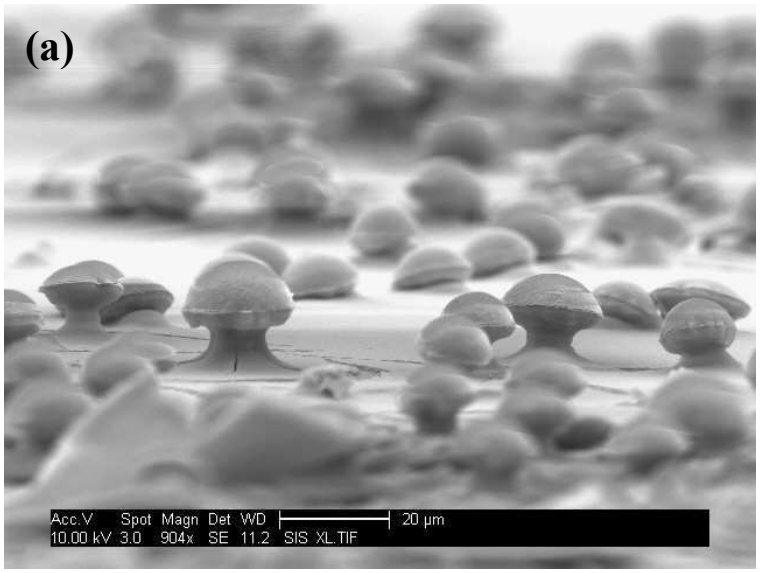

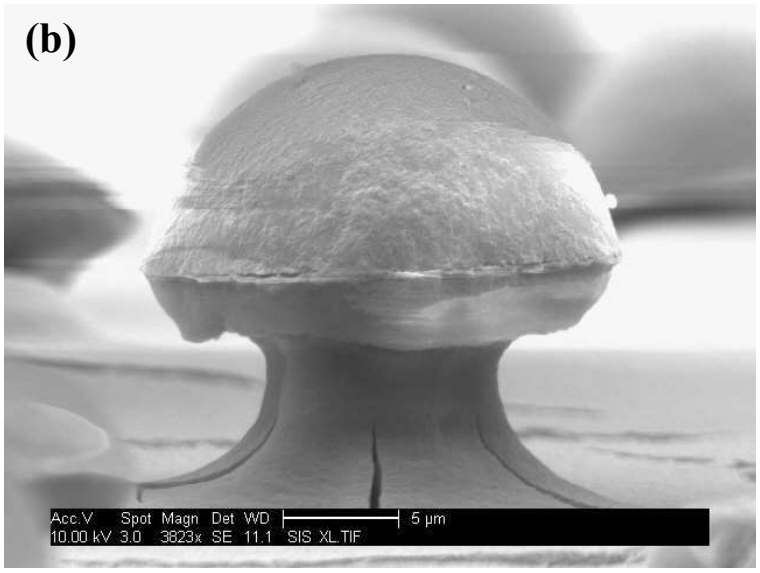

Figure D.3 A failed experiment yields art. SEM images, a and b, show the result of stopping the stripping process midway through. The upper cap is the polymer bead, the mid section is a polymer/silicon composite and the pedestal is porous silicon.

D.5 SUMMARY

A preliminary investigation into the bead patterning method did not result in freestanding polymer replicates exhibiting the spectral codes of the parent photonic structures. The investigation was passed onto other workers resulting in a publication.[1] However, freestanding polymer replicates exhibiting complete replication of the parent photonic structure still has not been achieved with this method.

D.6 REFERENCES

1. Park, Jennifer S.; Meade, Shawn O.; Segal, Ester; Sailor, Michael J. Porous silicon-based polymer replicas formed by bead patterning. *Physica Status Solidi A: Applications and Materials Science* (2007), 204(5), 1383-1387.

2. Li, Yang Yang; Cunin, Frederique; Link, Jamie R.; Gao, Ting; Betts, Ronald E.; Reiver, Sarah H.; Chin, Vicki; Bhatia, Sangeeta N.; Sailor, Michael J. *Polymer Replicas of Photonic Porous Silicon for Sensing and Drug Delivery Applications.* Science (Washington, DC, United States) (2003), 299(5615), 2045-2047.

3. Li, Y.Y., V.S. Kollengode, and M.J. Sailor, *Porous silicon/polymer nanocomposite photonic crystals by microdroplet patterning.* Adv. Mater., 2005. **17**(10): p. 1249-1251.